

UC Berkeley

Working Papers

Title

Modeling of the Brake Line Pressure to Tire Brake Force Subsystem

Permalink

<https://escholarship.org/uc/item/2cw289dp>

Authors

Xu, Z.
Ioannou, P.

Publication Date

1994-04-01

This paper has been mechanically scanned. Some errors may have been inadvertently introduced.

CALIFORNIA PATH PROGRAM
INSTITUTE OF TRANSPORTATION STUDIES
UNIVERSITY OF CALIFORNIA, BERKELEY

Modeling of the Brake Line Pressure to Tire Brake Force Subsystem

Z. Xu

P. Ioannou

University of Southern California

California PATH Working Paper

UCB-ITS-PWP-94-6

This work was performed as part of the California PATH Program of the University of California, in cooperation with the State of California Business, Transportation, and Housing Agency, Department of Transportation.

The contents of this report reflect the views of the authors who are responsible for the facts **and** the accuracy of the data presented herein. The contents do not necessarily reflect the official views or policies of the State of California. This report does not constitute a standard, specification, or regulation.

April 1994

ISSN 1055-1417

**Modeling of the Brake Line Pressure
to Tire Brake Force Subsystem**

by

Z. Xu and P. Ioannou

Report 92-05-03 May 1992

†This work was performed as part of the California PATH Program, in cooperation with the State of California Business, Transportation, and Housing Agency, Department of Transportation.

The contents of this paper reflect the views of the authors who are responsible for the facts and the accuracy of the data presented herein. The contents do not necessarily reflect the official views or policies of the State of California. This paper does not constitute a standard, specification or regulation.

Modeling of the Brake Line Pressure' to Tire Brake Force Subsystem

Z. Xu and P. Ioannou
Southern California Center
for Advanced Transportation Technologies
EE - Systems, **EEB 200B**
University of Southern California
Los Angeles, CA **90089-2562**

Abstract

One of the most challenging problems in automated vehicle control is when and how to apply the brakes. In order to deal with such a problem, a good understanding of the dynamical behavior of the braking mechanism is essential. In this report we use experimental data from a series of tests performed in collaboration with Ford research engineers to model the brake line pressure to tire brake force subsystem. This model will be used together with that of the master cylinder to line pressure currently under study, for developing an overall model for the braking mechanism. The brake model will later be used for longitudinal control design and automatic vehicle following.

***This work is supported by Caltrans through PATH of University of California and Ford Motor Company**

1 Introduction

The design of a control system for automatic braking that is reliable and safe under different road surface conditions requires a good understanding of the dynamical behavior of the brake mechanism. The brake mechanism may be divided into two parts. The first part involves the master cylinder pressure input to the brake line pressure subsystem and the second part the brake line pressure to the actual brake force subsystem. In this report we concentrate on the second part which is probably the most challenging one due to the variations in the tire and surface road characteristics. A series of experiments were conducted at Ford Motor Co. and the data collected were brought to USC for analysis and further processing. The results obtained are compared with those developed from physical laws [1, 2, 3, 4]. Our analysis reveals that the brake force can be expressed as an algebraic function of the slip index. Moreover, when the slip index is small, or before the wheel is about to be locked, the brake force is proportional to the brake line pressure. In this article, only longitudinal forces are considered.

2 Experimental Setup

The experimental set-up used by Ford engineers for performing the tests is shown in Figure 1 and is described as follows:

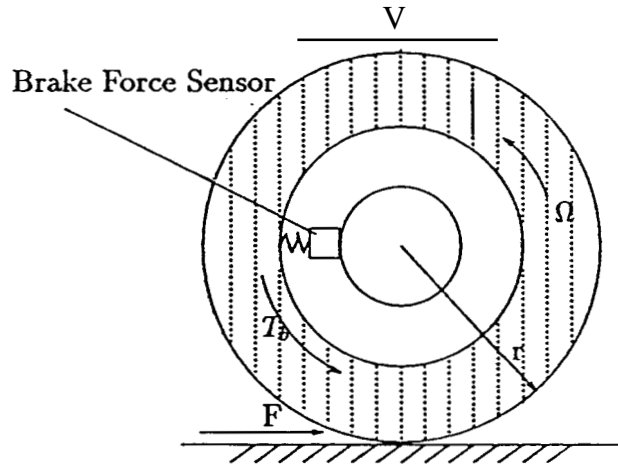


Figure 1: Tire System

The brake of the left front wheel has the capability of braking. The other three wheels are free to run. The measured variables are brake line pressure P , brake force F , wheel speed Ω , and vehicle speed V . In Figure 1 T_b represents the brake torque which is proportional to the brake line pressure P . Thus in the tire system considered, the brake line pressure P is the input, the brake force F is the output, and the vehicle speed V and wheel speed Ω are the state variables. The brake line pressure P is generated by a high frequency pump which

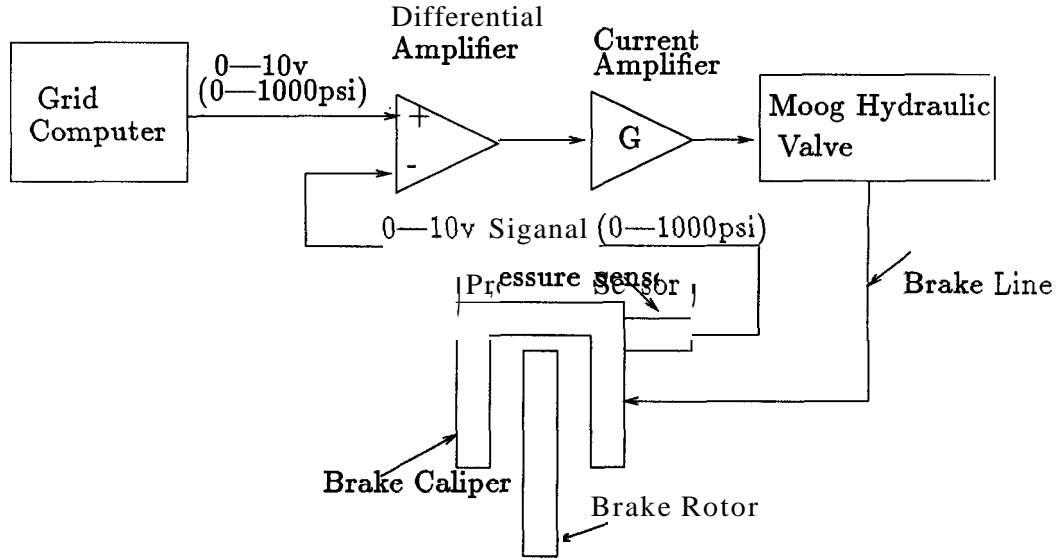


Figure 2: Hardware set-up for generating the line pressure Input

is controlled by the electric circuit shown in Figure 2. The brake force F is measured by a sensor mounted close to the shaft of the wheel and connected to the rim through a spring as shown in Figure 1. The vehicle speed is measured by an optical sensor and is normalized by the radius of the wheel. It is therefore expressed in terms of rad/sec. In our analysis, we will omit this normalization and treat V as the vehicle speed in m/sec .

The tests were conducted on two different road surfaces. One is a dry asphalt and the other is wet jennite and therefore more slippery. Three different inputs for the line pressure were applied: step, triangular, and staircase. The data obtained are presented in Figures A.1 – A.28 in Appendix, Note that the line pressures in Figures A.1 – A.14 are equal to those in Figures A.15 – A.28, respectively.

3 Data Processing and Modeling

Due to the road surface effects, the brake force measurements contain high frequency noise. This can be clearly seen from Figures A.1 – A.28. In order to filter out the noise effects, we design the sixth order low pass filter

$$H(z) = \frac{10^{-3}(0.5573 + 3.344z^{-1} + 8.359z^{-2} + 11.15z^{-3} + 8.359z^{-4} + 3.344z^{-5} + 0.5573z^{-6})}{111.2 - 545.1z^{-1} + 1122.2z^{-2} - 1241.4z^{-3} + 777.7z^{-4} - 261.4z^{-5} + 36.82z^{-6}}$$

which is based on a sampling rate of 200Hz and has a cut-off frequency of about 10Hz. This choice of cut-off frequency is based on our observation of the measured data and brake

frequency band. The magnitude versus frequency of this low pass is plotted in Figure 3. The filtered data are shown in Figures A.29 — A.56 in Appendix which are corresponding

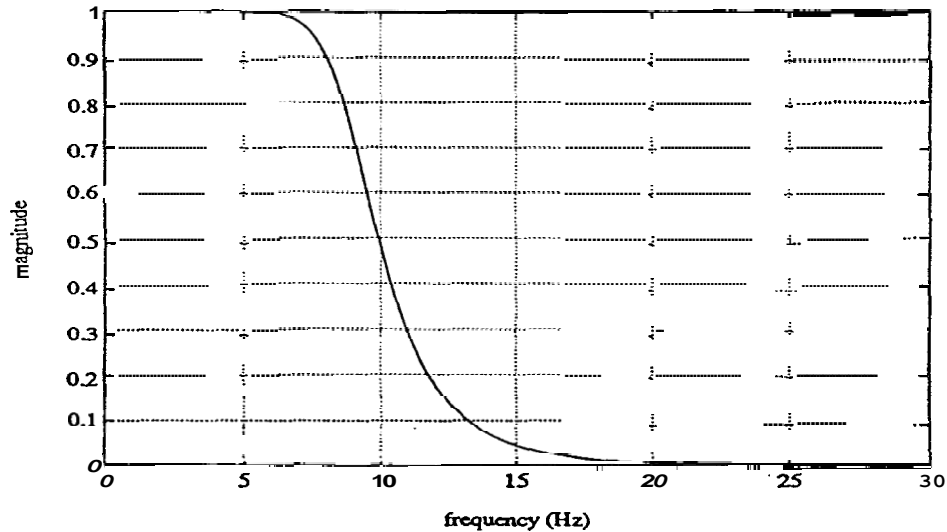


Figure 3: Low Pass Filter

to Figures A.1 — A.28, respectively except that we substitute the slip index vs time curves for wheel speed vs time curves. Note that although the line pressure, vehicle speed, and wheel speed measurements are less noisy than the measurements of the brake force, for consistency all data were filtered by the same filter. Using the filtered data, we make the following observations:

1. When the brake line pressure P is **small** i.e. $P < 500$ *psi* or when the slip index S_l , defined as

$$S_l := \frac{V - r\Omega}{V} \quad (1)$$

where r is the radius of the wheel, is **small**, both dry asphalt road and wet jennite road produce similar brake forces as shown in Figures 4—6. In these three figures, the brake forces are generated by the line pressure shown in Figures A.1 — A.3 in Appendix, respectively.

2. When the brake line pressure $P \geq 500$ *psi*, the dry asphalt and jennite roads produce different brake force responses as shown in Figures A.4 — A.14 and Figures A.18 — A.28 in Appendix. The difference is due to the fact that the more slippery wet jennite road caused the wheel to be locked when $P \geq 500$ *psi* which results in a slip index $S_l = 1$. However, for the dry asphalt road, $S_l < 0.1$ even when P is as large as **1000** *psi*.

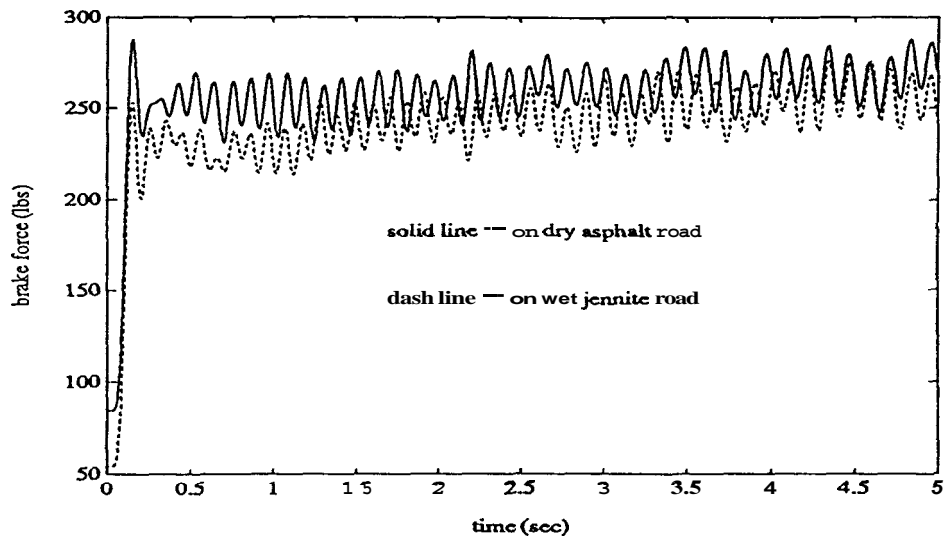


Figure 4: Filtered brake force vs time for dry asphalt and wet jennite road

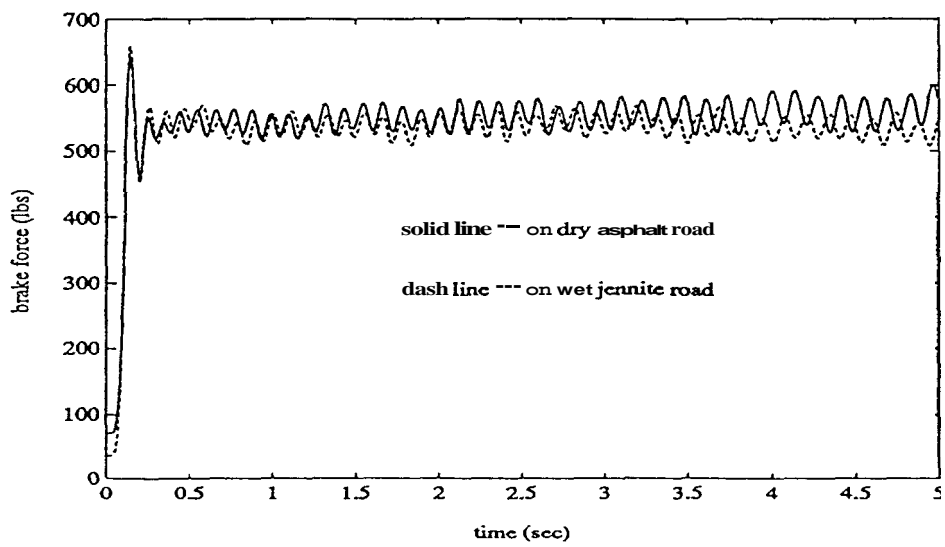


Figure 5: Filtered brake force vs time for dry asphalt and wet jennite-road

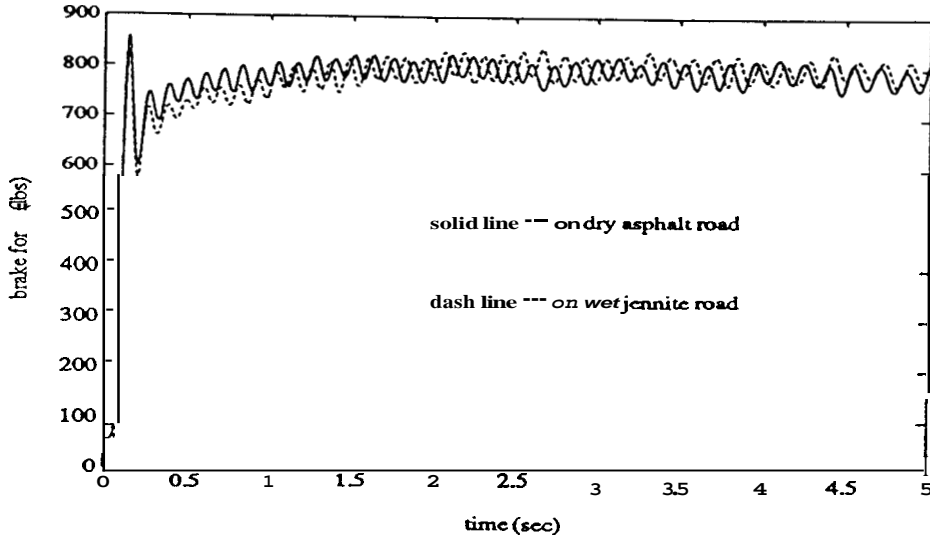


Figure 6: Filtered brake force vs time for dry asphalt and wet jennite road

- The tests confirm that the brake force can be approximated as an algebraic function of the slip index as suggested in [1, 2]. This function according to [1, 2] is given by

$$\begin{aligned} F &= d \sin(c \tan^{-1}(b\phi)), \\ \phi &= (1 - e)S_l + (e/b) \tan^{-1}(bS_l), \end{aligned} \quad (2)$$

where S_l is expressed as a percentage and b, c, d, e are parameters that depend on the vehicle load, tire characteristics, road condition etc. The graph of F vs S_l as depicted by (2) for $b = 0.21, c = 1.67, d = 1369 \text{ lb} (= 6090 \text{ Newton}), e = 0.686$ obtained from [1], is shown in Figure 7. In Figure 8 we show the corresponding curve developed using the experimental data shown in Figure A.20 in the Appendix. It is clear that the two curves are quite similar except for the scales that are different due to the difference in the values of the constants b, c, d, e .

- When the slip index is small i.e. $S_l < 0.1$ or the point where the brake force reaches maximum and the wheel locks is not yet reached, the brake force F is almost proportional to the brake line pressure P (i.e. $F \approx \alpha P$) as shown in Figure 9. This graph is developed from the experimental data shown in Figure A.8 in the Appendix. The gain α between P and F varies from 1.4 to 1.9 depending on the test and value of P . This observation agrees with the theoretical results as explained below:

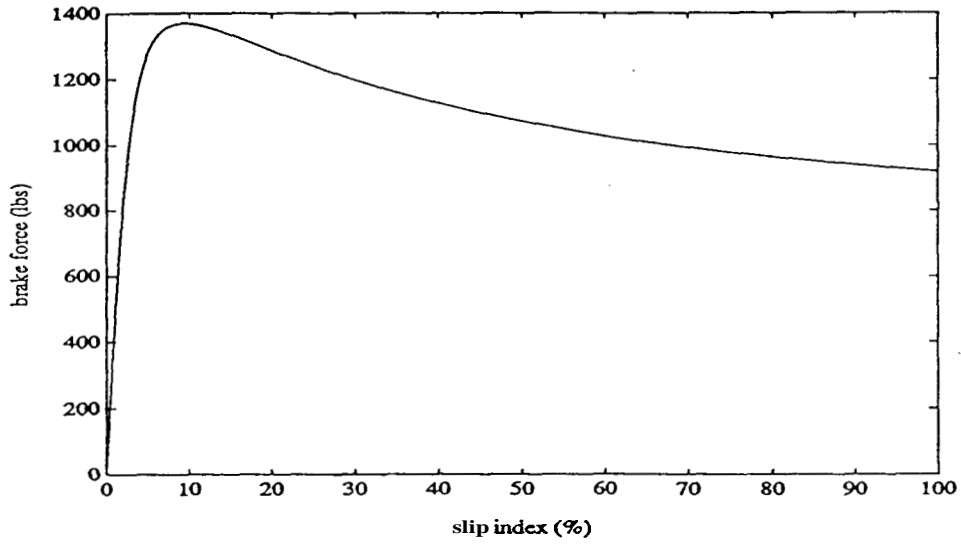


Figure 7: Brake force vs slip index from theory

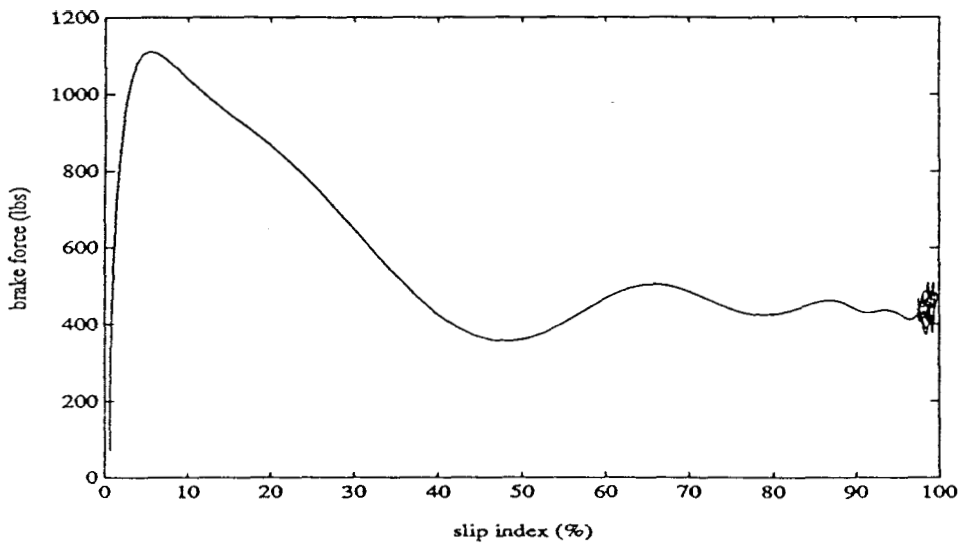


Figure 8: Filtered tested brake force vs slip index from experiment

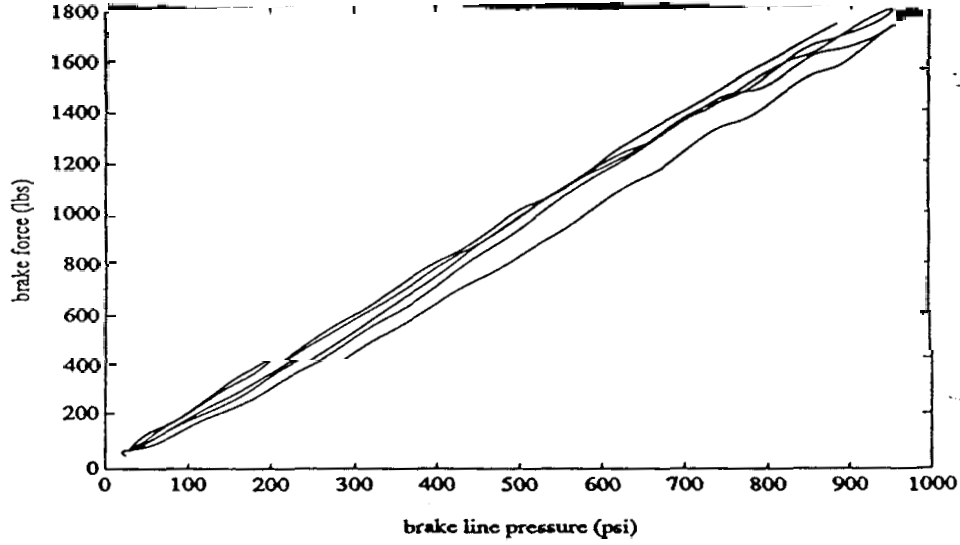


Figure 9: Filtered brake force vs brake line pressure **from** experiment

According to references [1, 2], the tire brake model is described by

$$\begin{aligned}
 \mathbf{V} &= F/M \\
 \dot{\Omega} &= (-T_b + rF)/J \\
 F &= d \sin(c \tan^{-1}(b\phi)) \\
 \phi &= (1 - e)S_l + (e/b) \tan^{-1}(bS_l)
 \end{aligned} \tag{3}$$

where T_b is the brake torque, M is the **mass** of the vehicle, and J is the rotational inertia of the wheel. Since $S_l = 1 - r\Omega/V$, we have that

$$\dot{S}_l = \frac{r}{V} [(rF - T_b)/J - F(1 - S_l)/(\tau M)]. \tag{4}$$

As shown in Figure 7, when S_l is small, $F \approx KS_l$. Thus

$$\dot{S}_l = -\frac{r}{V} [(\frac{r}{J} - 1/(\tau M))KS_l + KS_l^2/\tau M - T_b/J]. \tag{5}$$

We rewrite the above equation as

$$\dot{S}_l = -\frac{r}{V} [(\frac{r}{J} - \frac{1}{\tau M} + \frac{S_l}{\tau M})KS_l - \frac{T_b}{J}]. \tag{6}$$

Since M is large, the above equation may be approximated as

$$\dot{S}_l \approx -\frac{r^2}{VJ}KS_l + \frac{r}{VJ}T_b. \tag{7}$$

From $K S_l = F = M V$, we have that

$$K = M \dot{V} / S_l. \quad (8)$$

After processing the experimental data, we find that

$$\dot{V} / S_l > 3g \quad (9)$$

for small slip index, where g is the acceleration due to gravity, which implies that $K > 3Mg$. Let m be the mass of the rotational part connected to the wheel. Then $J < m r^2$. Since $M/m \gg 10$, we have $\frac{r^2}{J} K \gg 10$. This means that S_l changes quite fast. On the other hand, the vehicle speed V changes relatively slowly. We may therefore assume that V is almost constant relative to S_l . Thus, by assuming V constant in (7), it follows that for constant input T_b , S_l will reach the steady state value $T_b/(rK)$ very fast. Since any continuous function can be approximated by a series of step functions, then for any input T_b , we have that

$$S_l \approx T_b / (K r). \quad (10)$$

Since $F \propto K S_l$ when S_l is small, and T_b is proportional to P , it follows from (10) that

$$F \approx \alpha P \quad (11)$$

for some constant α . Note that K depends on the characteristics of the road surface. The more slippery the road is, the smaller the value of K is. Equation (10) tells us that for the same brake line pressure, a slippery road will produce a larger slip index, which agrees with intuition. However, since $F \approx K S_l$, the brake force is almost independent of the road condition when the slip index is small or when the brake line pressure is small.

Using (11) and Newton's second law of motion, the tire brake model is

$$F = M \dot{V}$$

which implies

$$V \approx \alpha P / M. \quad (12)$$

We must emphasize that this approximate model is valid only when the slip index is small. This condition can be satisfied by limiting the brake line pressure to a certain range. Also the anti-lock brake system will help to prevent the slip index becoming too large. The parameter α however changes as a function of the line pressure and road condition. Its value is found to be around 1.6.

4 Further Comments and Observations

1. The system shown in Figure 2 that is used to generate the line pressure consists of a feedback loop and some dynamics. These dynamics are responsible for the steady state small oscillations in the line pressure response shown in the Figures in the Appendix. It is not clear to what extent these oscillations are contributing to the oscillations that appear in the response for the brake force and vehicle and wheel speed.
2. The step response of the brake force shows some overshoot indicating the possibility of some unknown dynamics between the line pressure and brake force. However, the presence of occasional overshoots of comparable size at steady state (see Figure A.3) indicates that these overshoots may be due to noise introduced by the road characteristics. The consistency of the overshoots however suggests that further analysis is required in order to understand their cause. For this we need more details about the properties of the sensor and its dynamics and additional tests need to be performed. It is possible that the overshoots are due to sensor dynamics.

Acknowledgments

We would like to thank Dr. Steve Eckert of Ford Motor Co. for performing the brake experiments and supplying us with the data and for taking the time to visit us at USC and help us with discussions on brake and vehicle dynamics.

References

- [1] Egbert Bakker, Lars Nyborg, and Hans B. Pacejka. Tyre Modelling for Use in Vehicle Dynamics Studies. SAE **870421**, pages **1-14**.
- [2] Egbert Bakker, Hans B. Pacejka, and Lars Lidner. A New Tire Model with an Application in Vehicle Dynamic Studies. SAE **890097**, pages **83-91**.
- [3] A. Van Zanten, et al. Measurement and Simulation of Transient Tire Forces. SAE **890640**.
- [4] A. Van Zanten, et al. Measurement and Simulation of Transients in Longitudinal and Lateral Tire Forces. SAE **900210**, pages **133-151**.

Appendix

Figures A.1 — A.14: The raw tested data for the experiments on the dry asphalt road.

Figures A.15 — A.28: The raw tested data for the experiments on the wet jennite road.

Figures A.29 — A.42: The filtered data for the experiments on the dry asphalt road.

Figures A.43 — A.46: The filtered data for the experiments on the wet jennite road.

Figure A.1

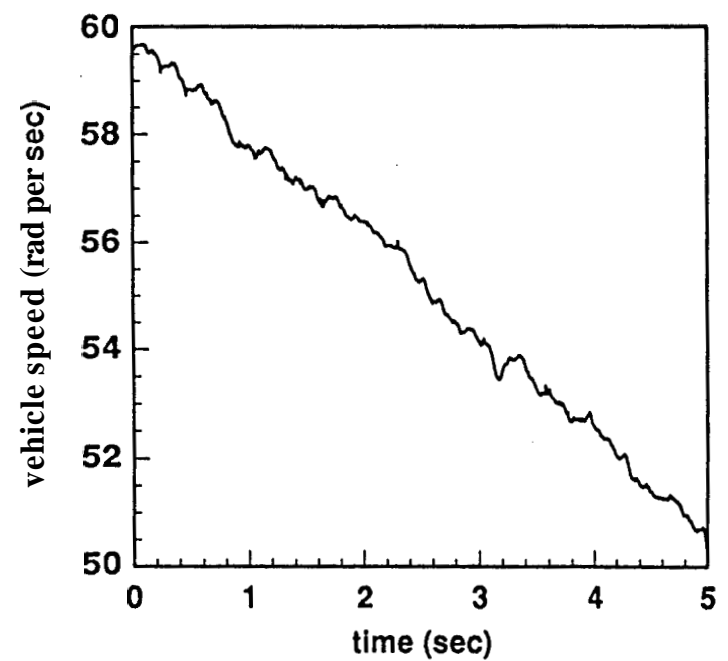
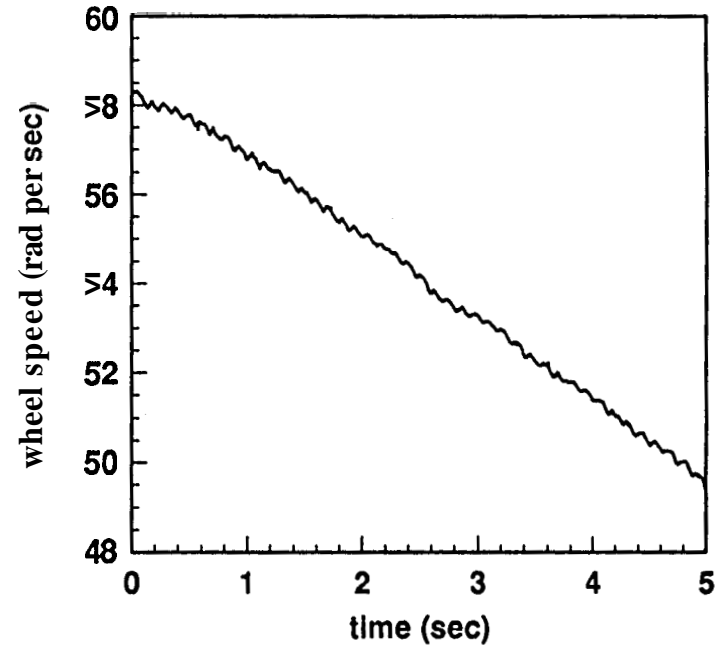
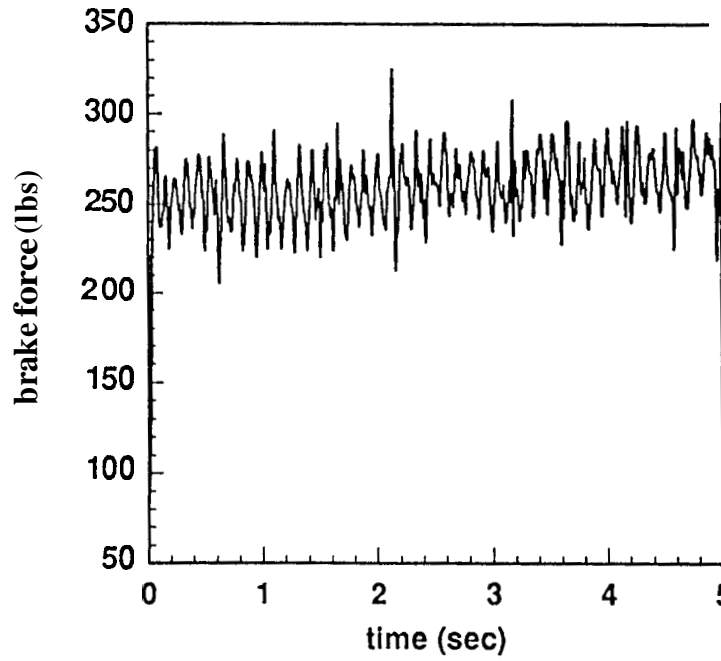
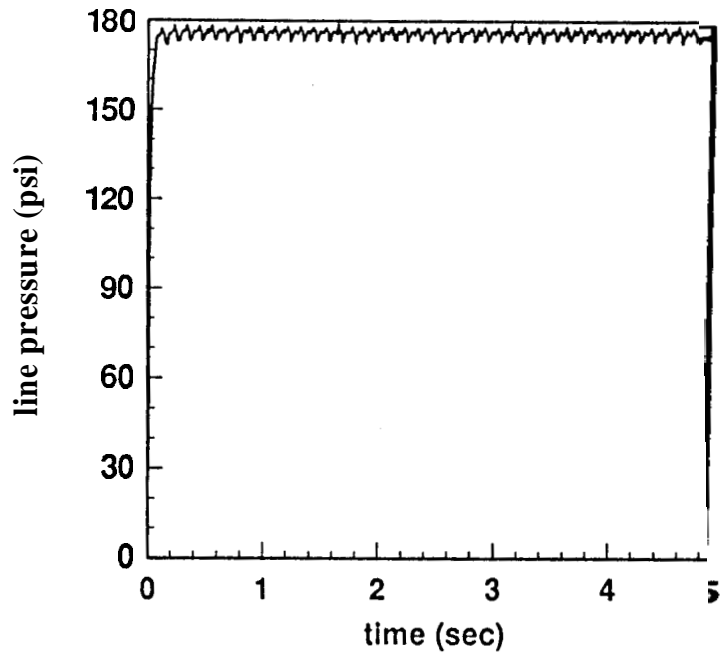


Figure A 2

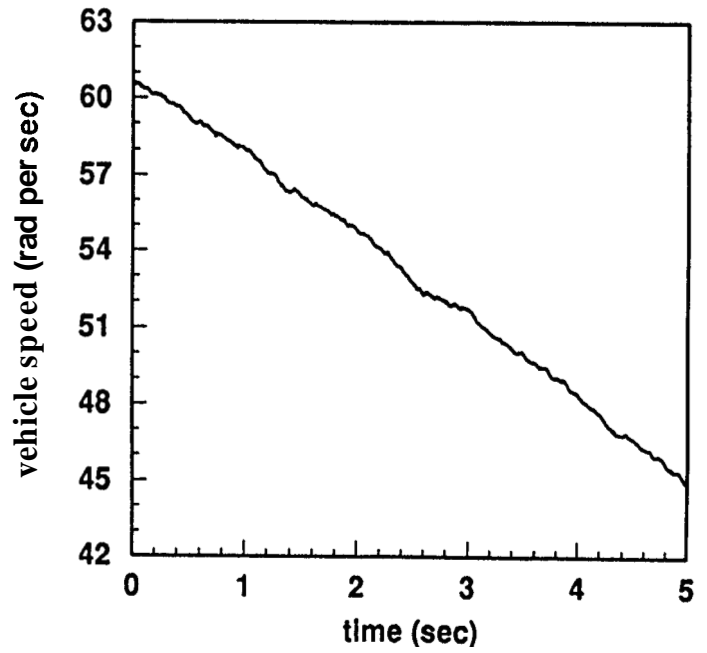
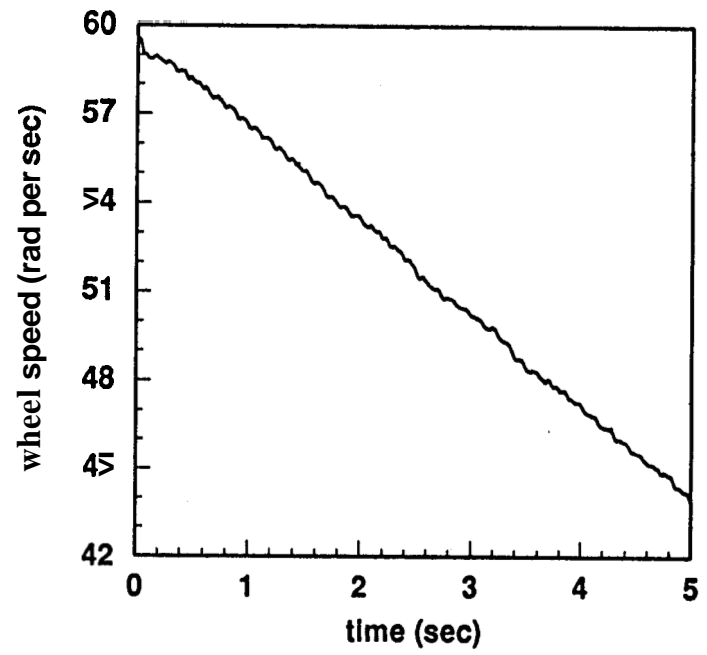
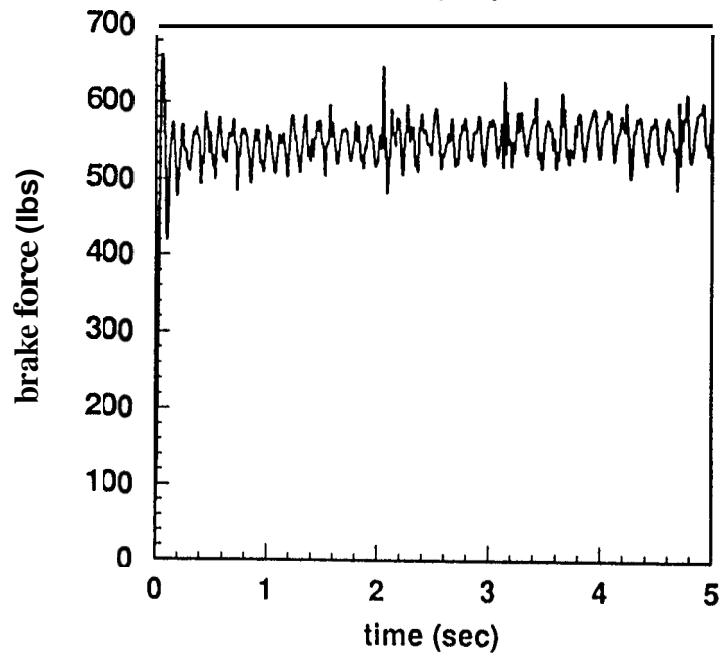
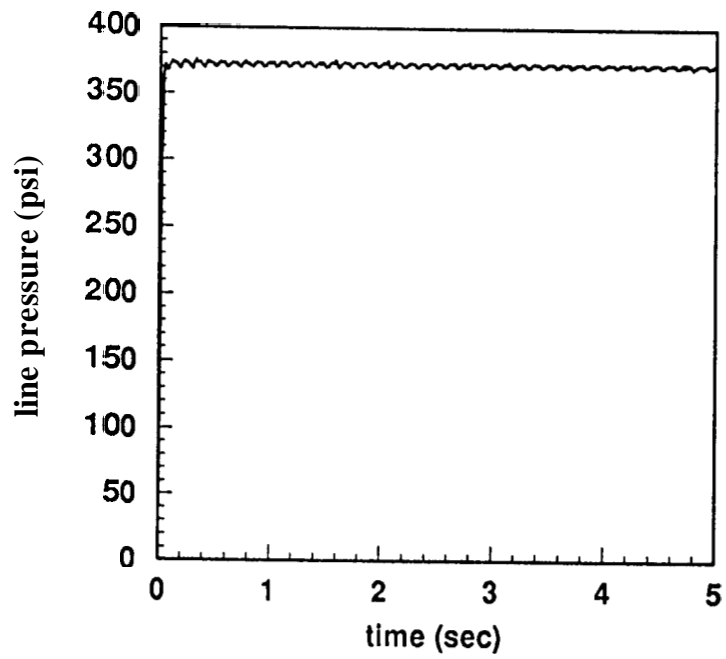


Figure A.3

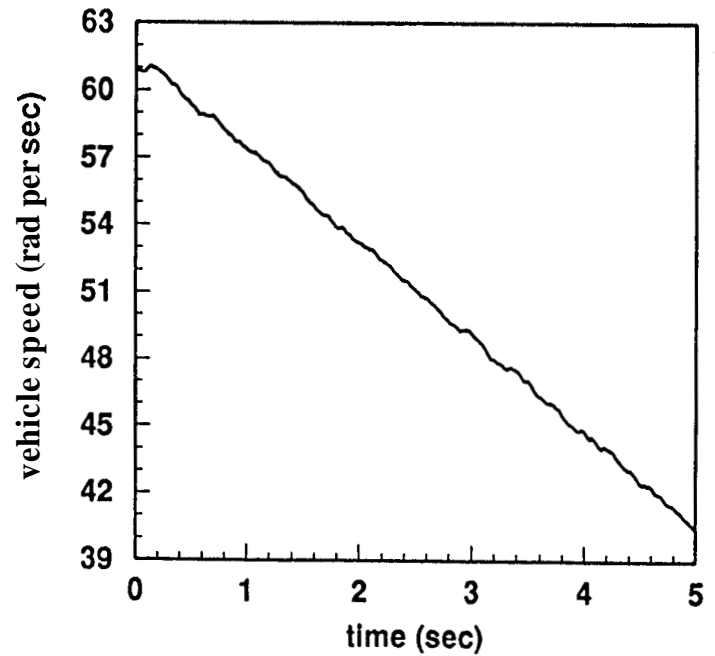
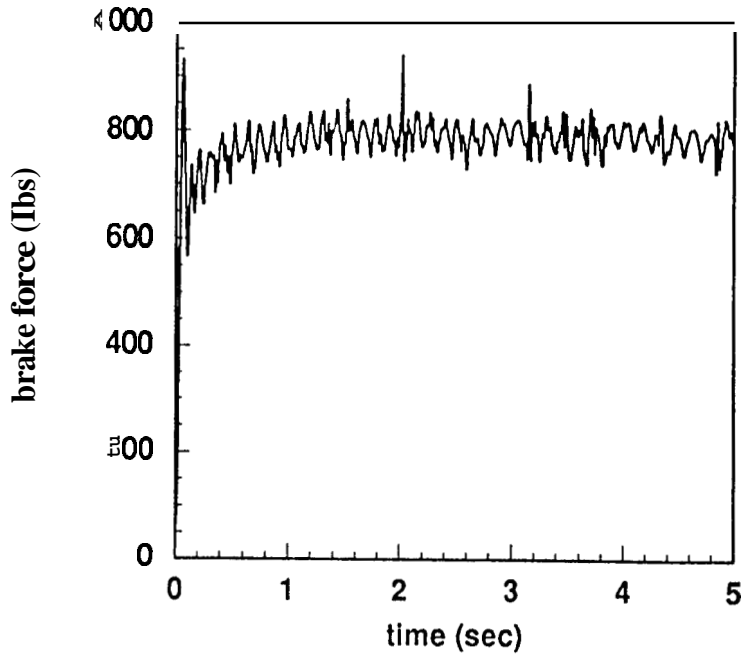
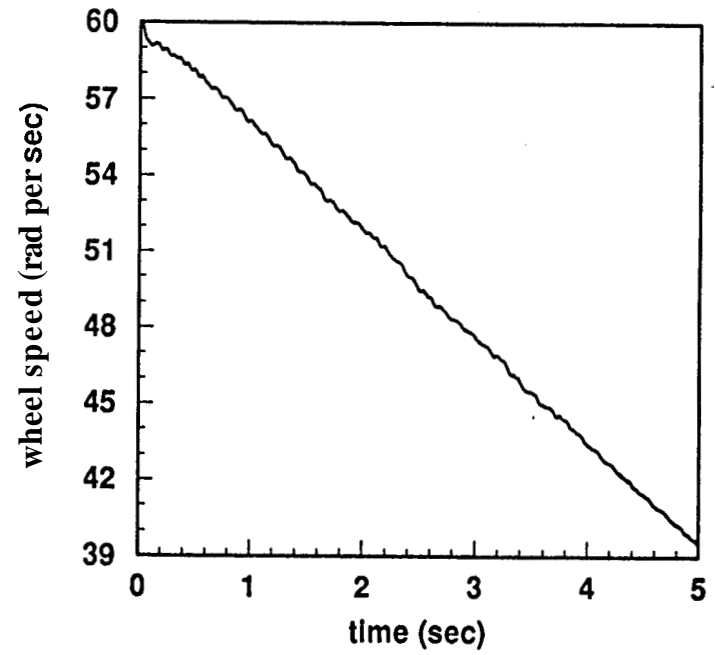
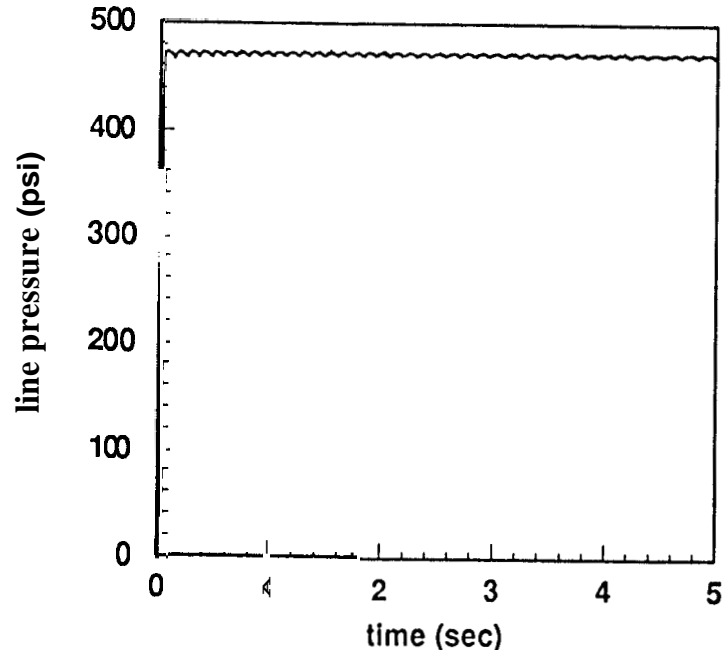


Figure A 4

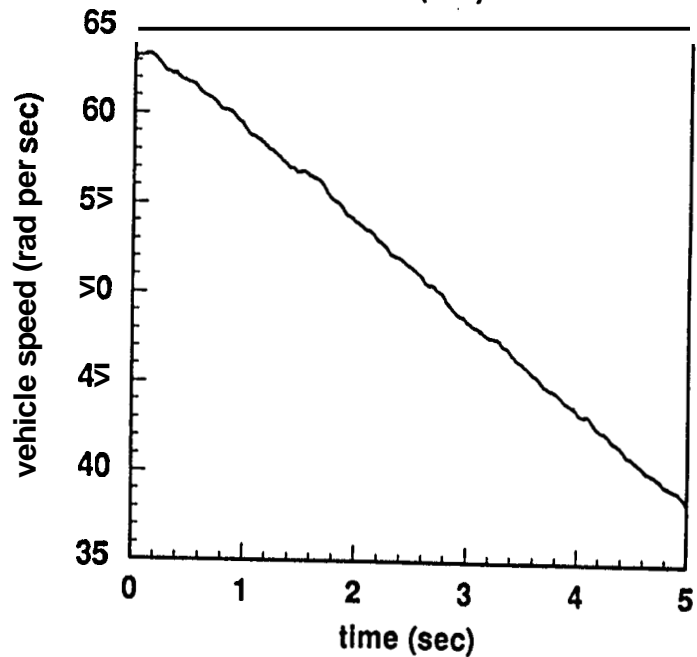
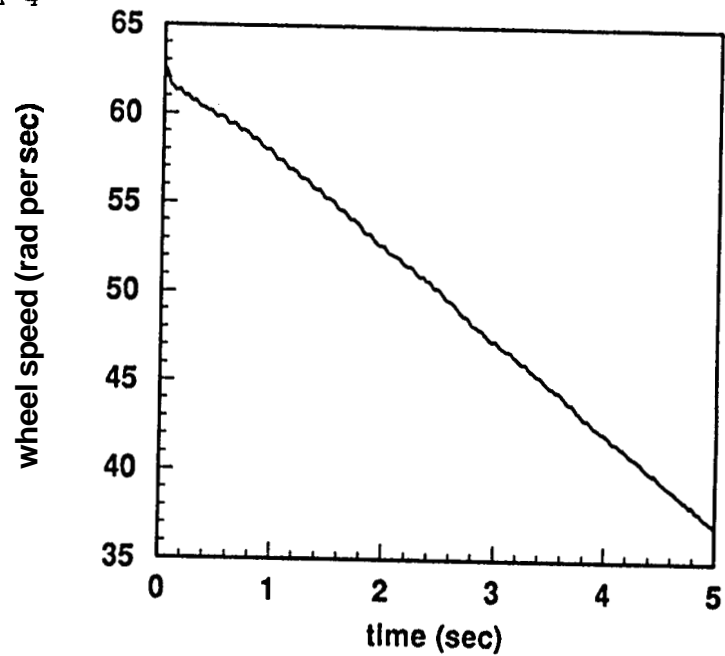
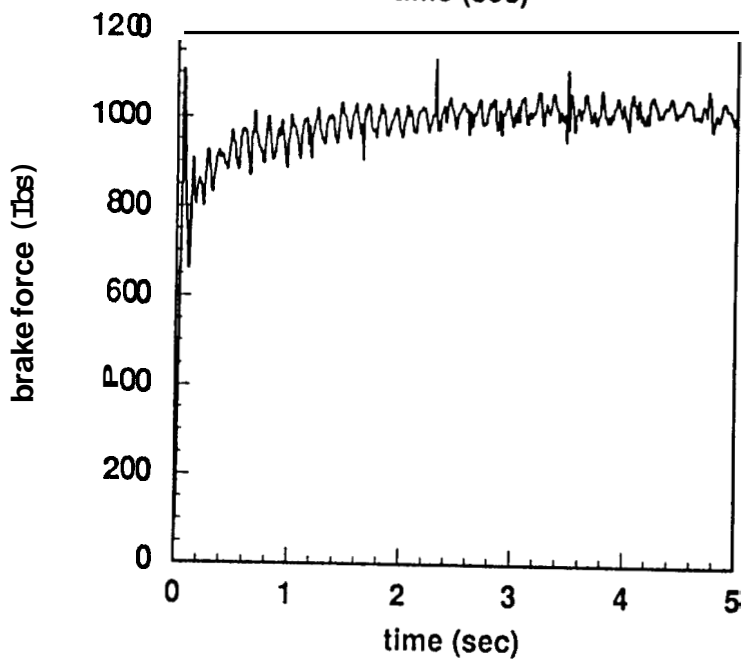
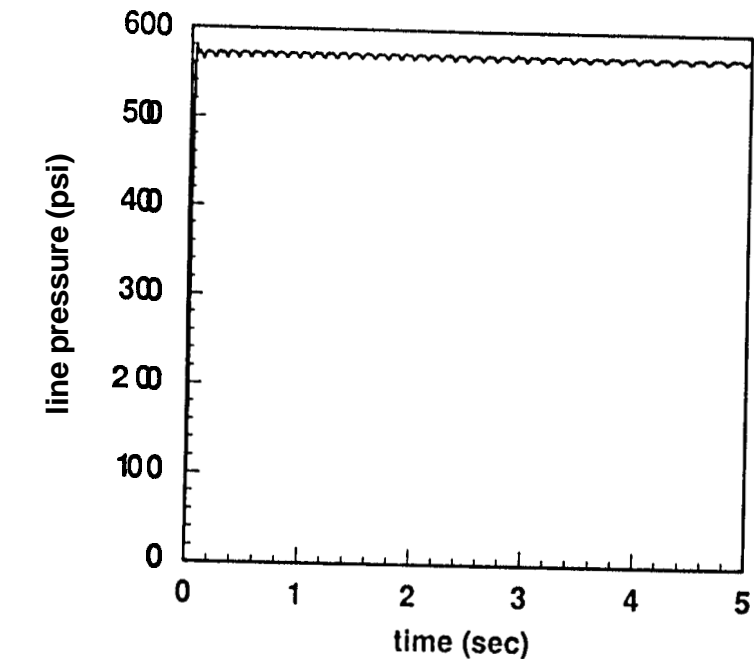


Figure A.5

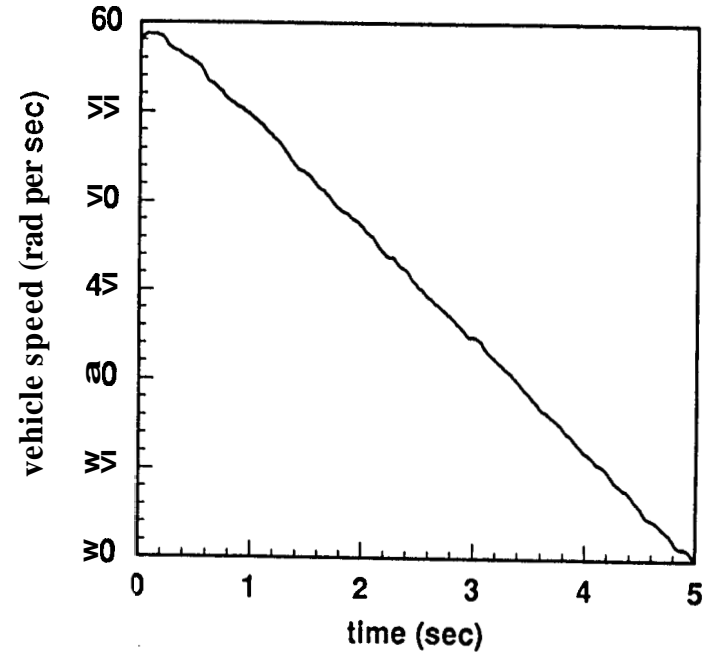
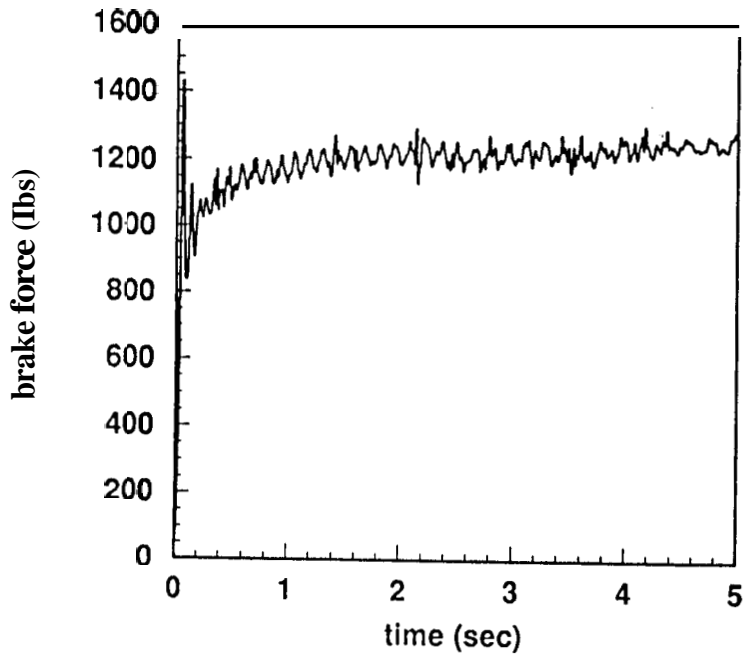
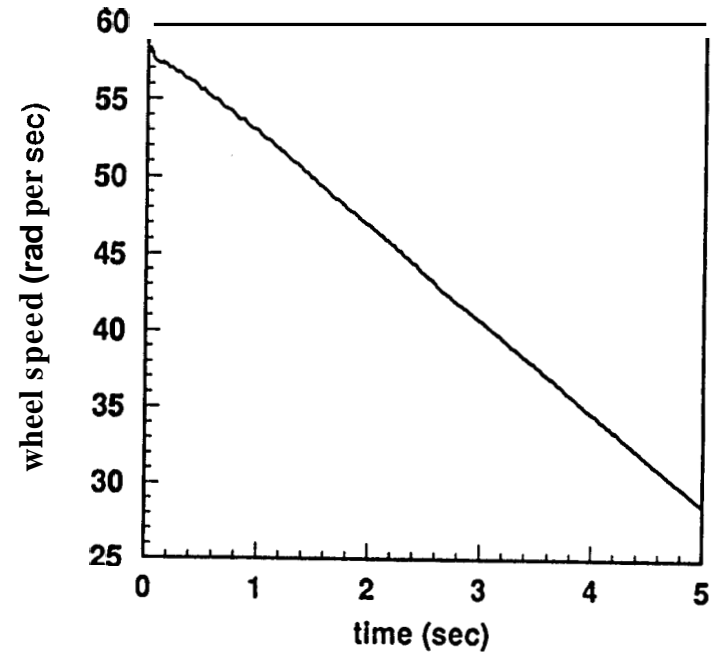
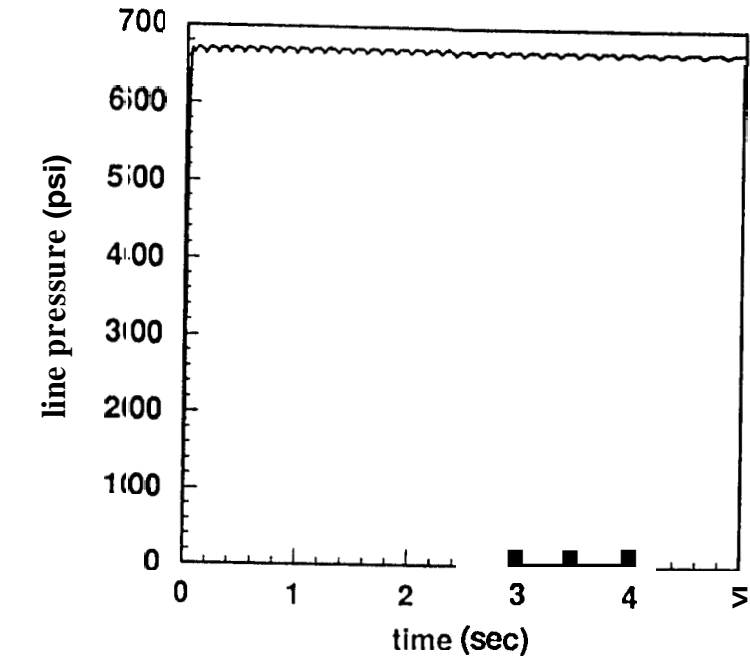


Figure A.6

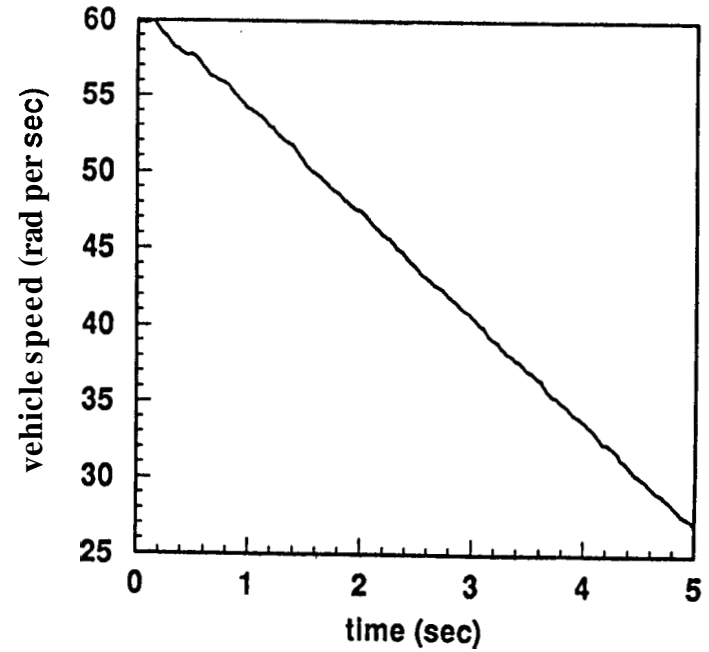
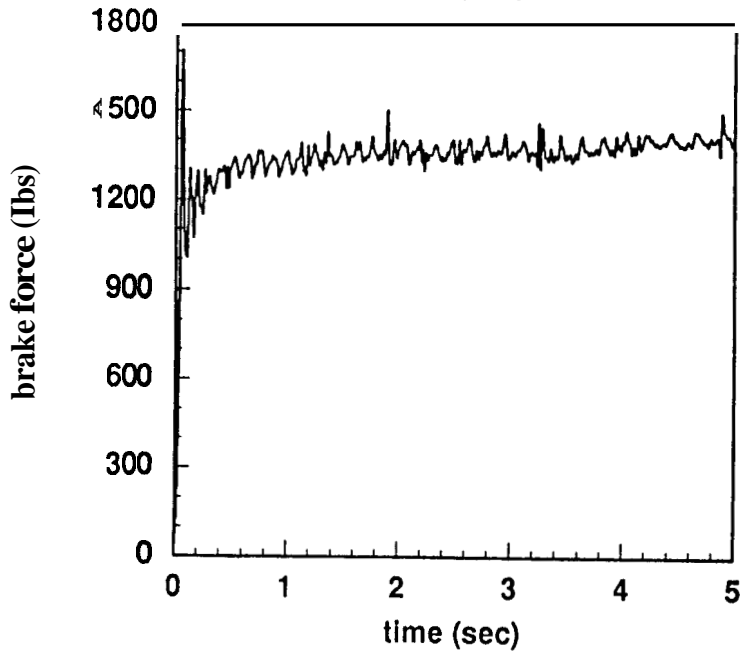
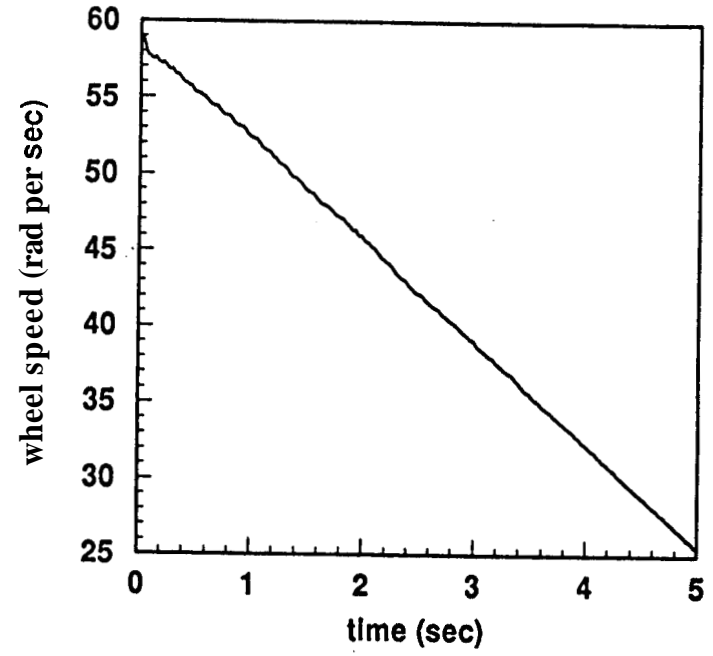
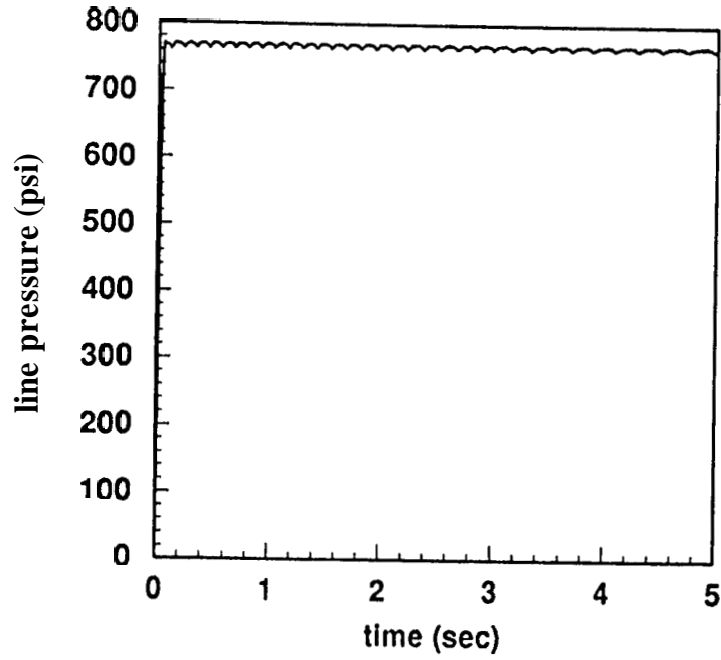


Figure A.7

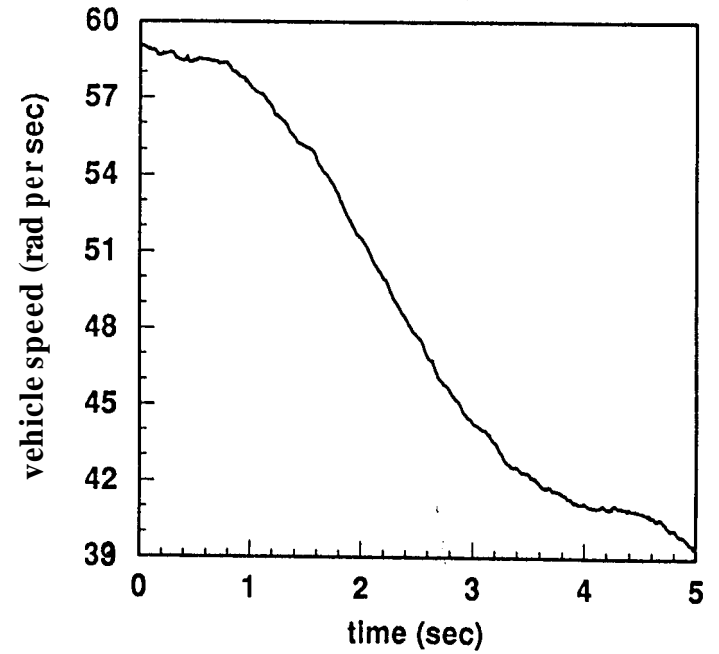
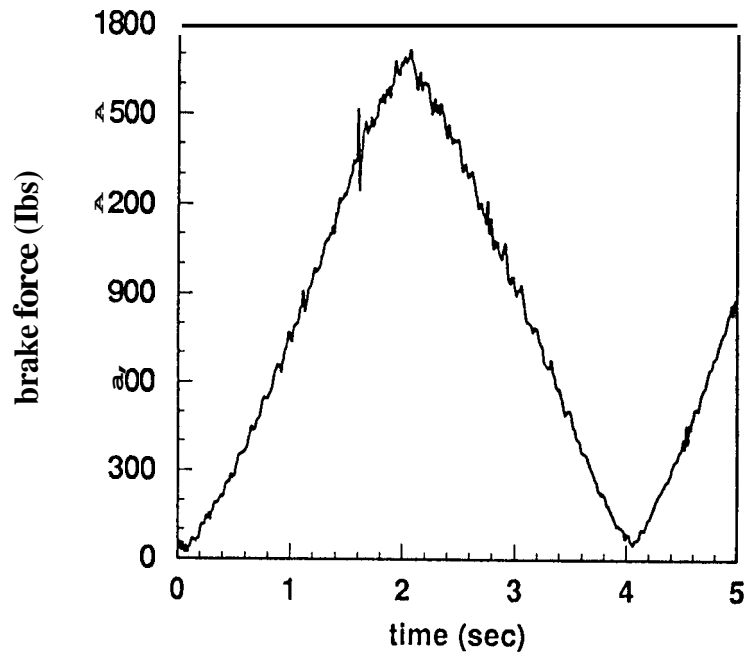
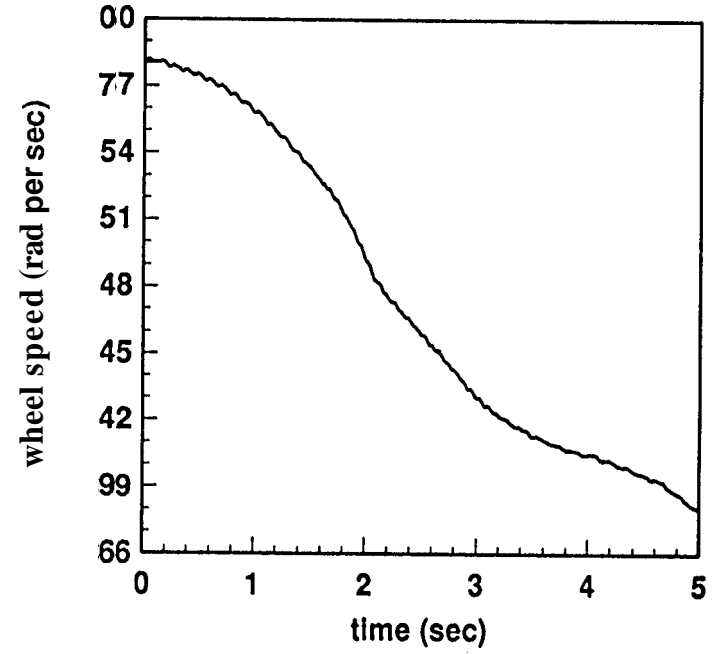
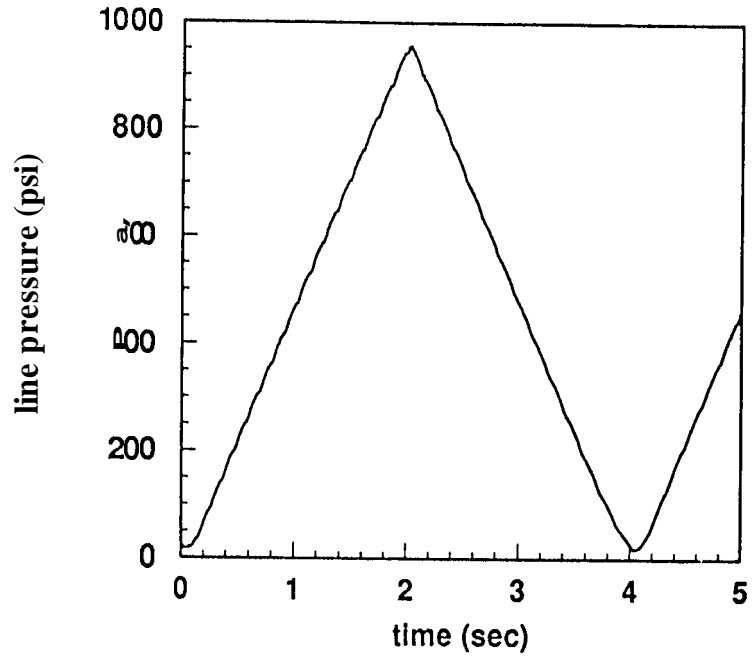


Figure A.8

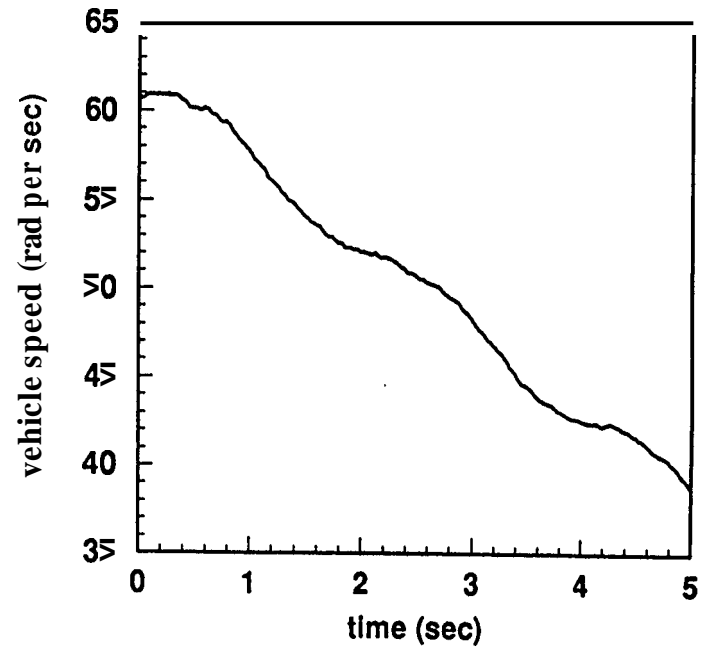
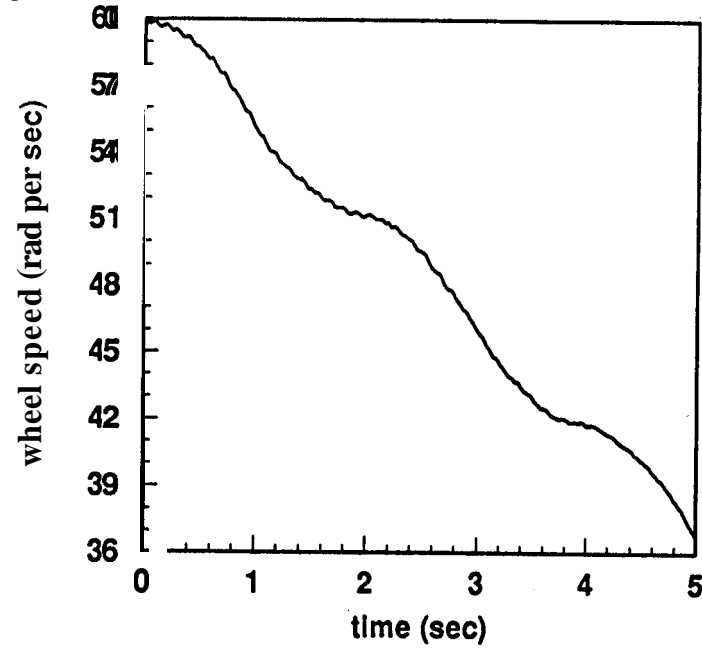
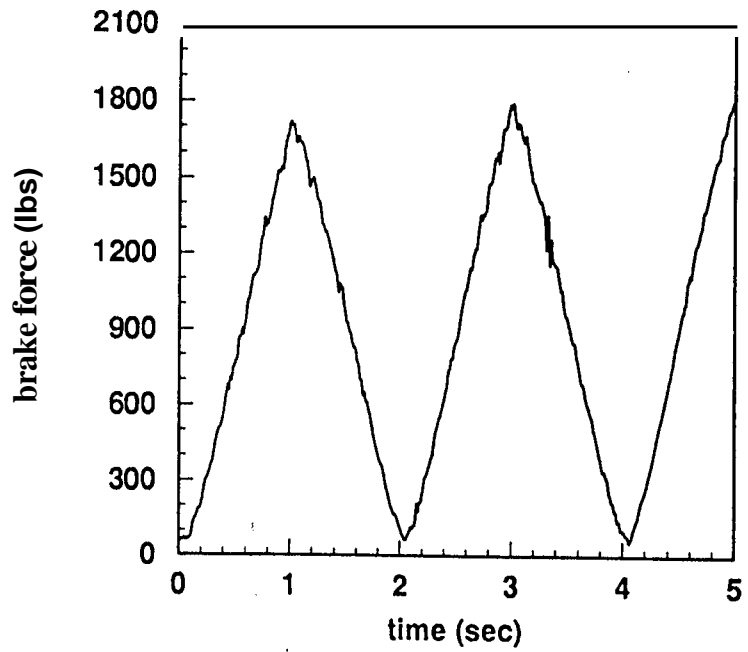
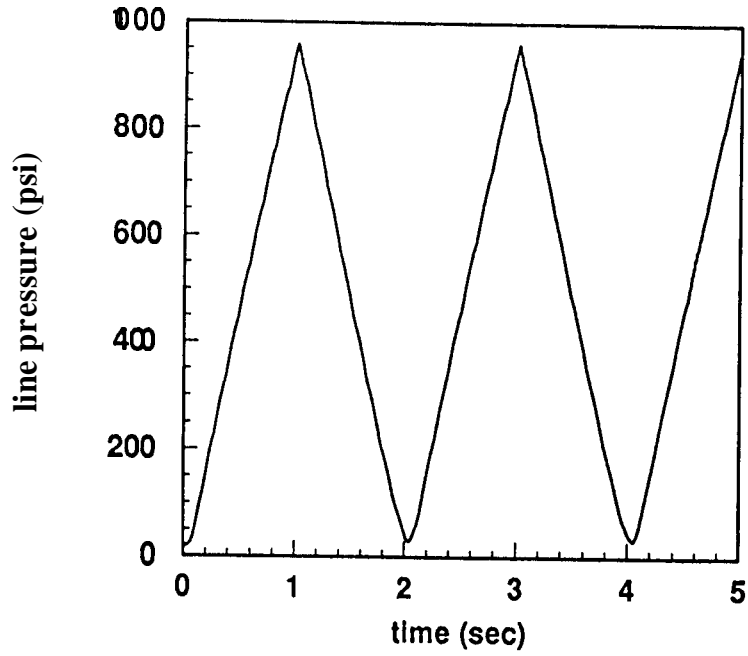


Figure A.9

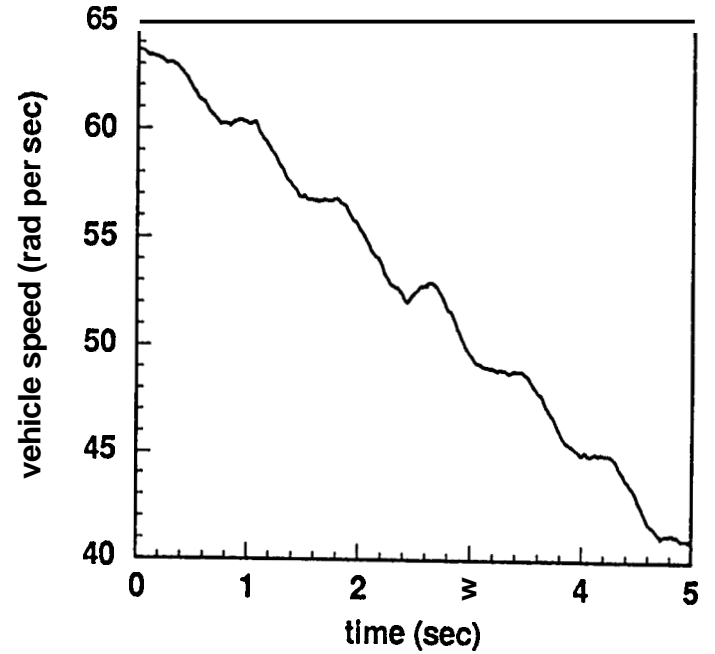
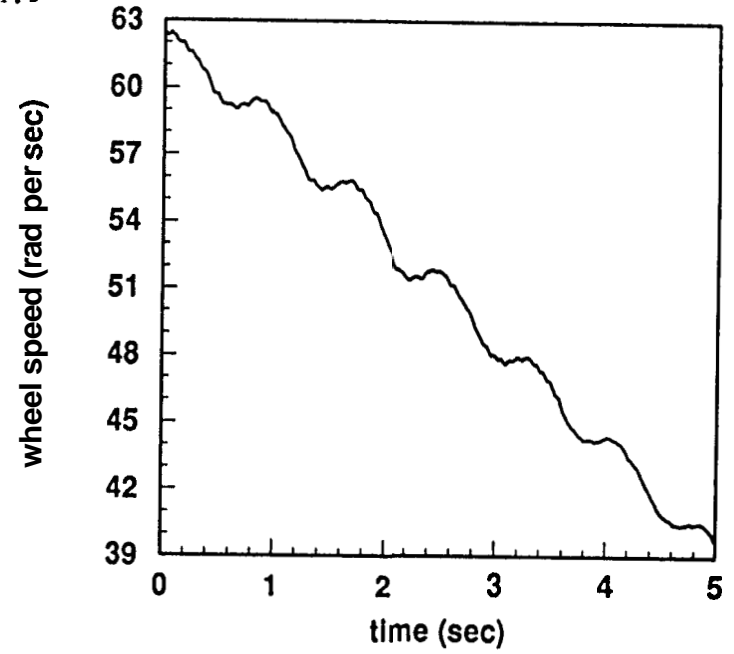
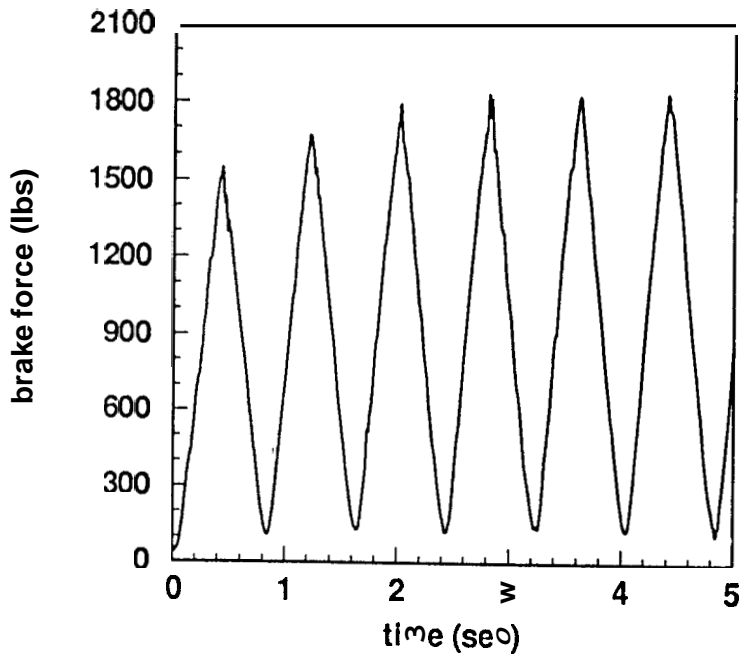
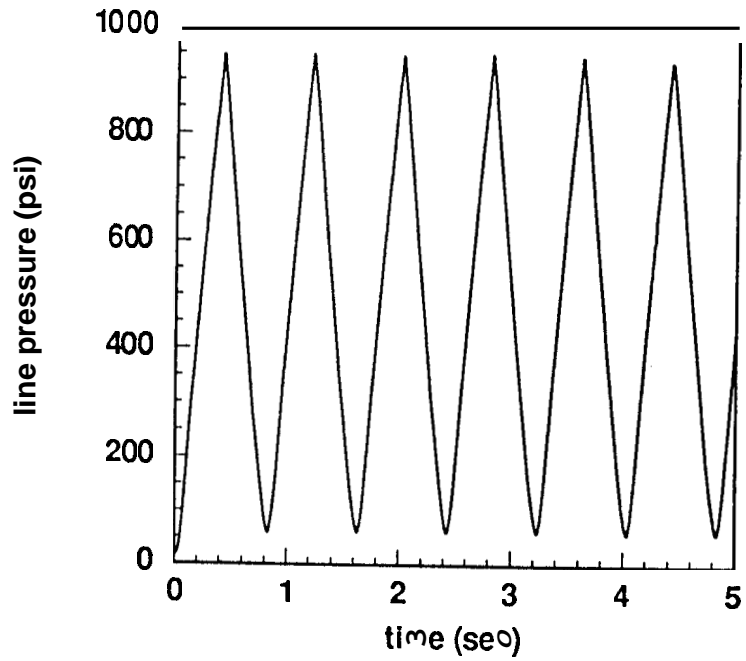


Figure A.10

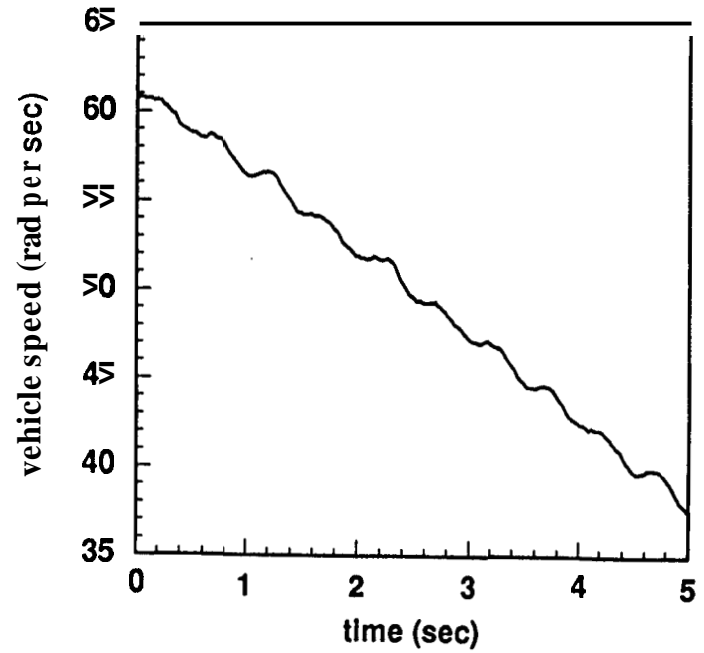
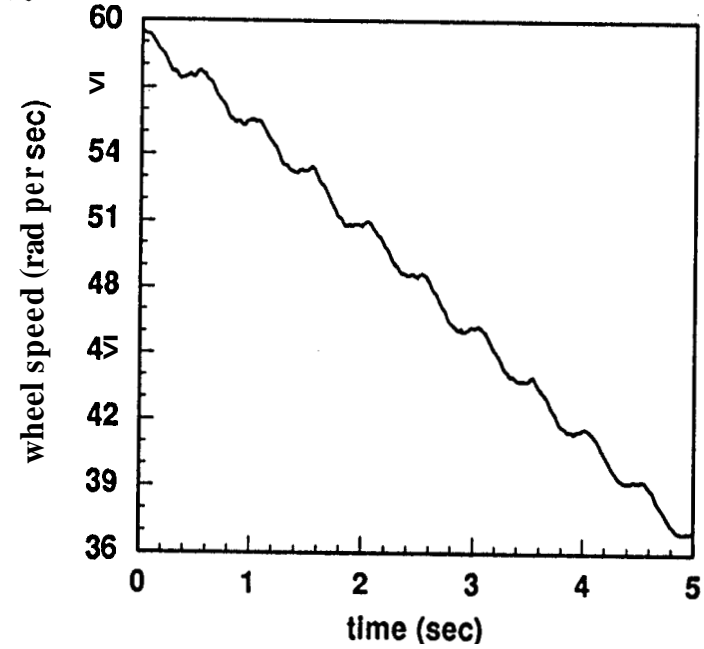
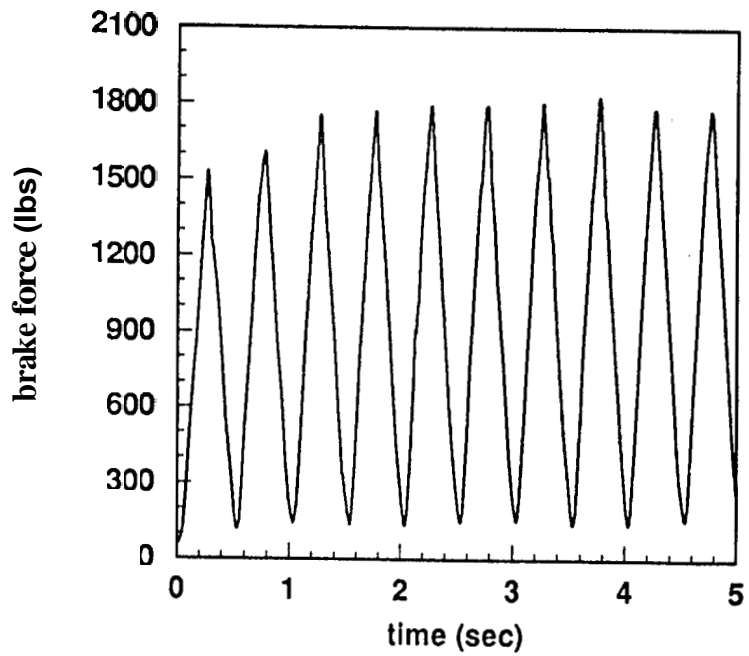
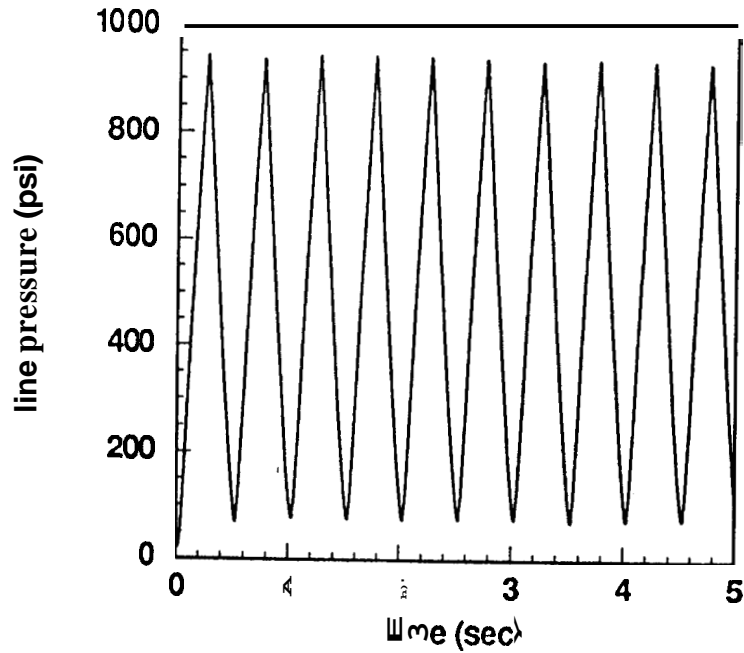


Figure A.11

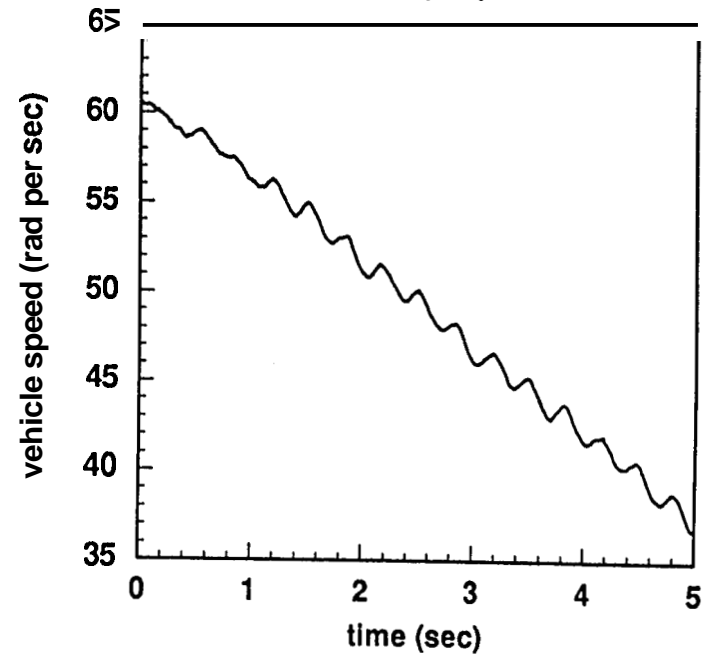
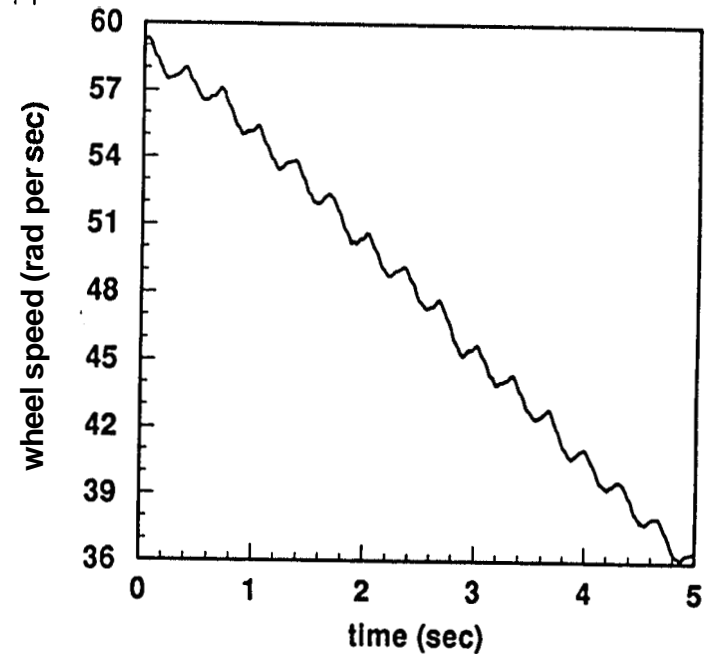
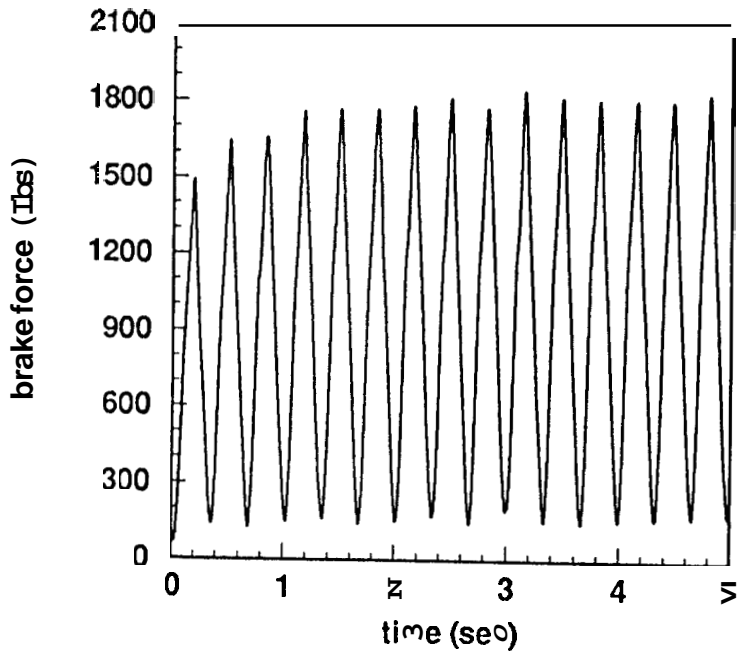
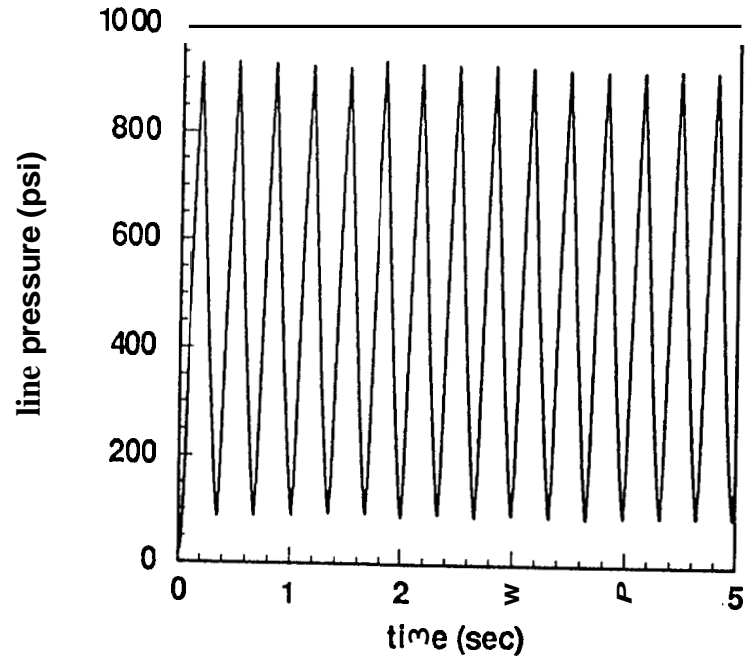


Figure A.12

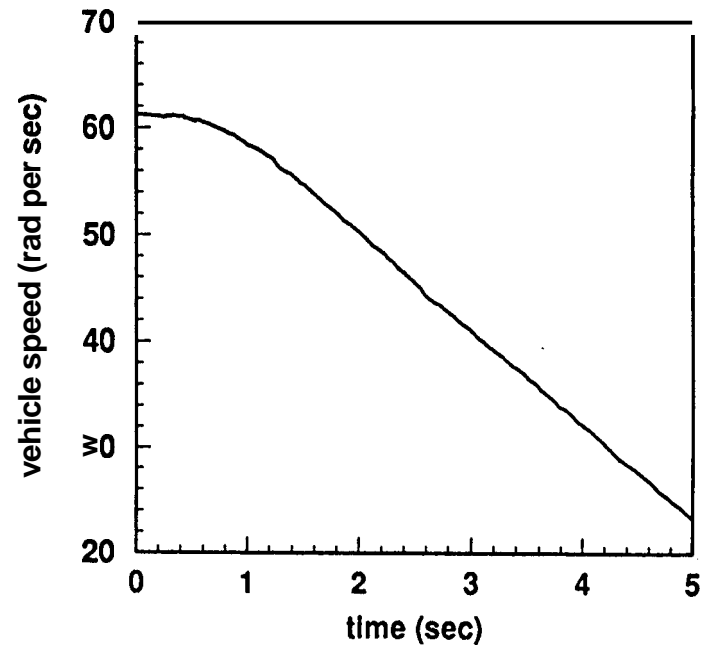
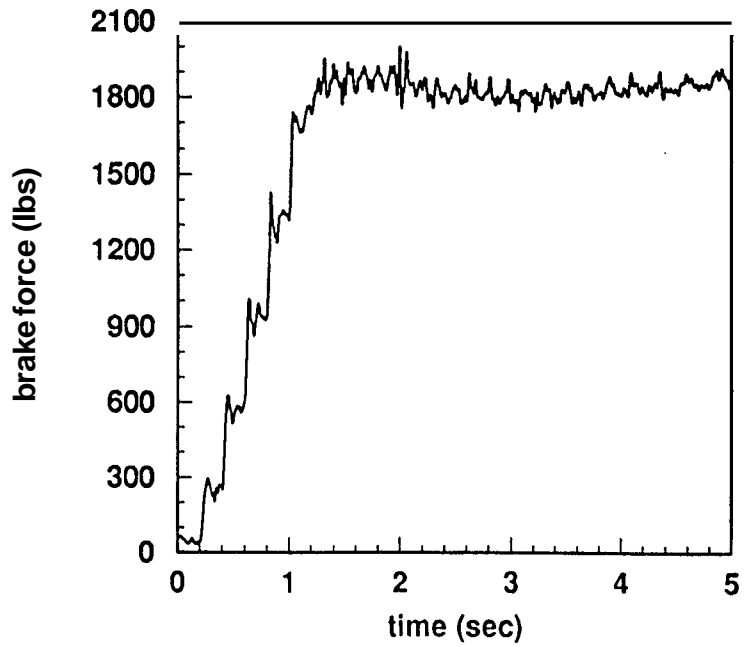
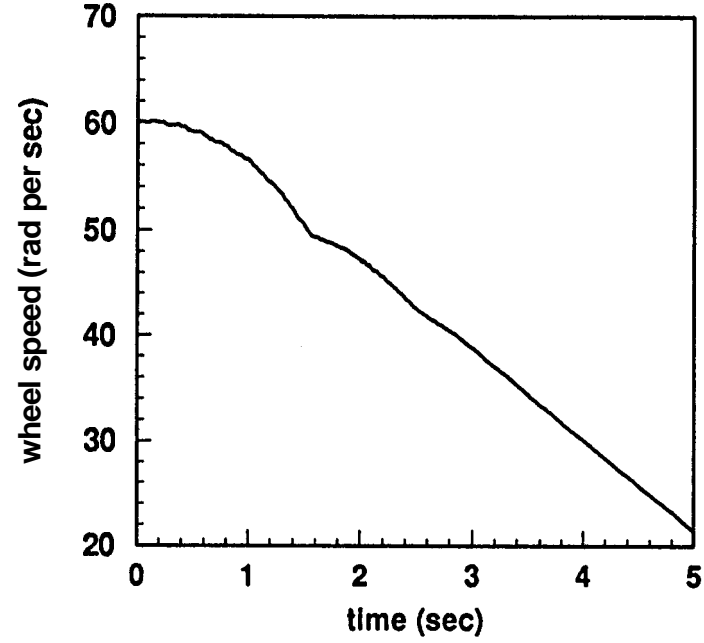
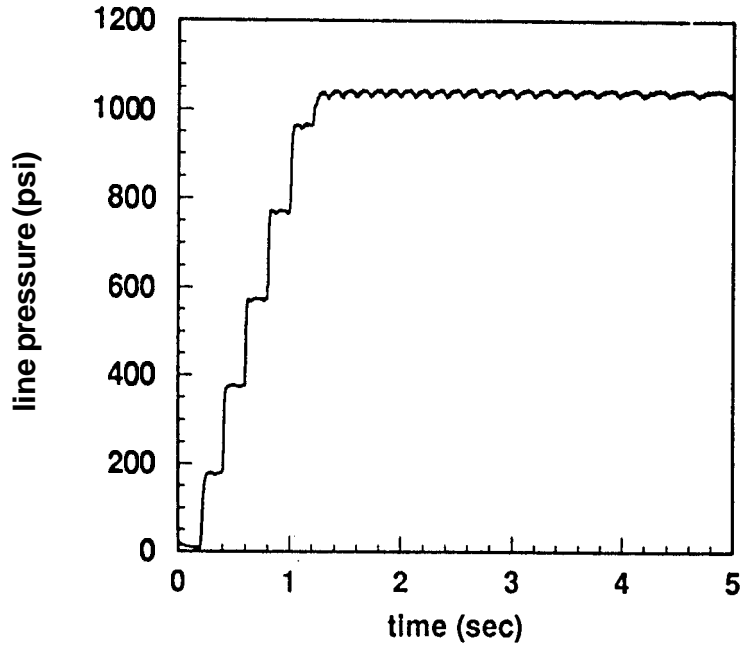


Figure A.13

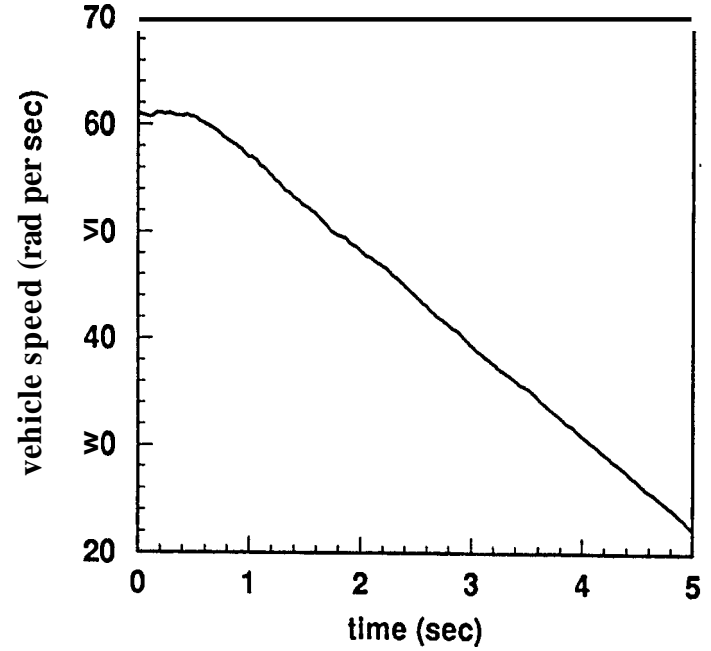
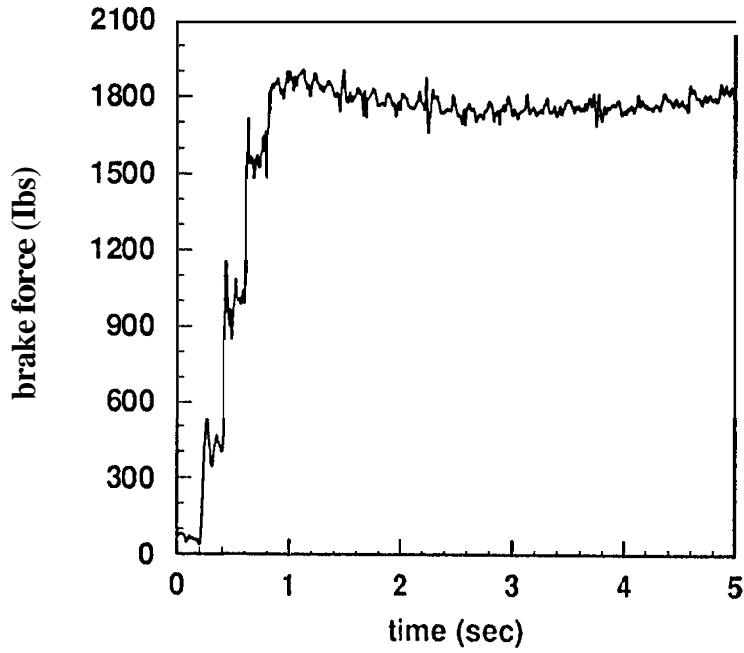
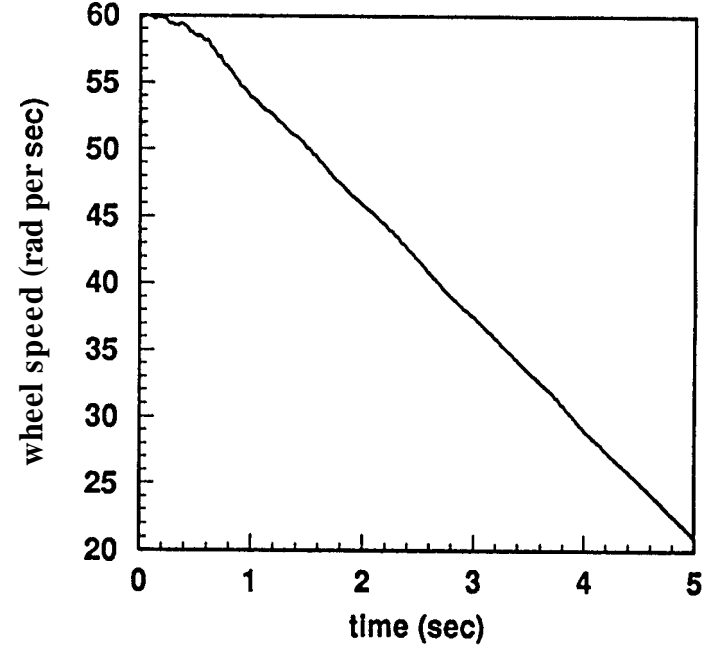
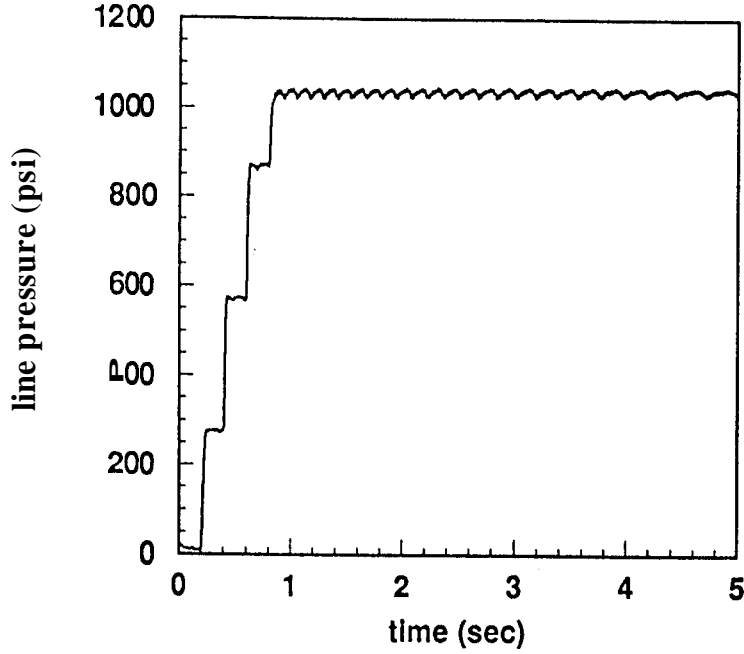


Figure A 14

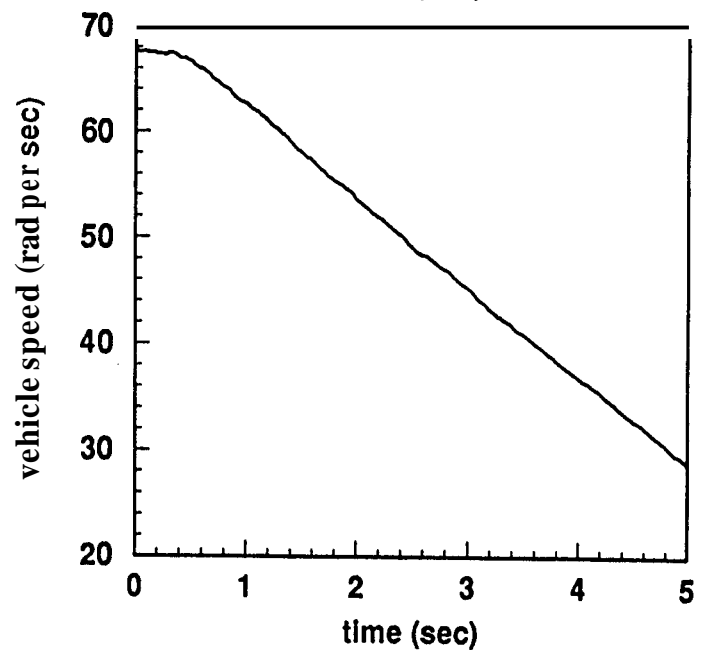
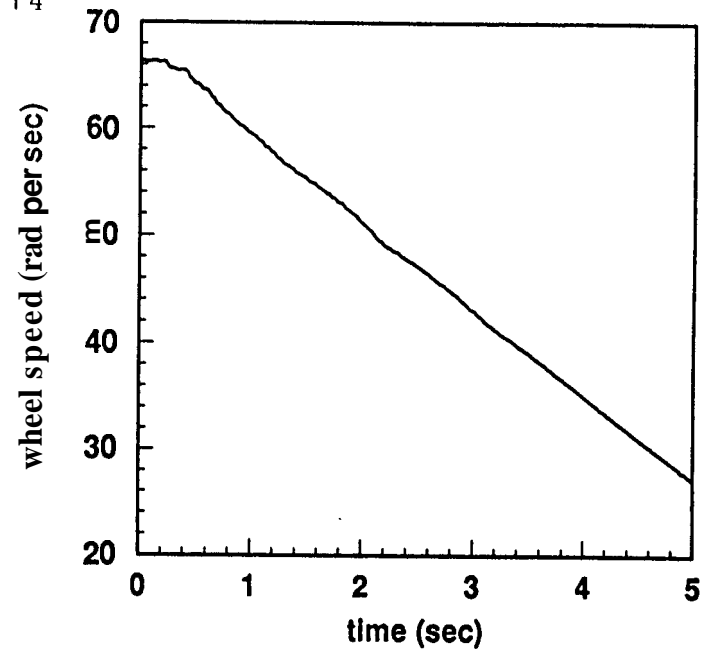
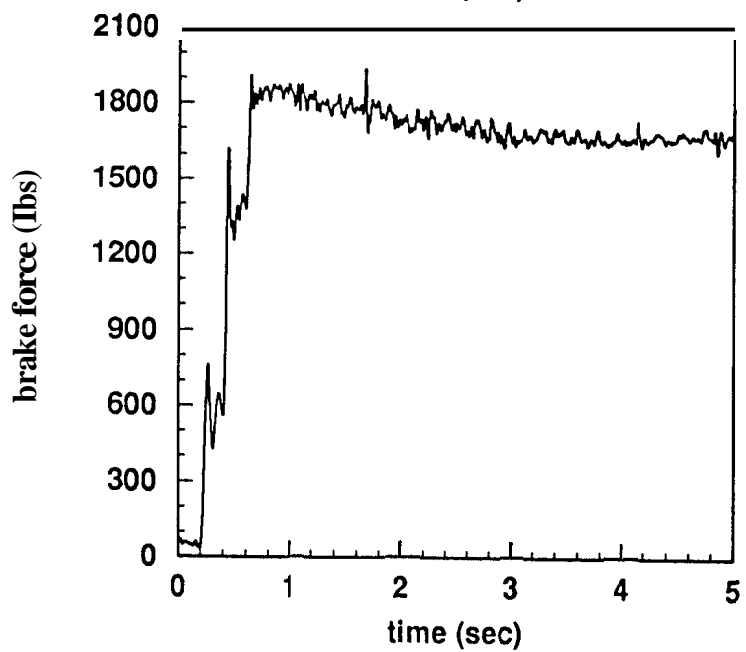
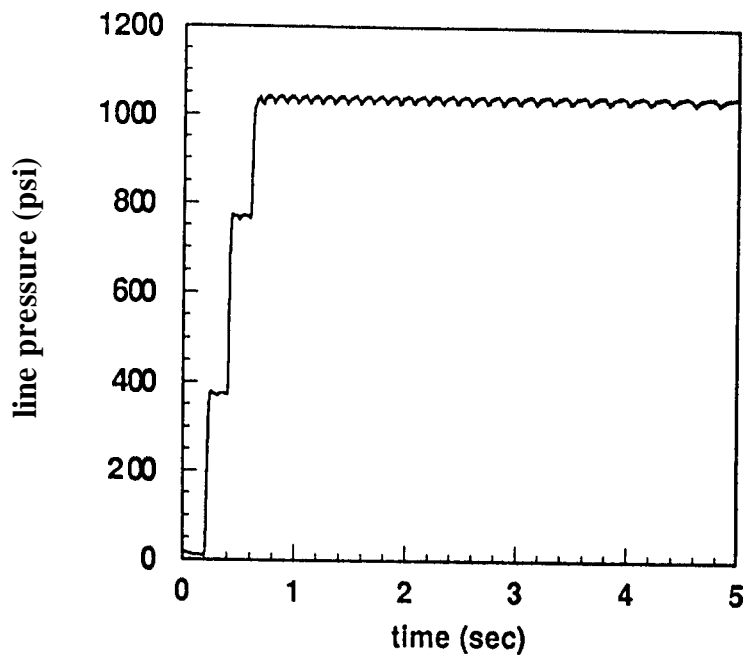


Figure A.15

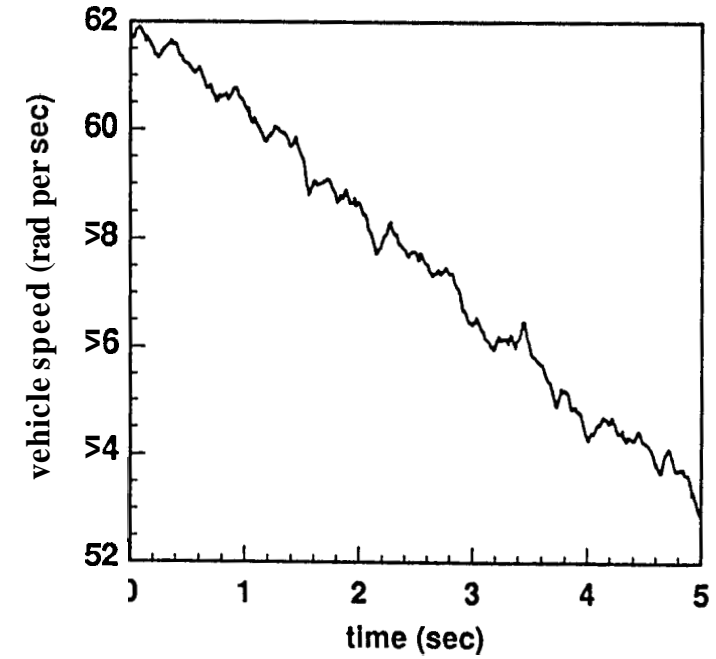
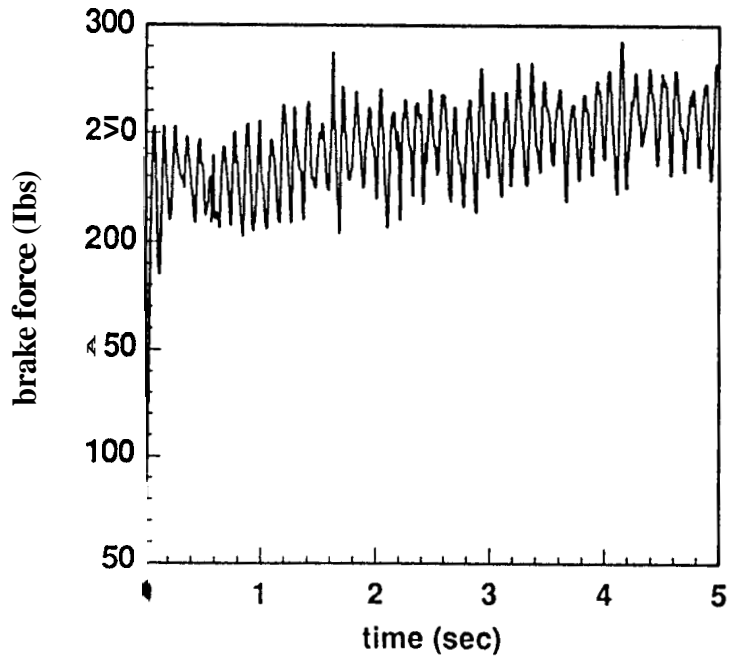
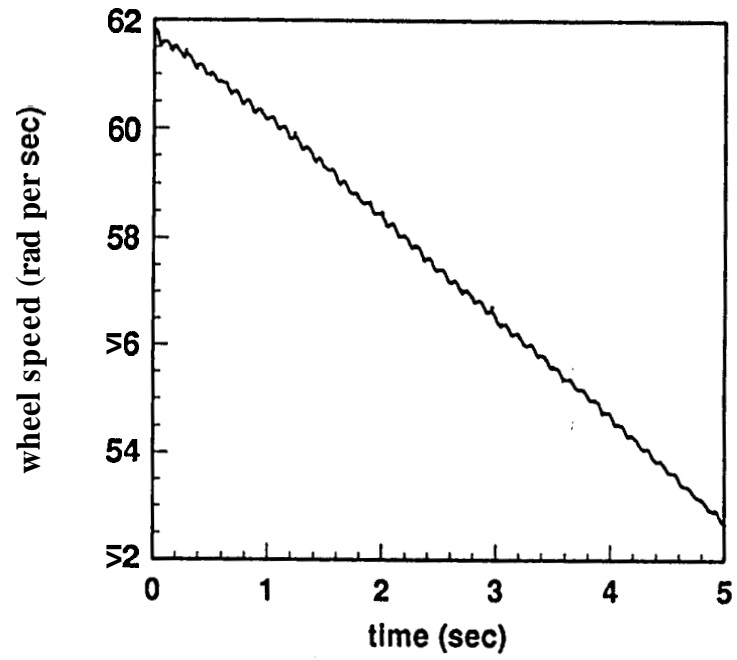
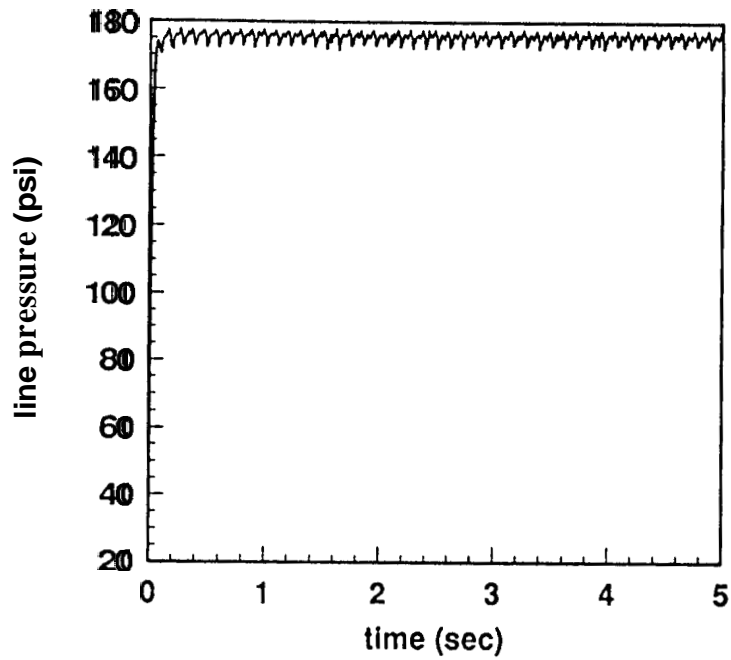


Figure A 1 6

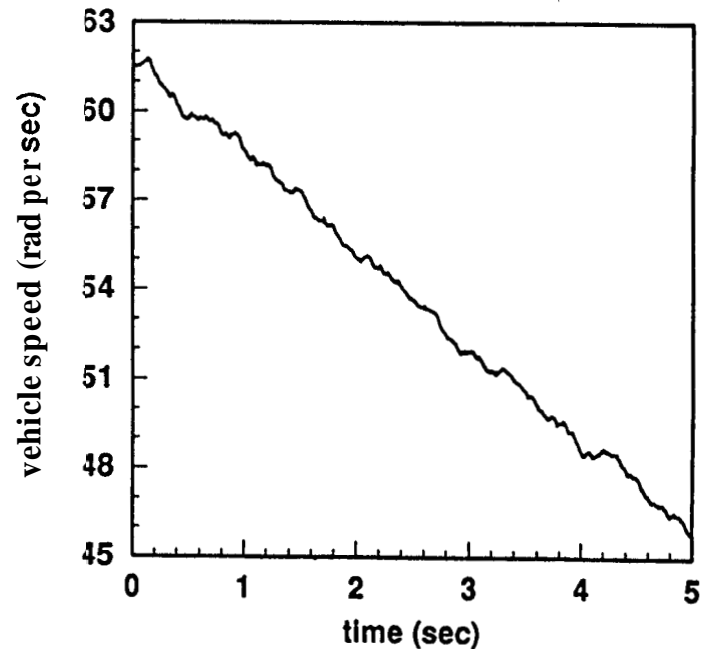
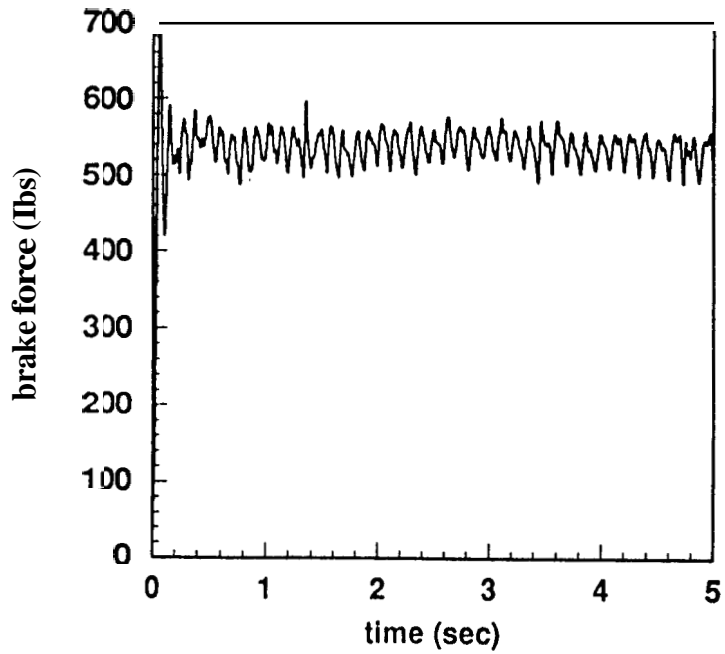
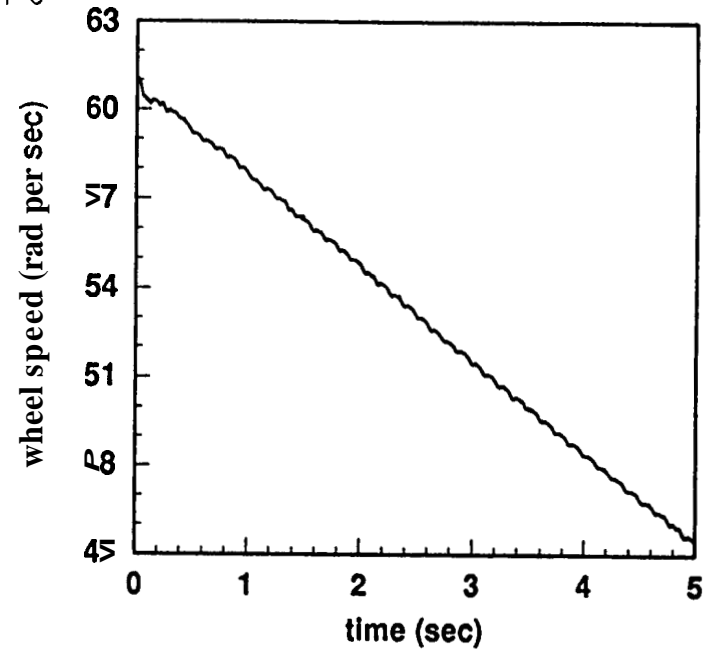
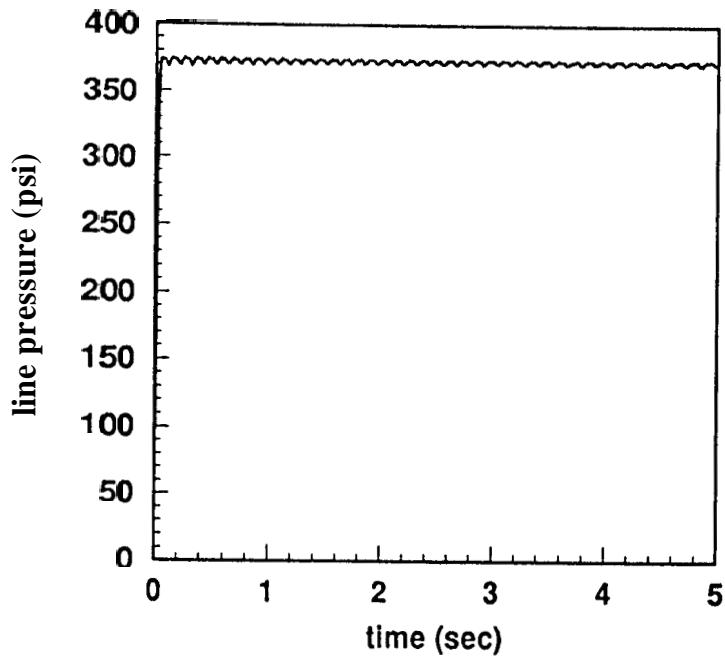


Figure A.17

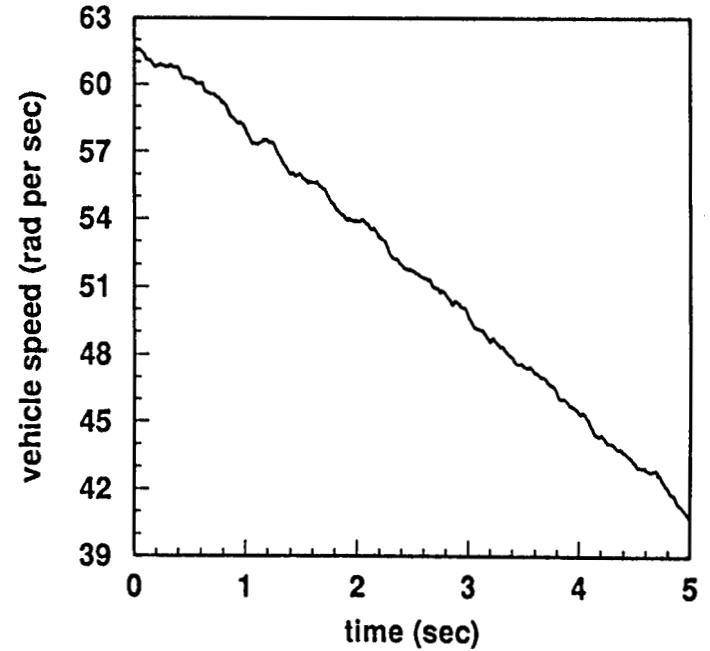
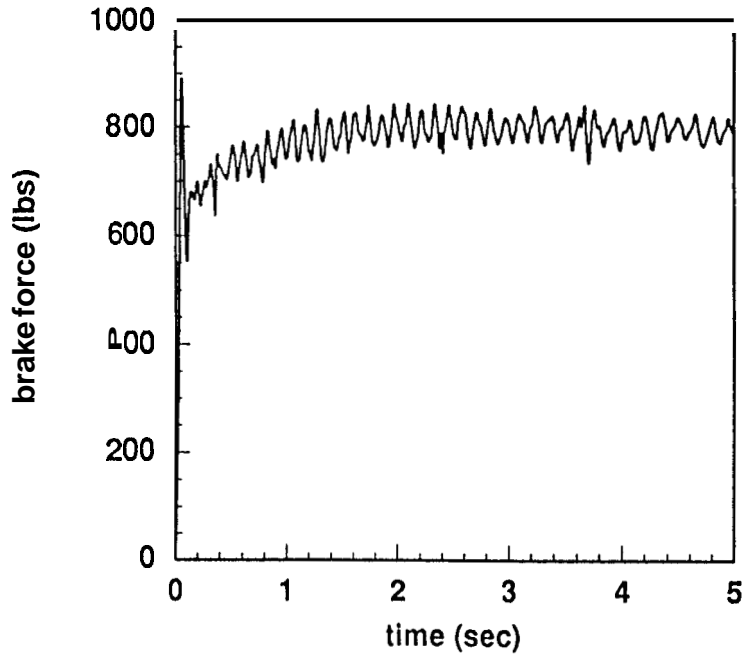
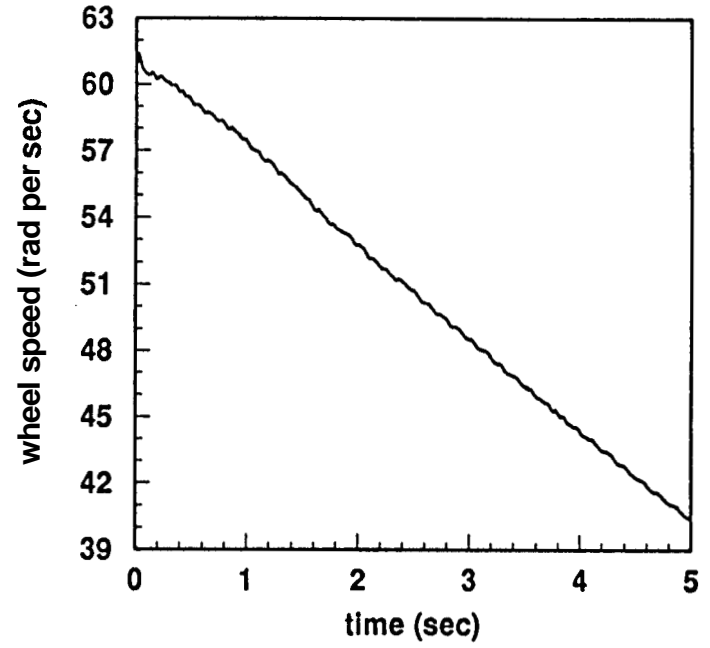
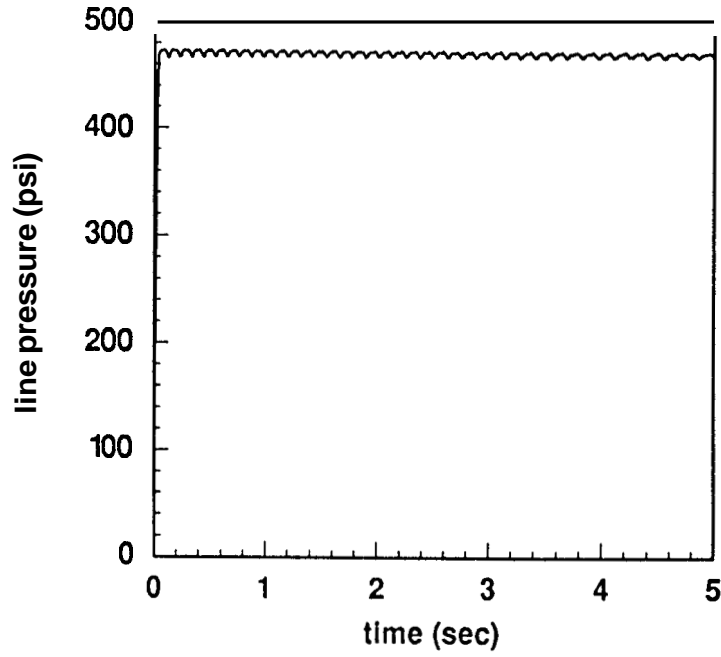


Figure A.18

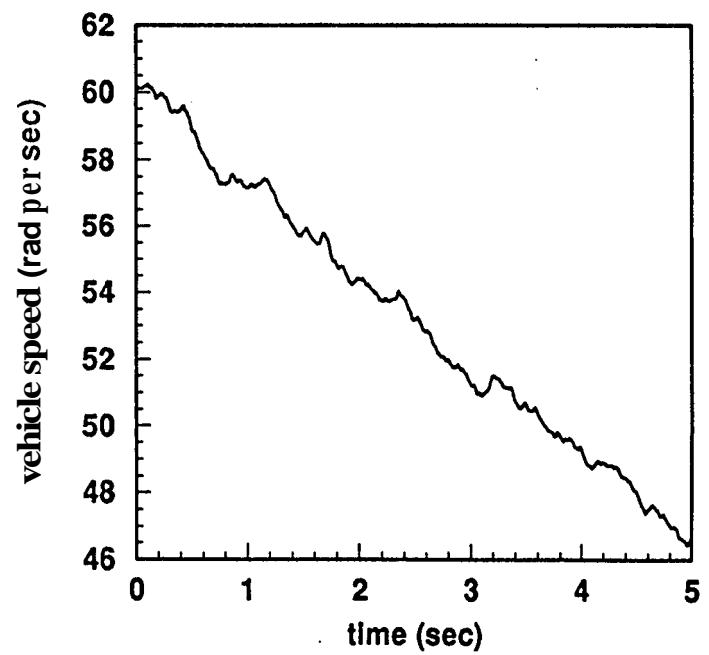
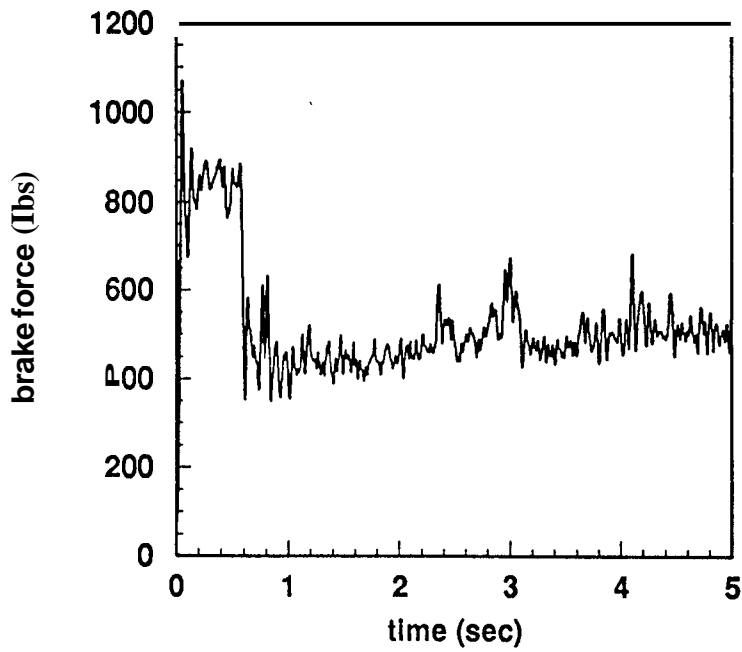
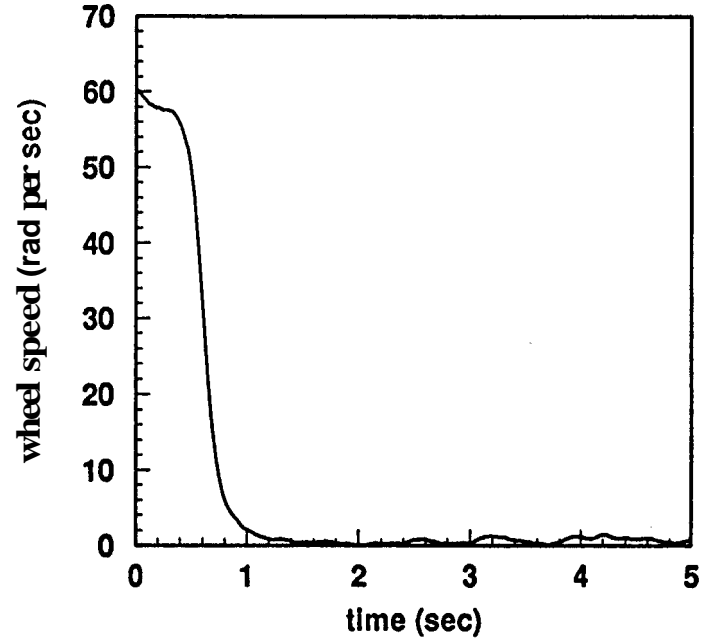
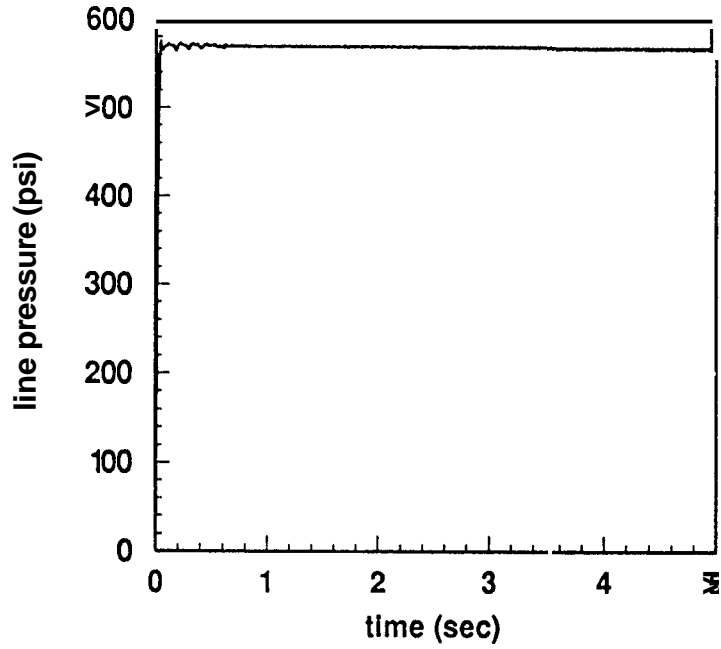


Figure A.19

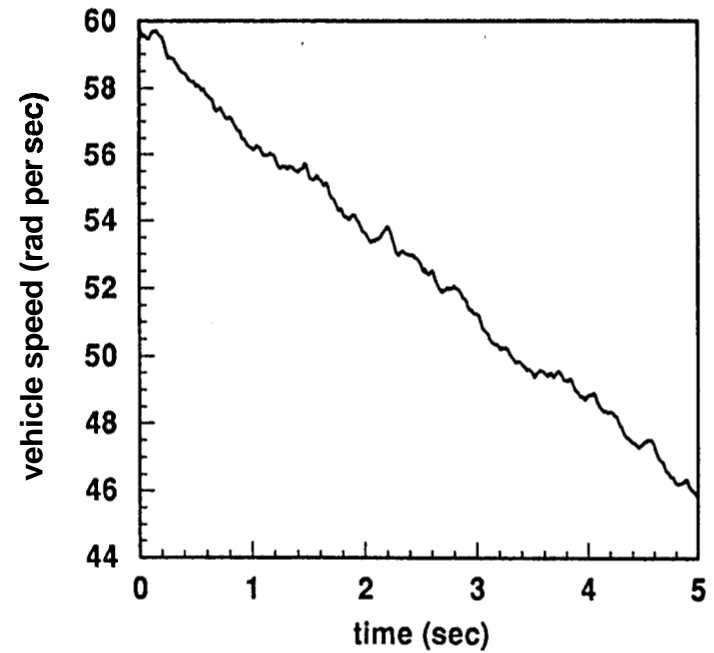
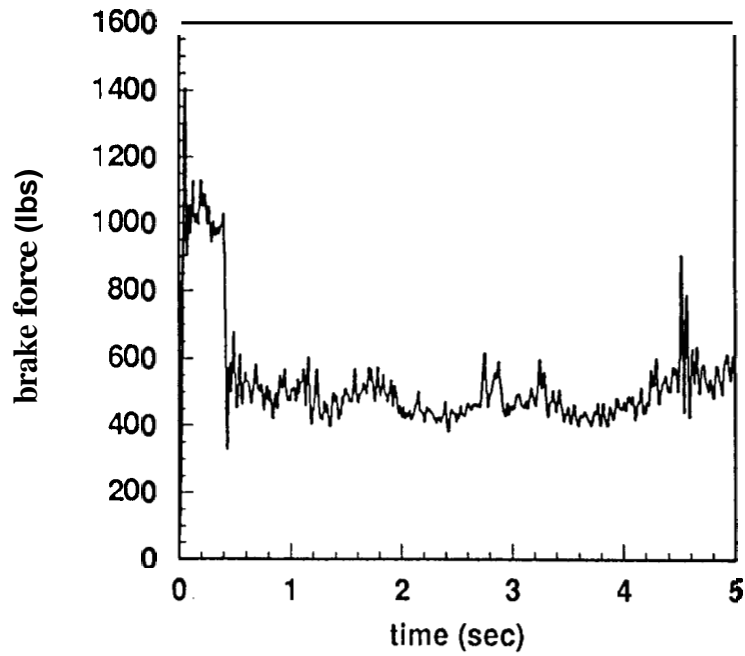
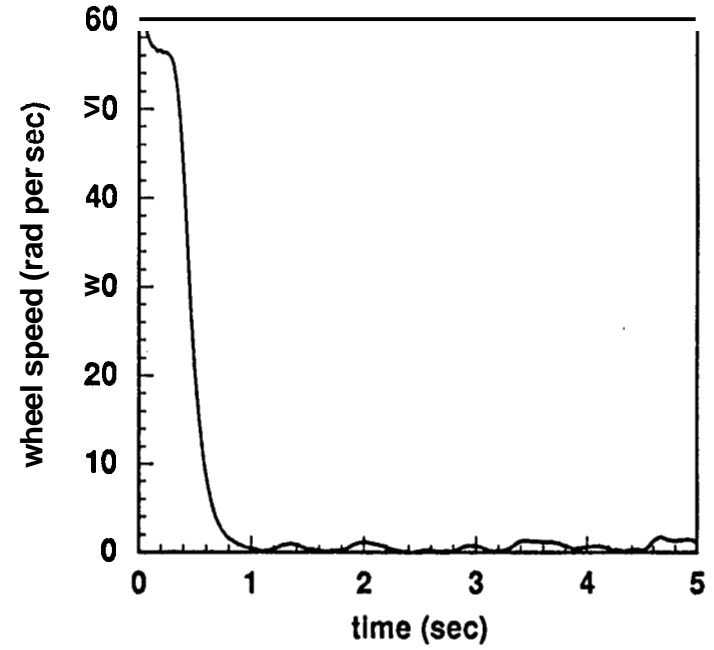
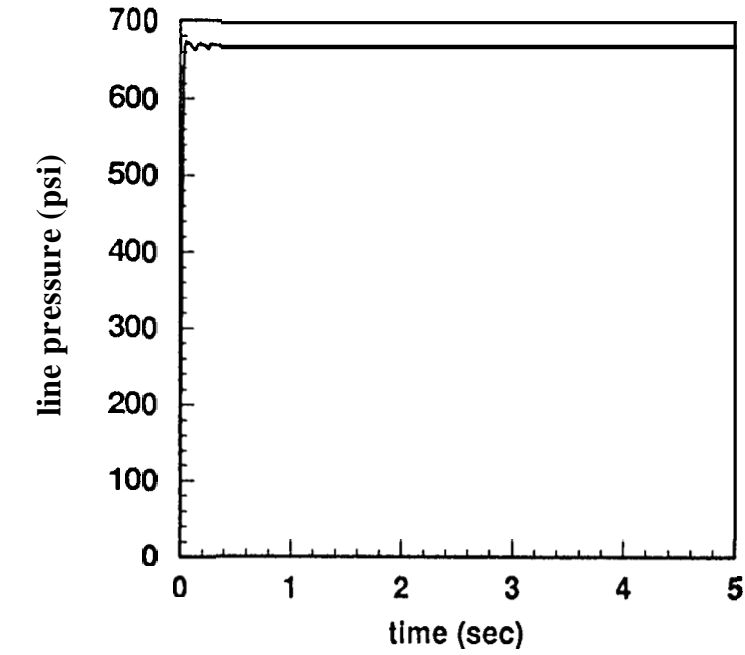


Figure A.20

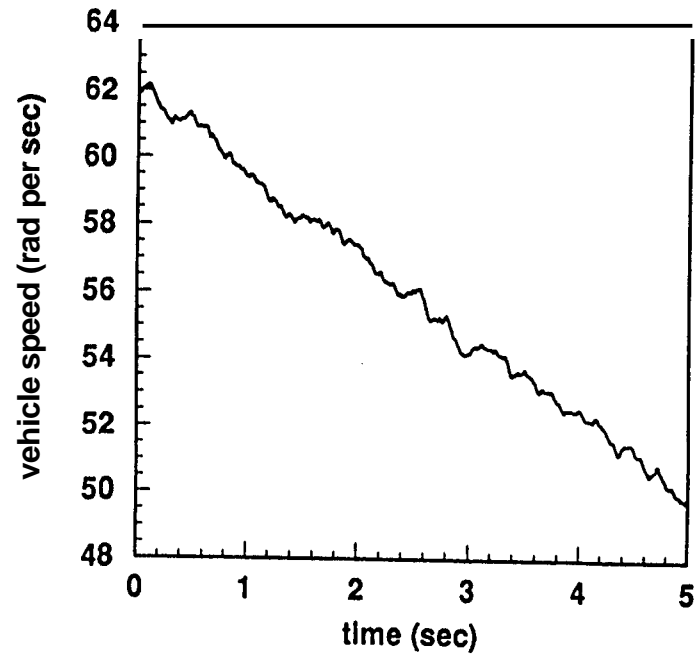
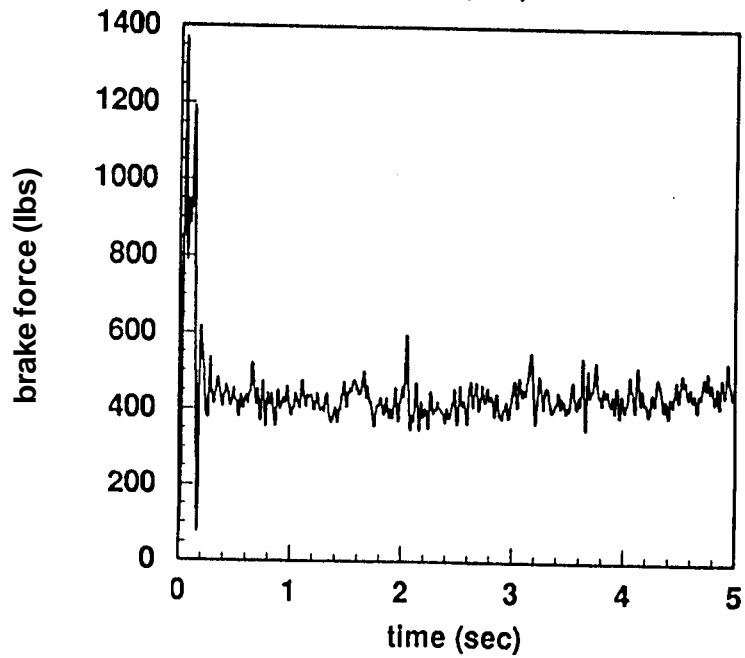
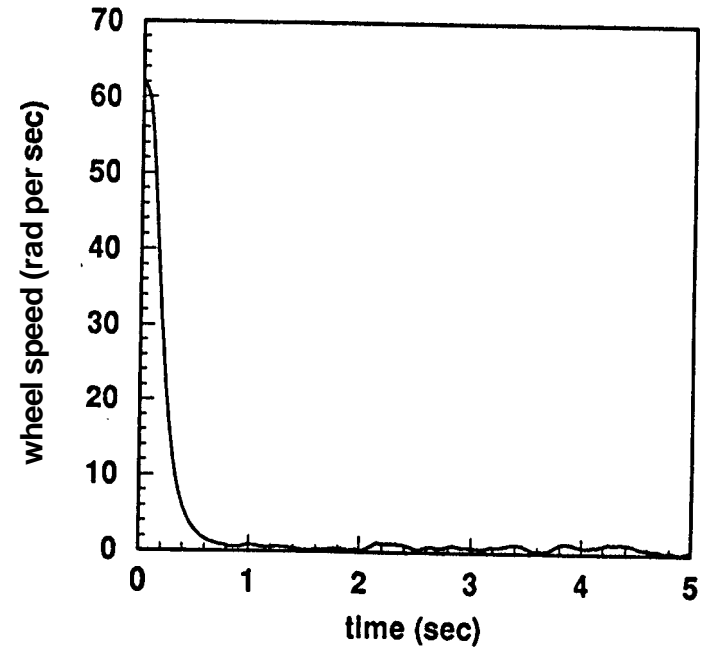
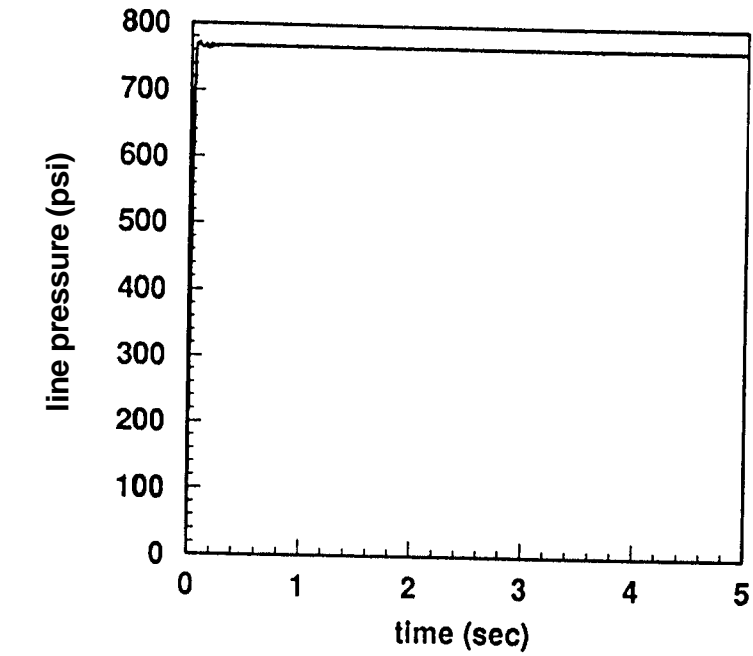


Figure A.21

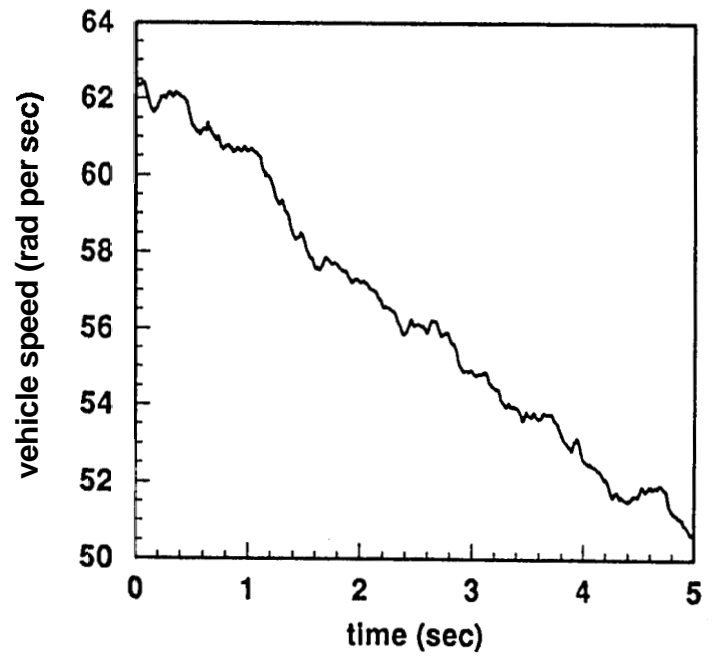
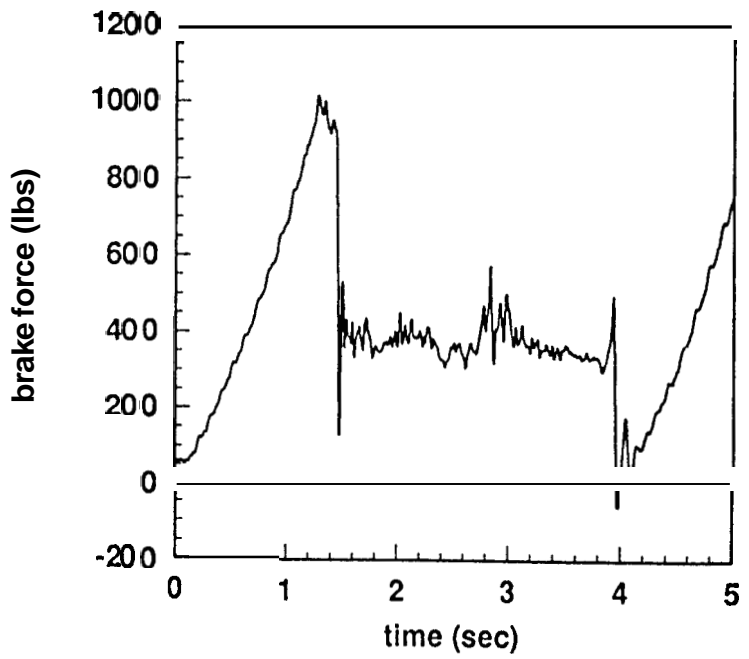
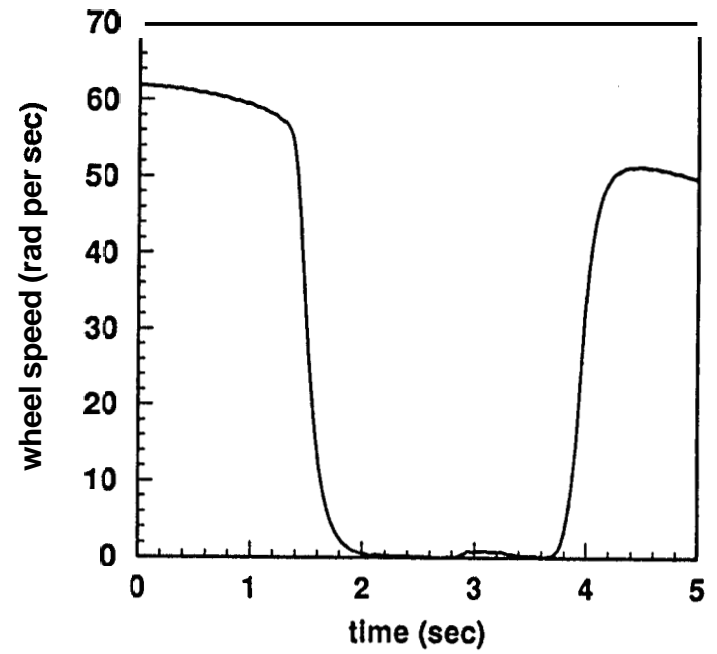
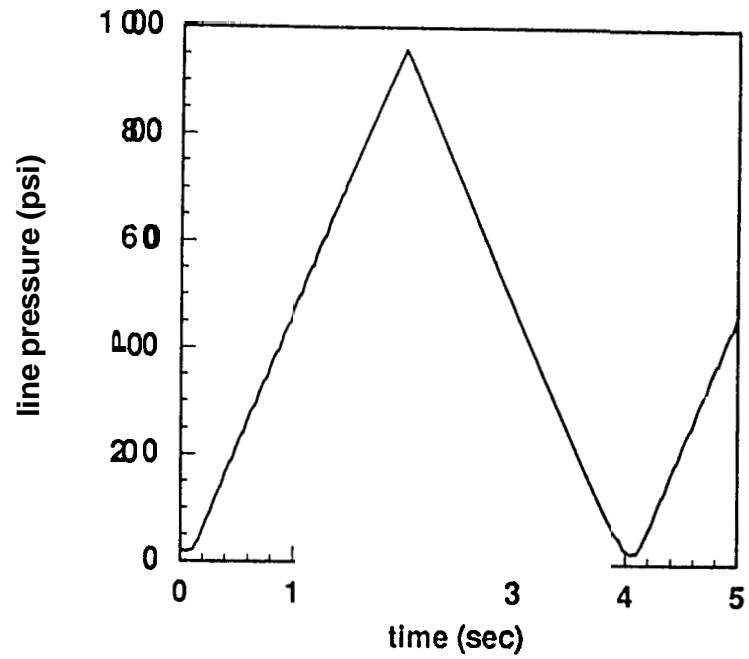


Figure A.22

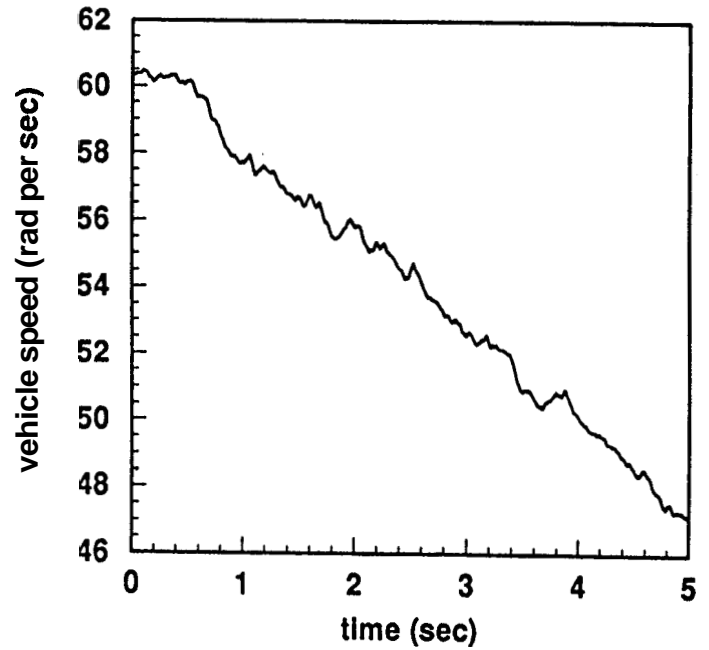
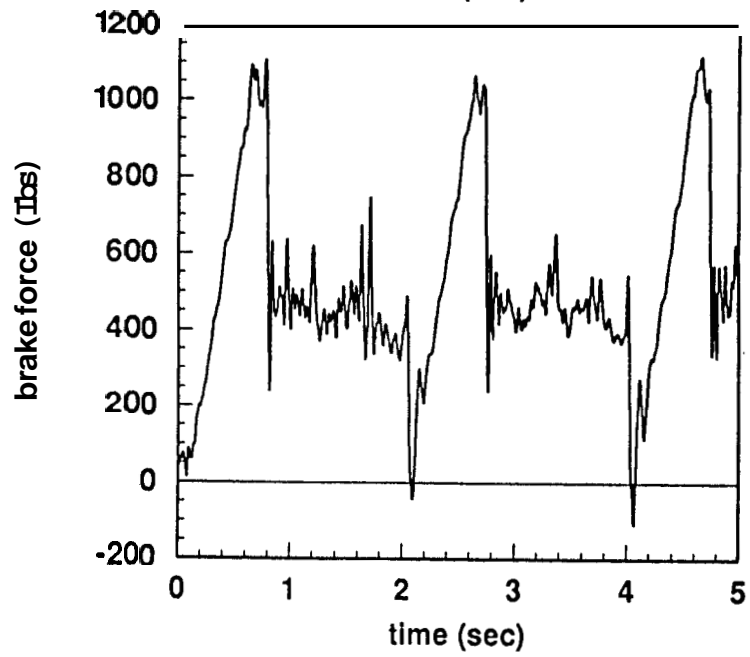
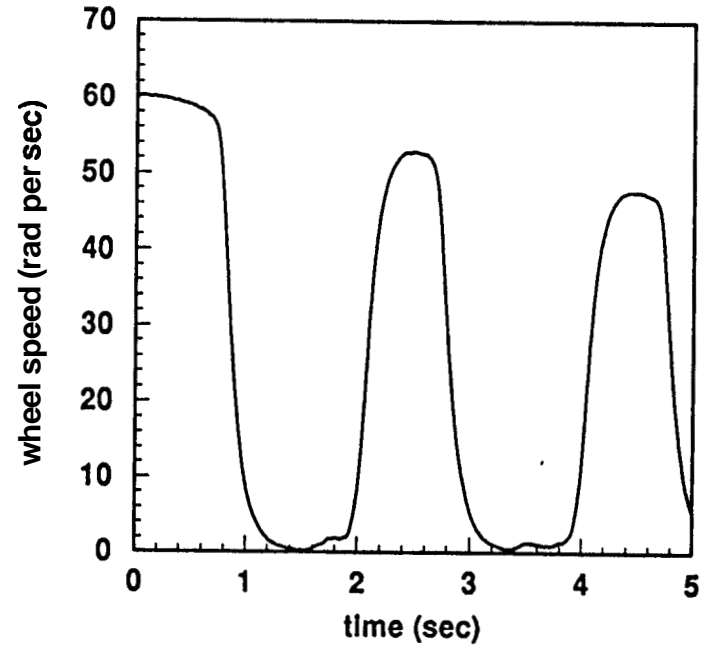
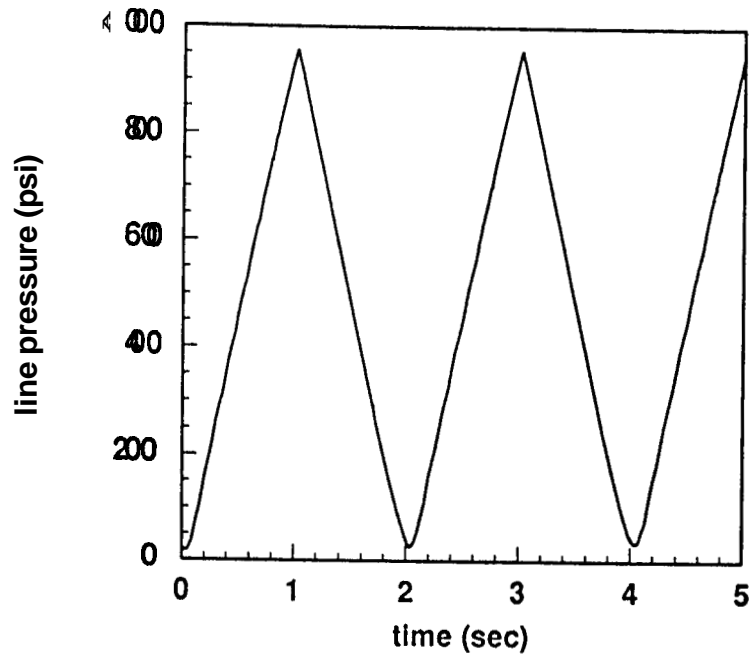


Figure A.23

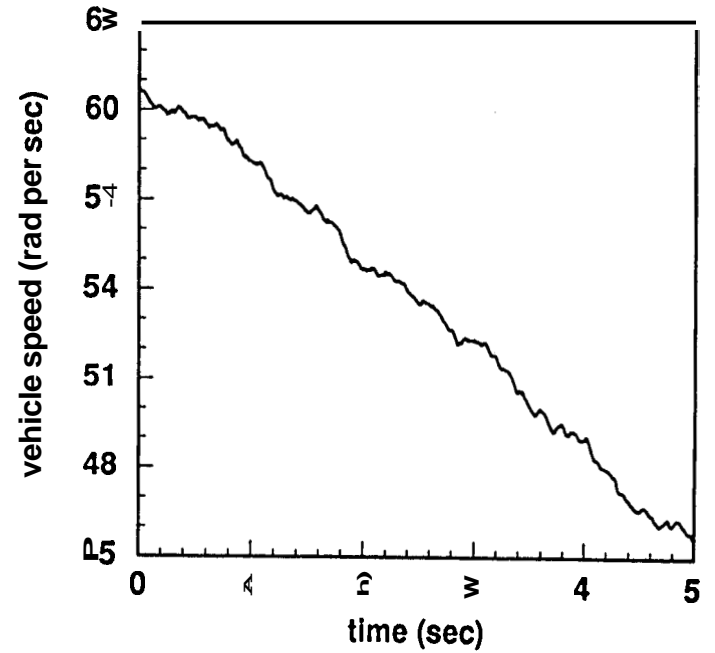
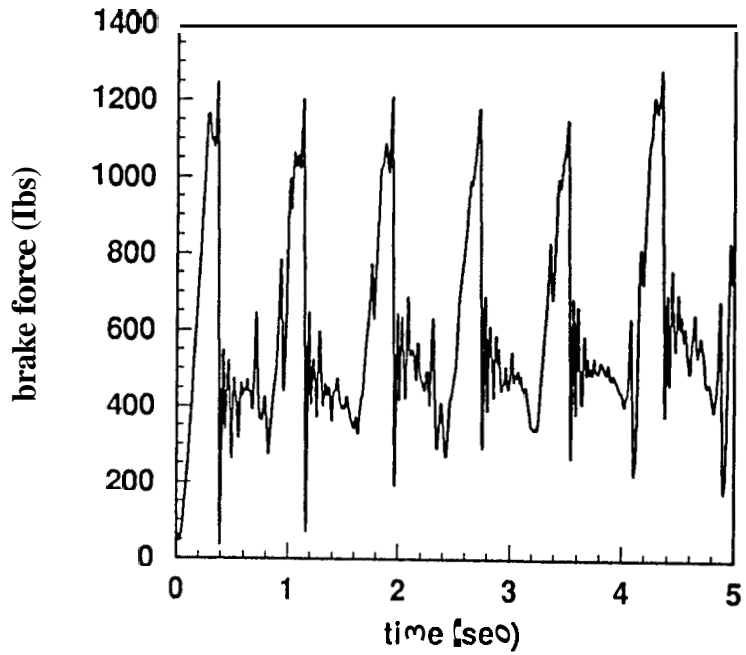
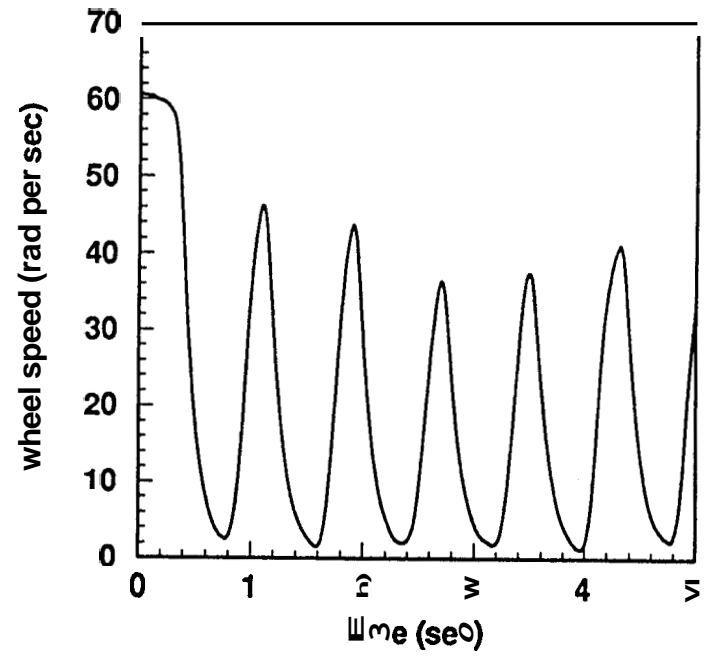
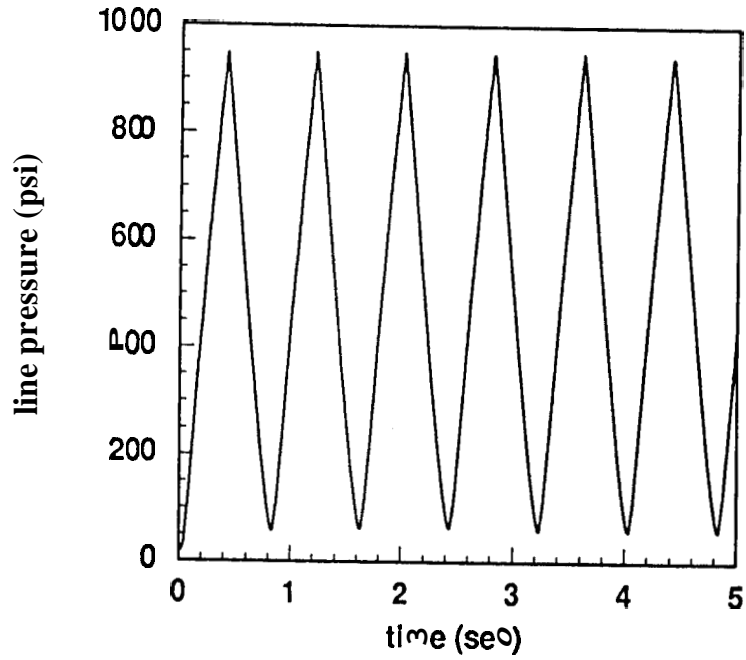


Figure A.24

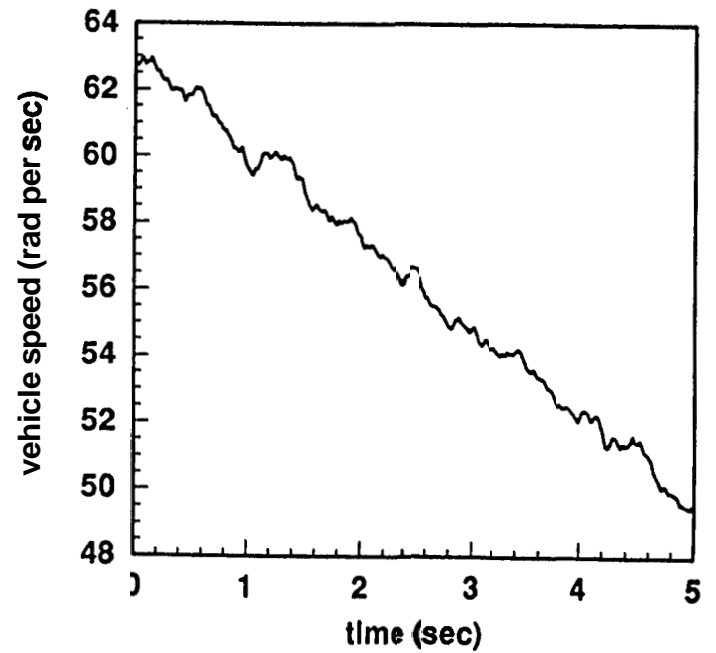
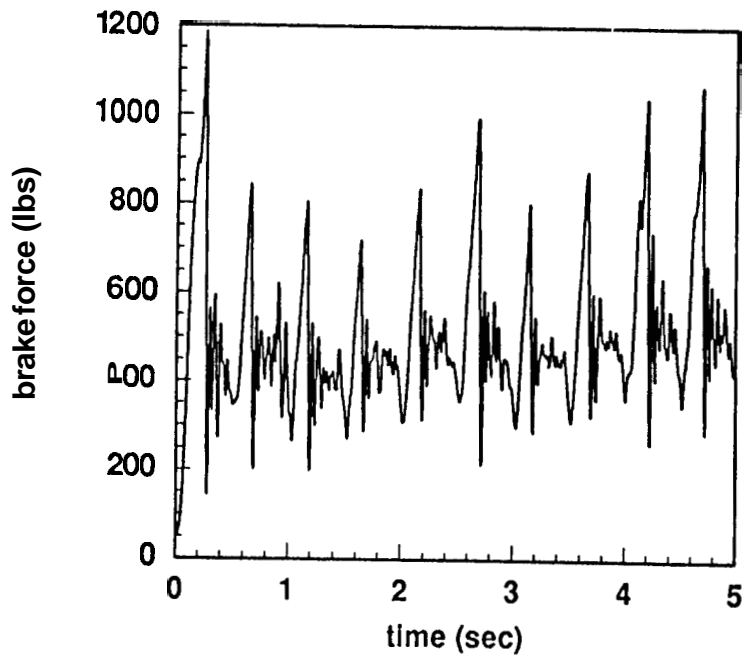
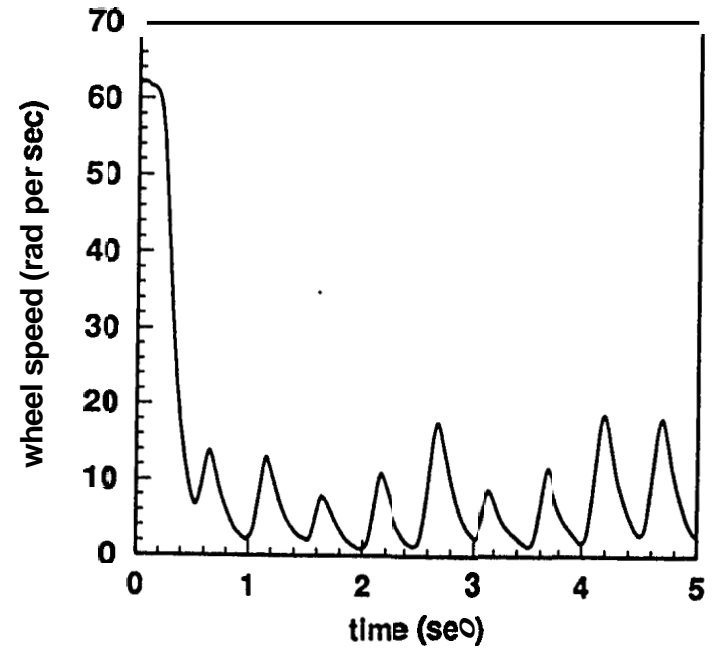
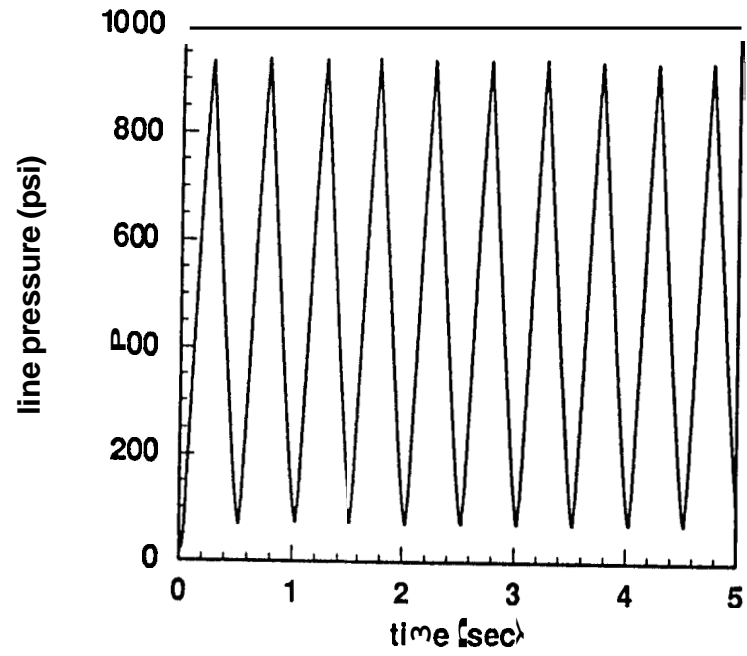


Figure A.25

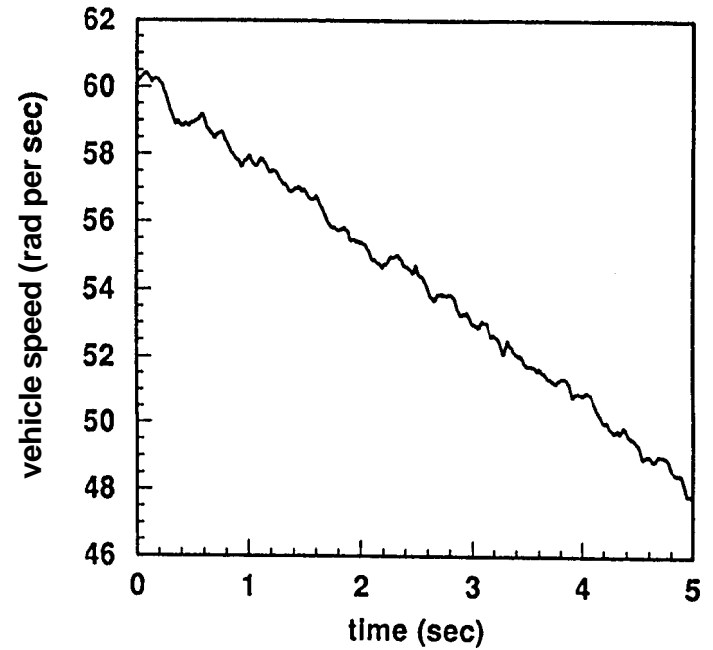
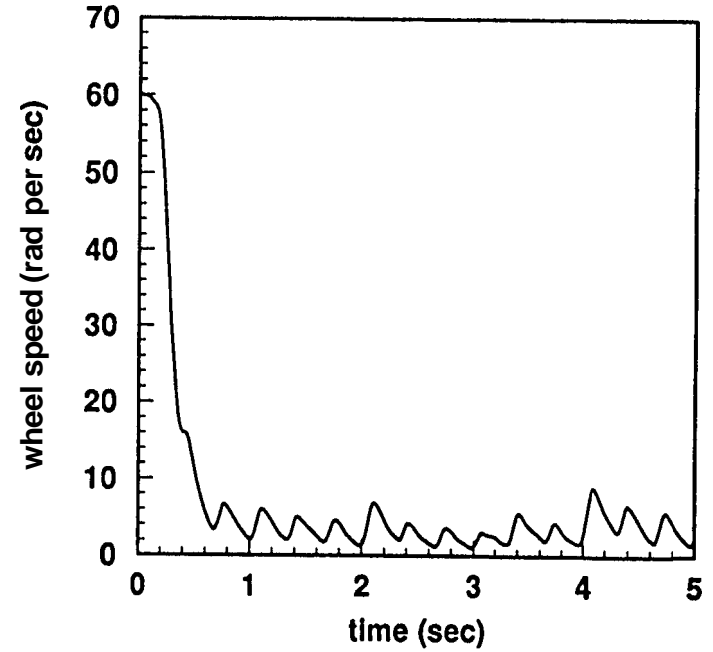
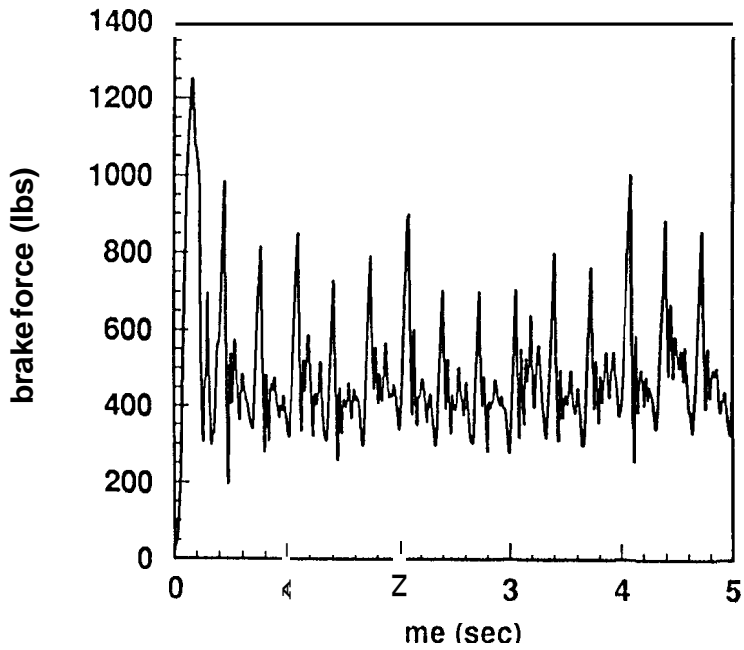
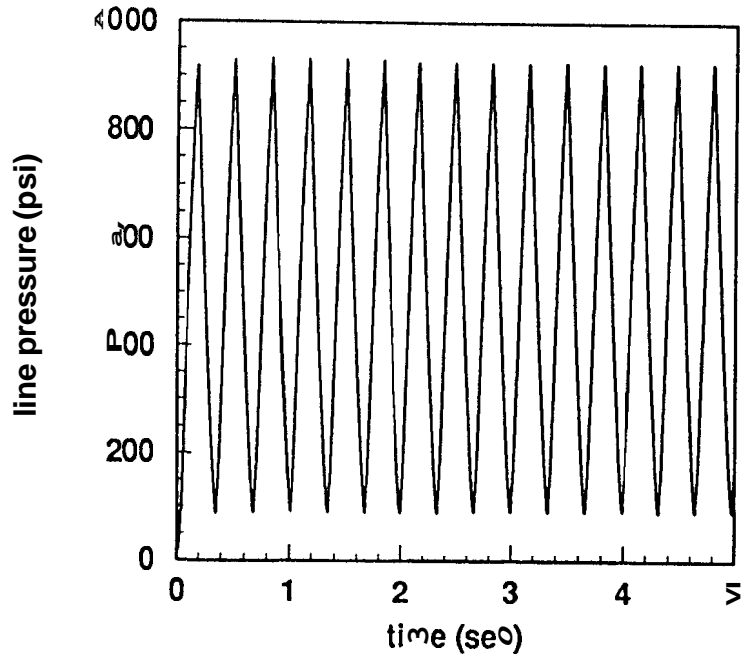


Figure A.26

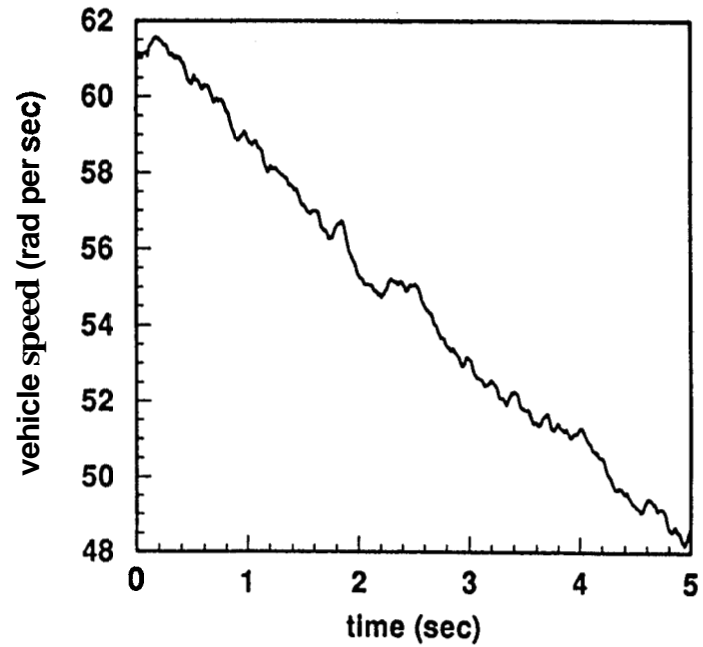
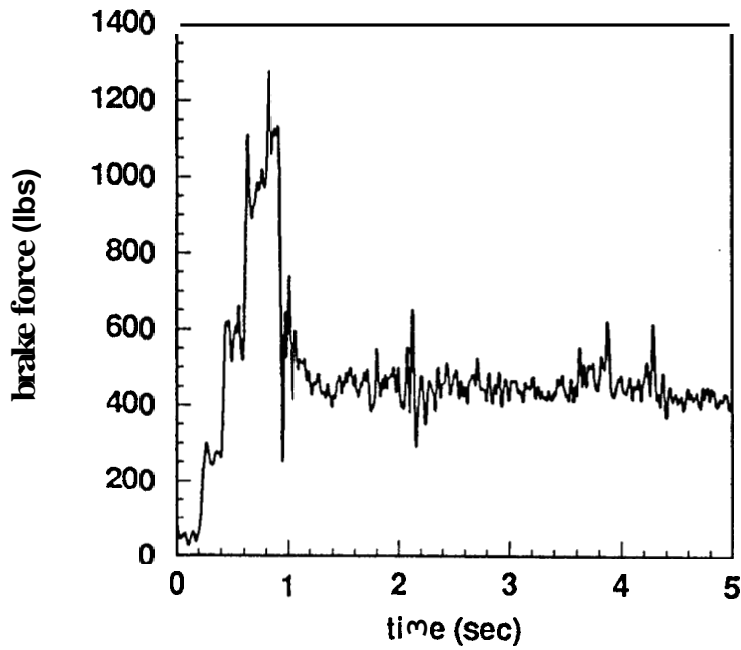
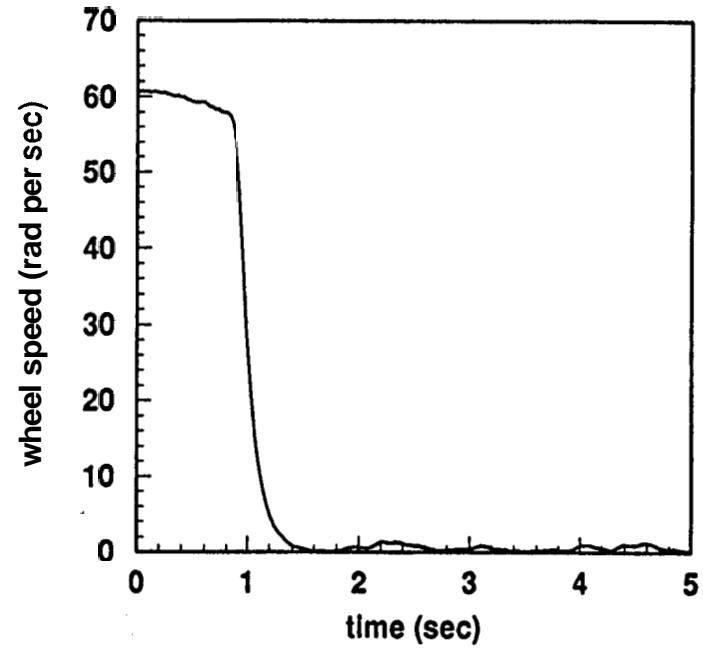
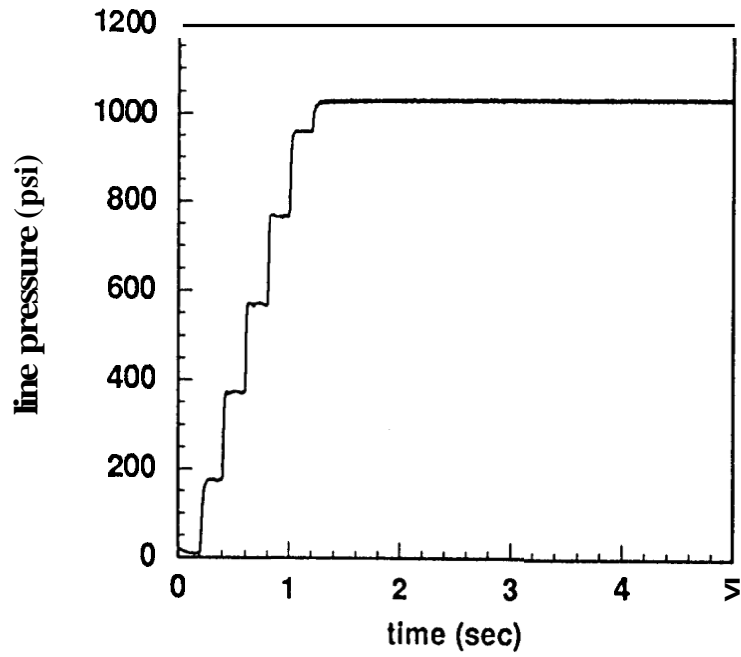


Figure A.27

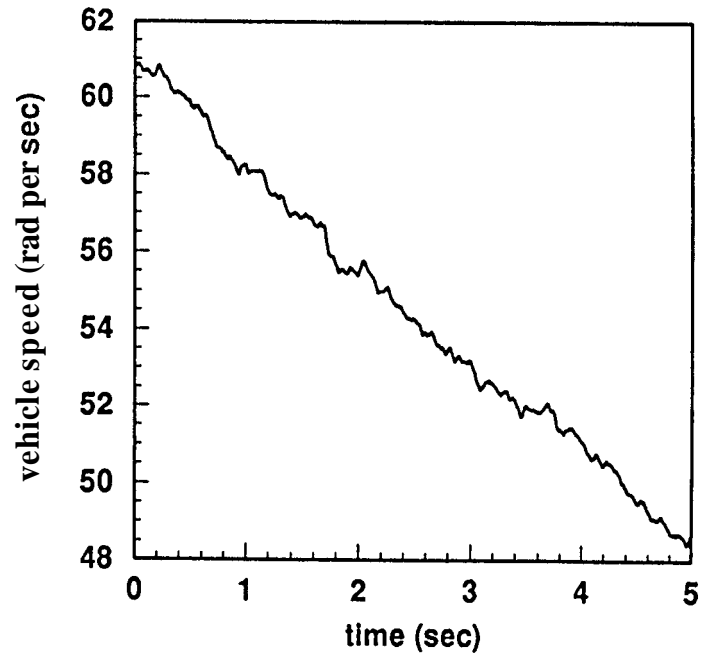
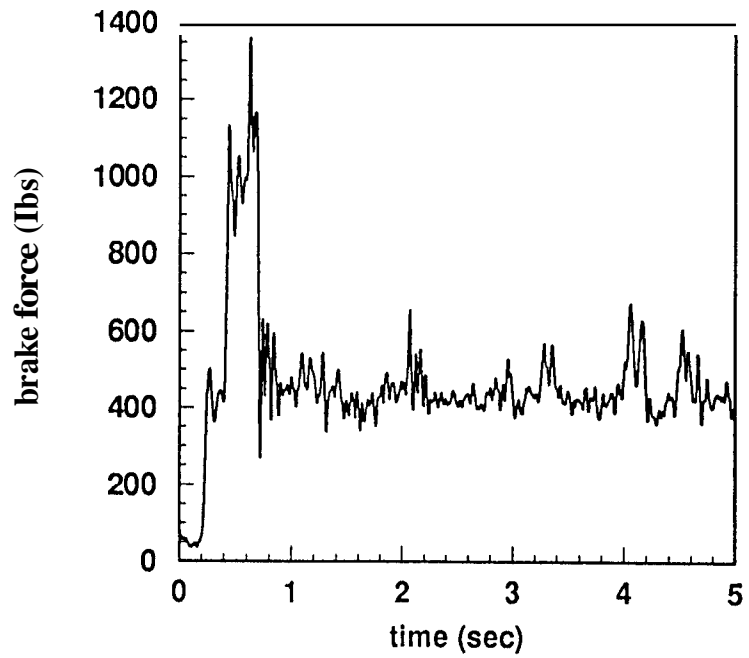
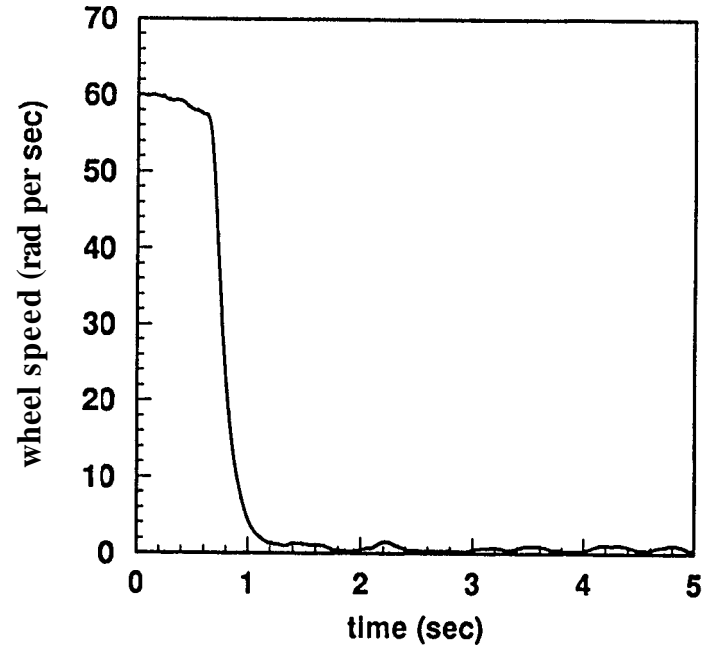
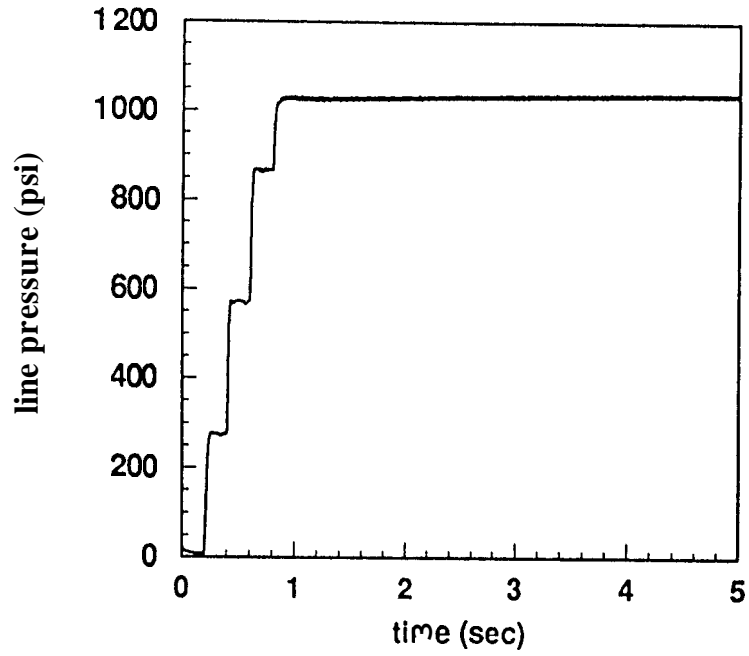


Figure A.28

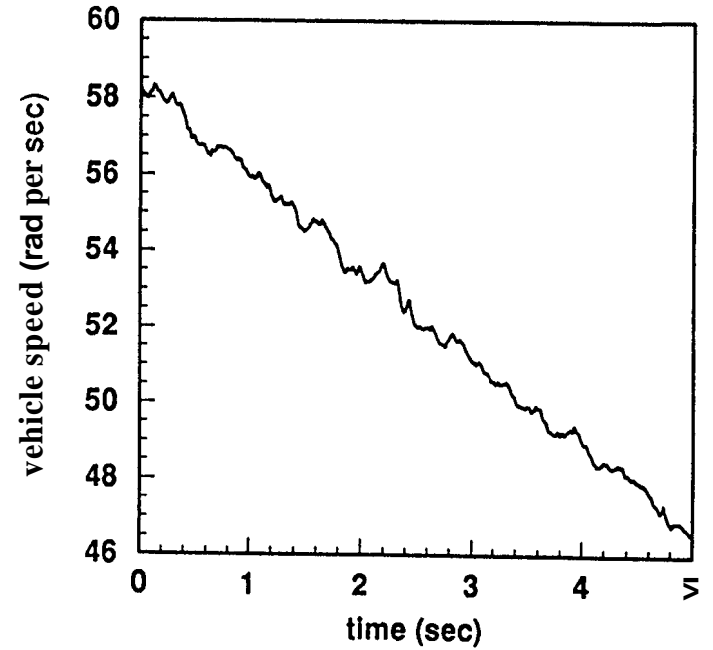
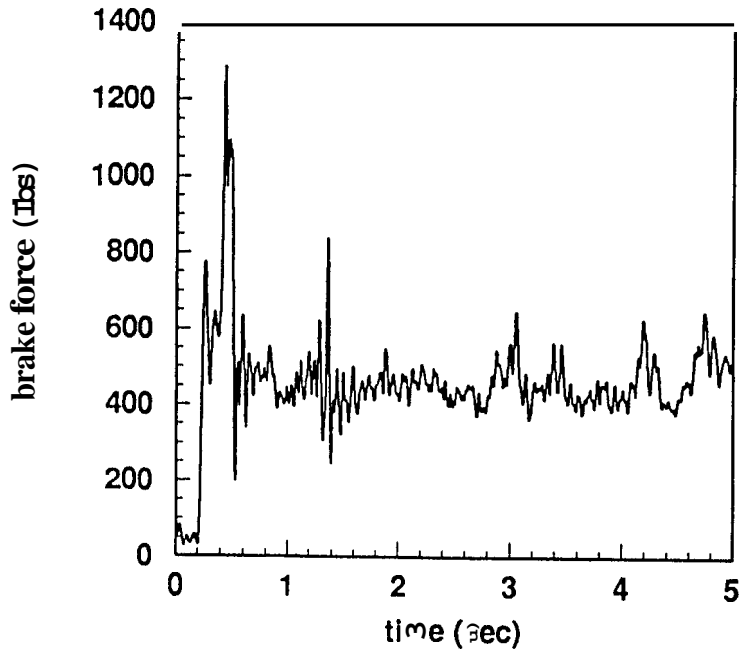
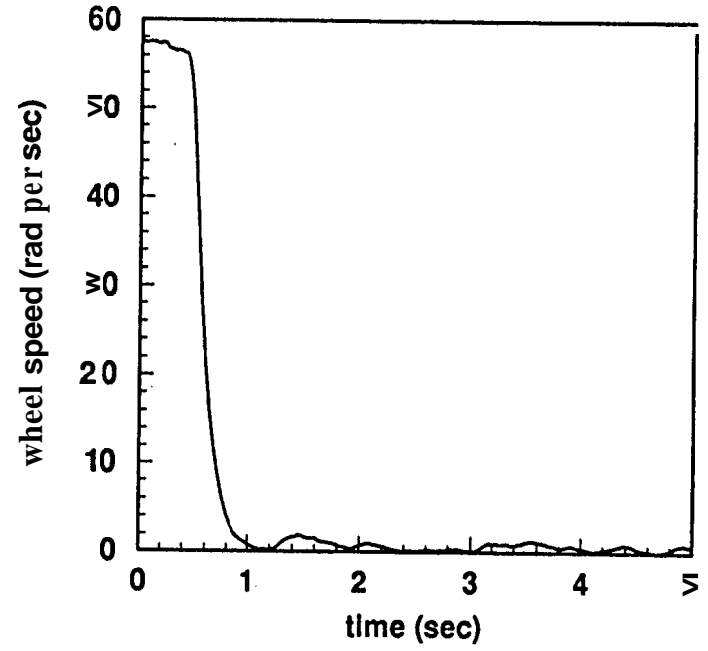
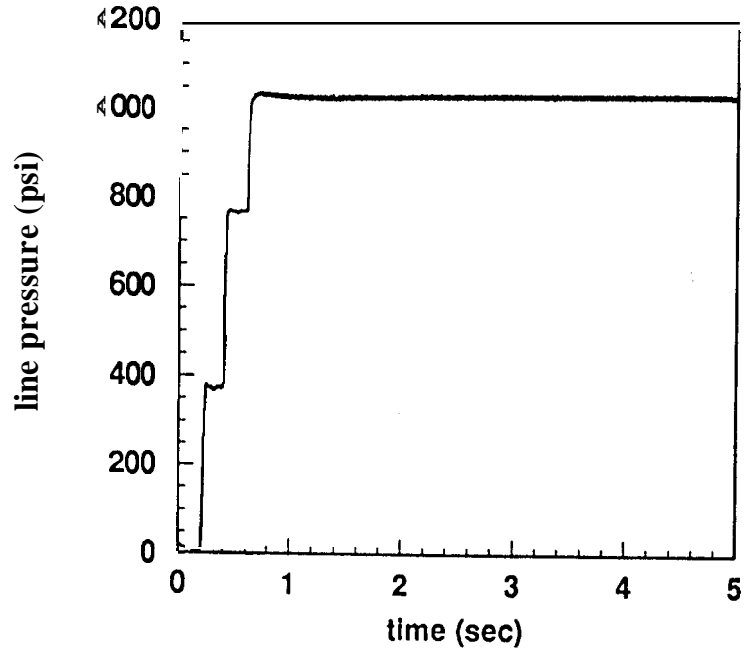


Figure A.29

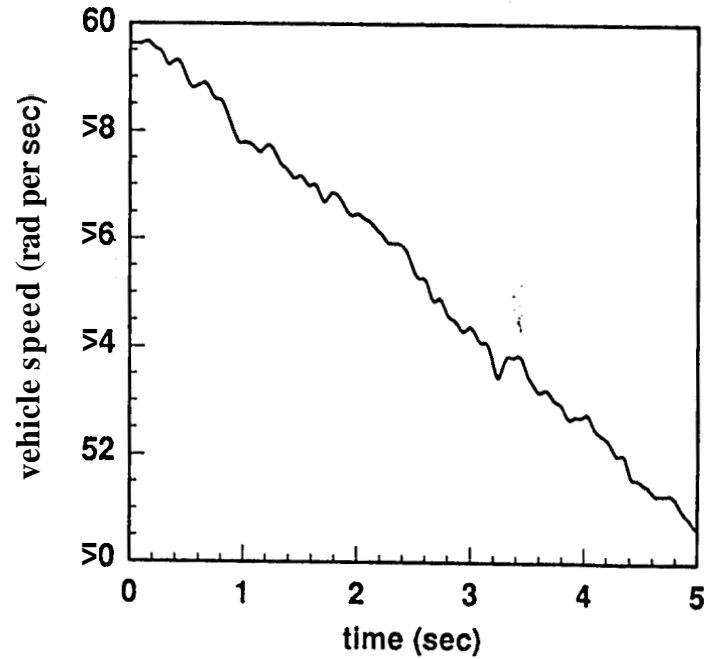
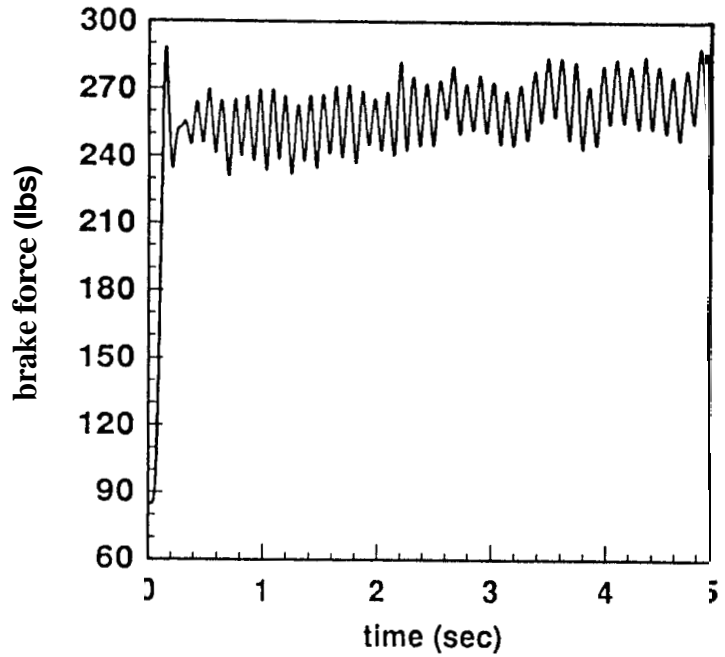
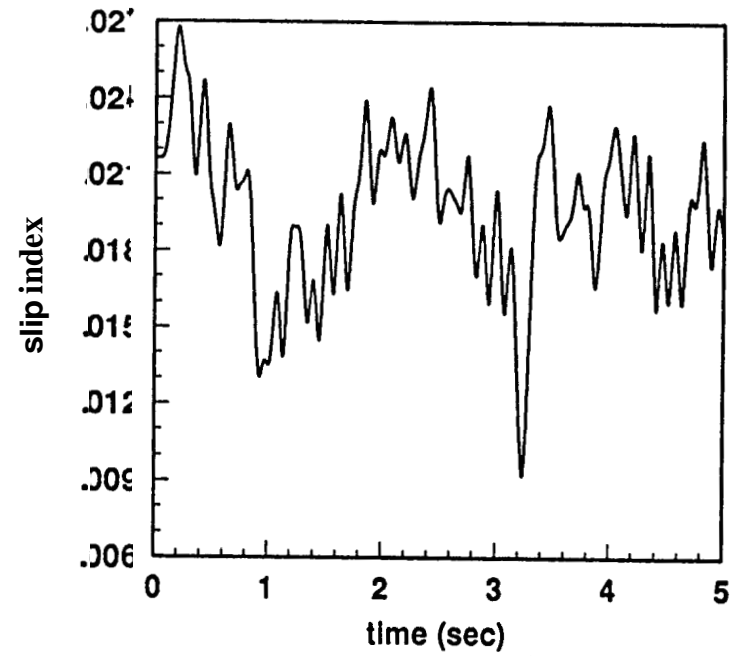
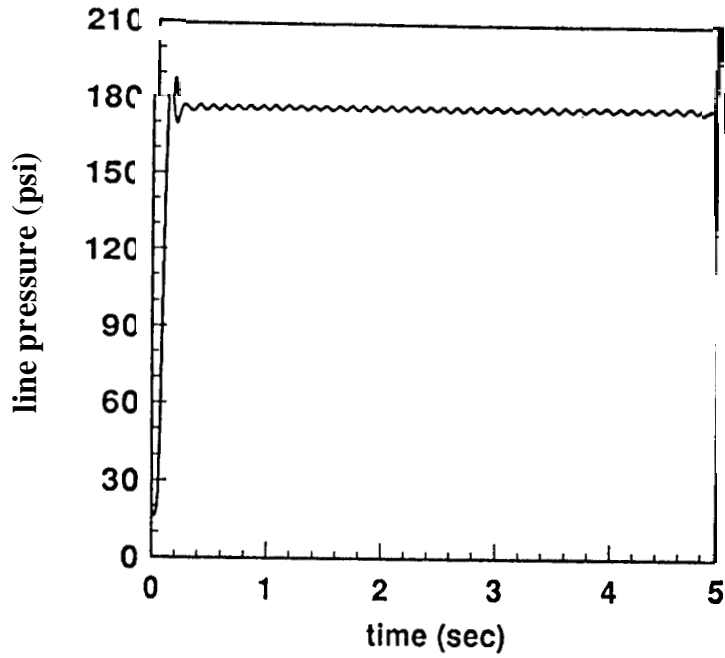


Figure A.30

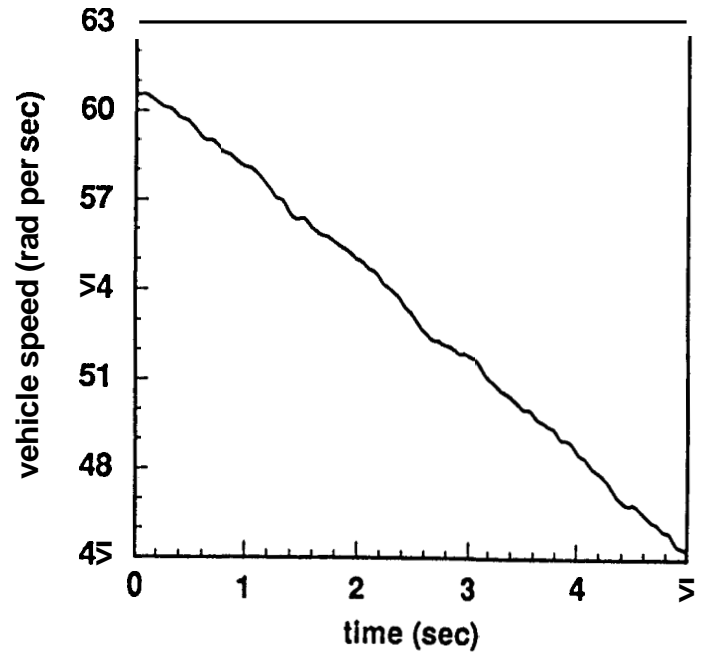
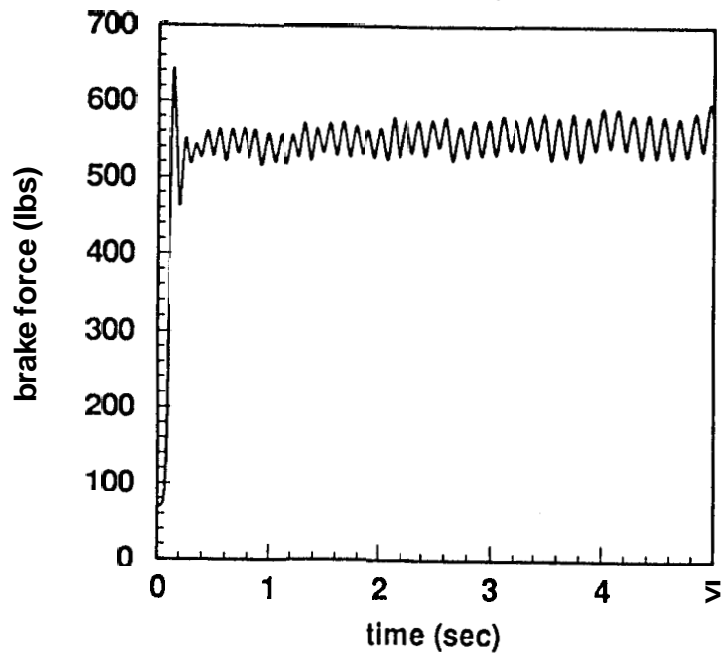
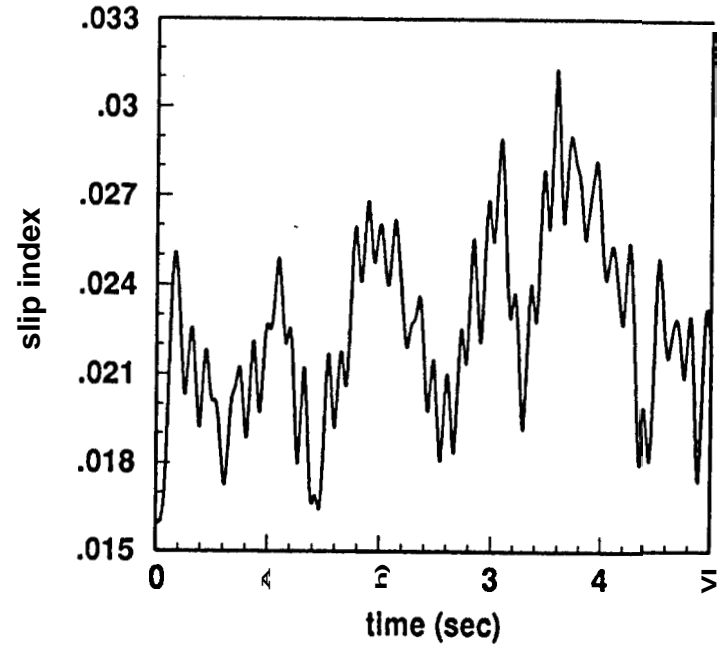
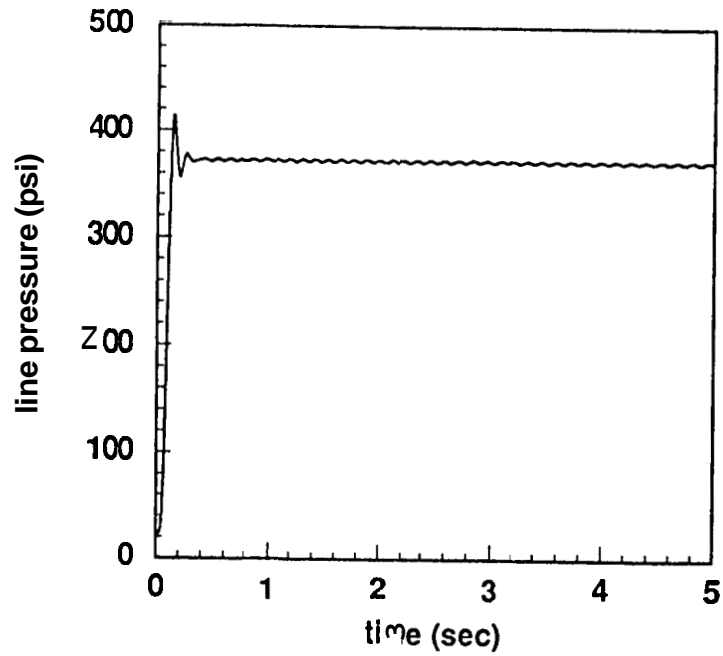


Figure A.31

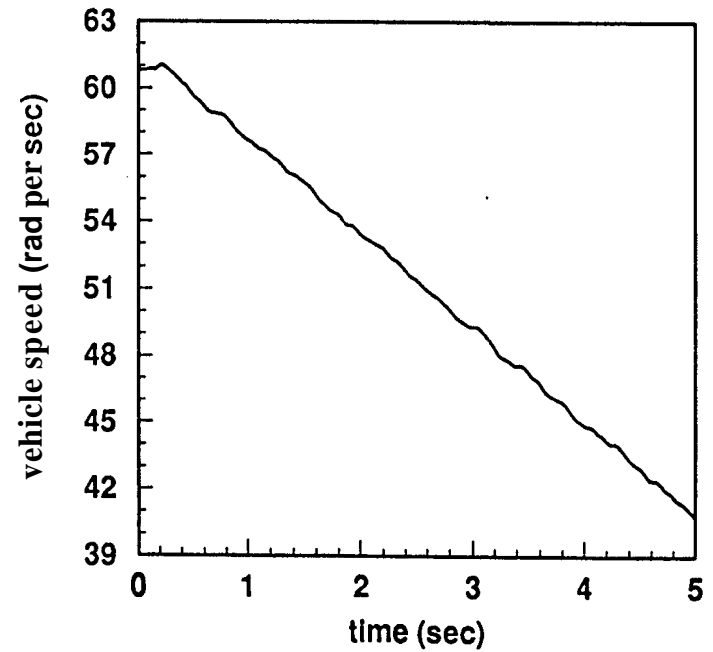
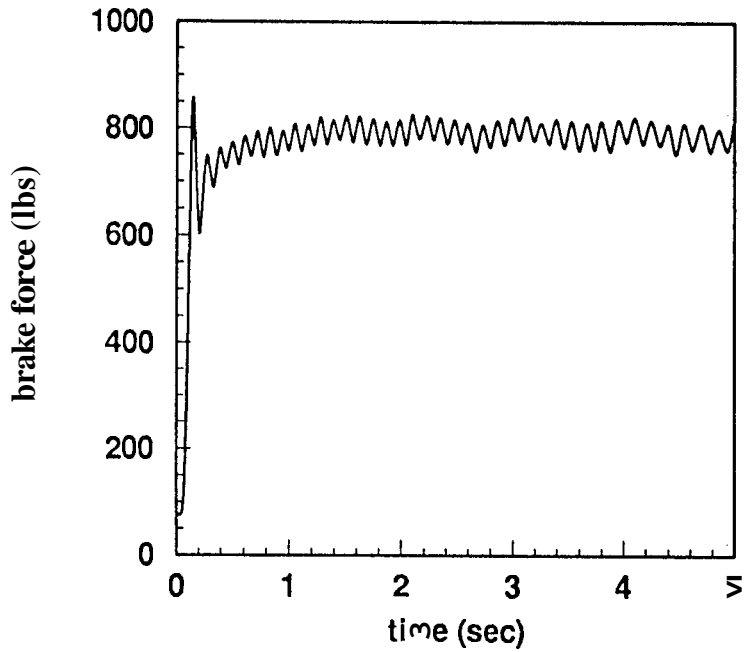
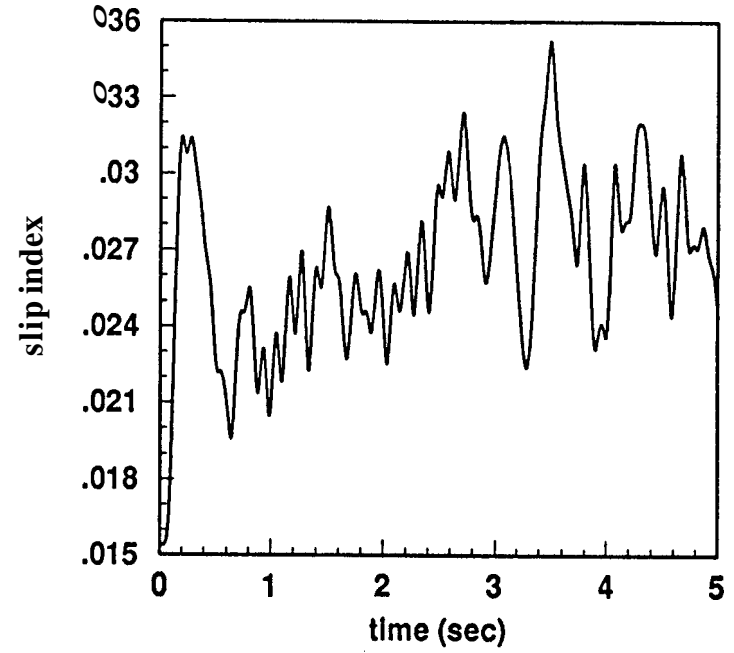
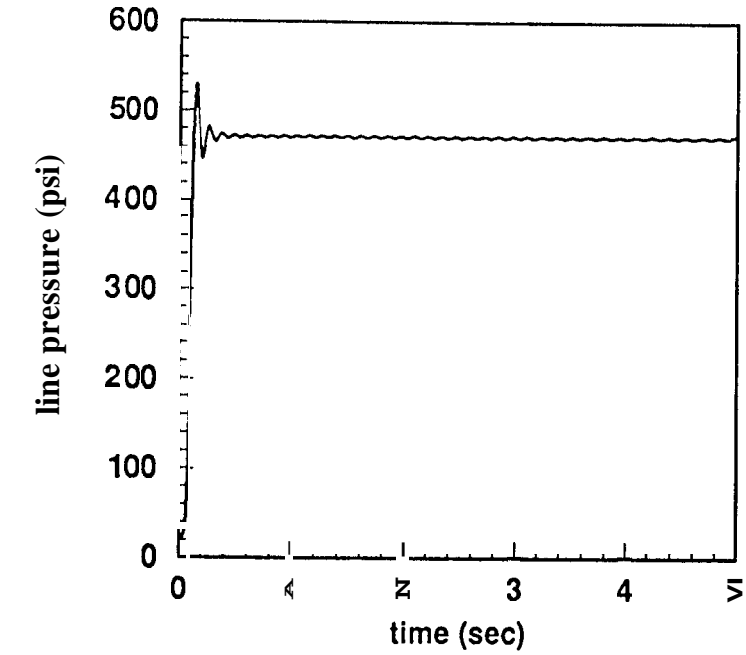


Figure A.32

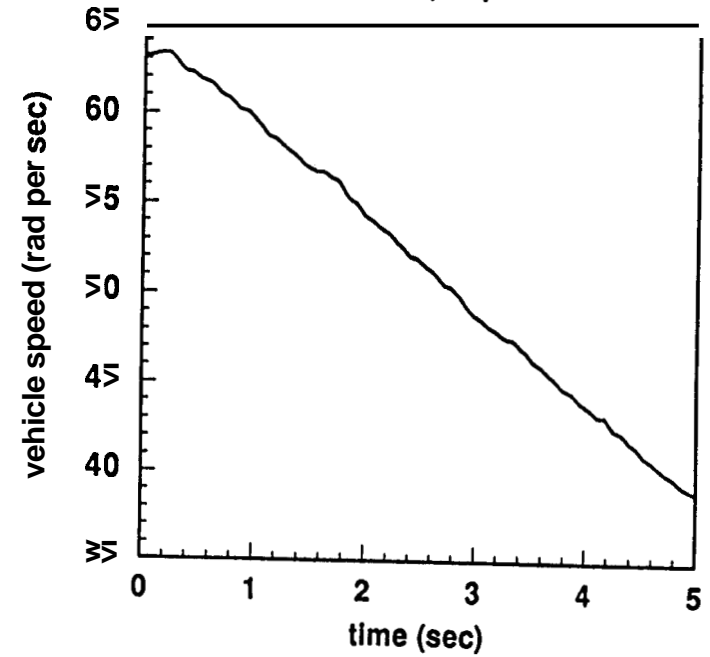
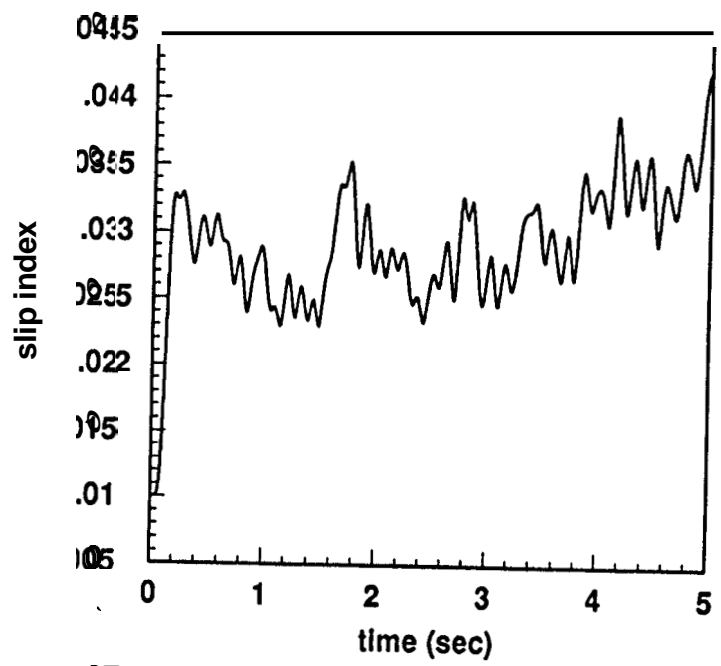
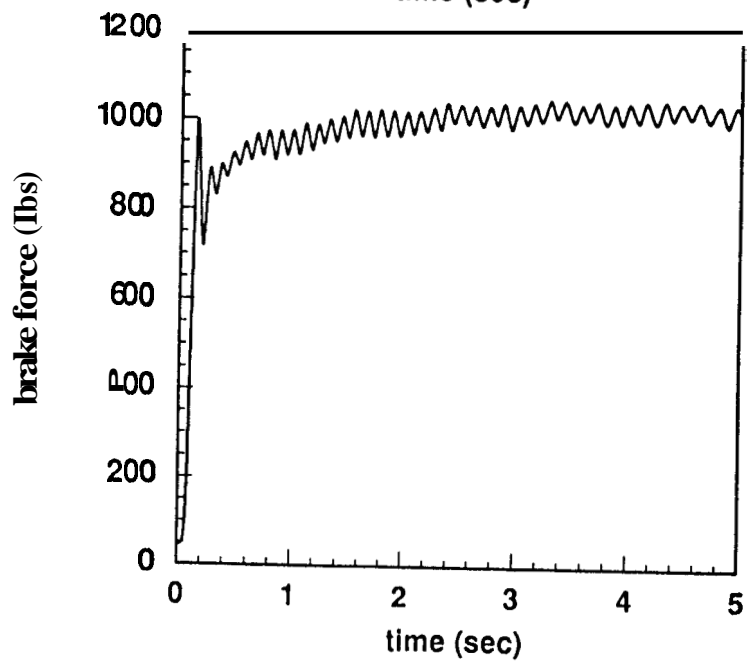
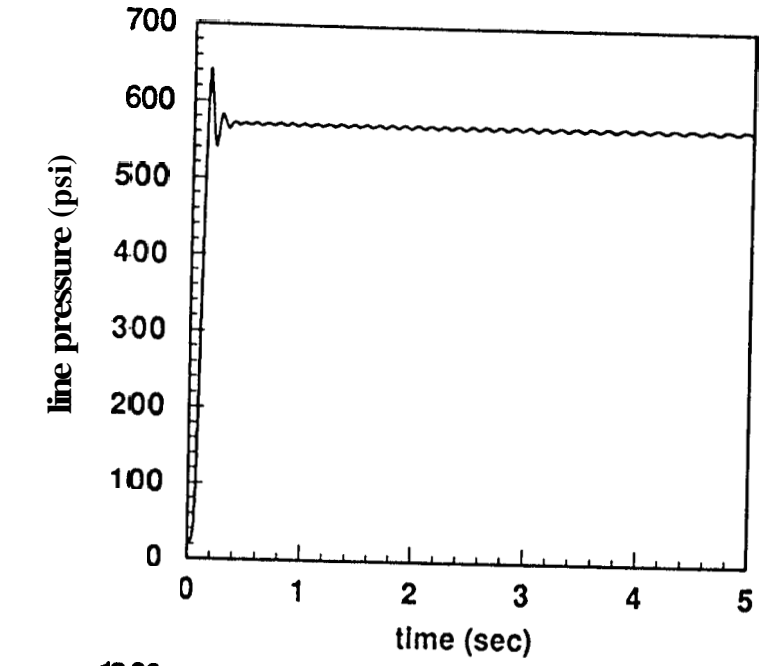


Figure A.33

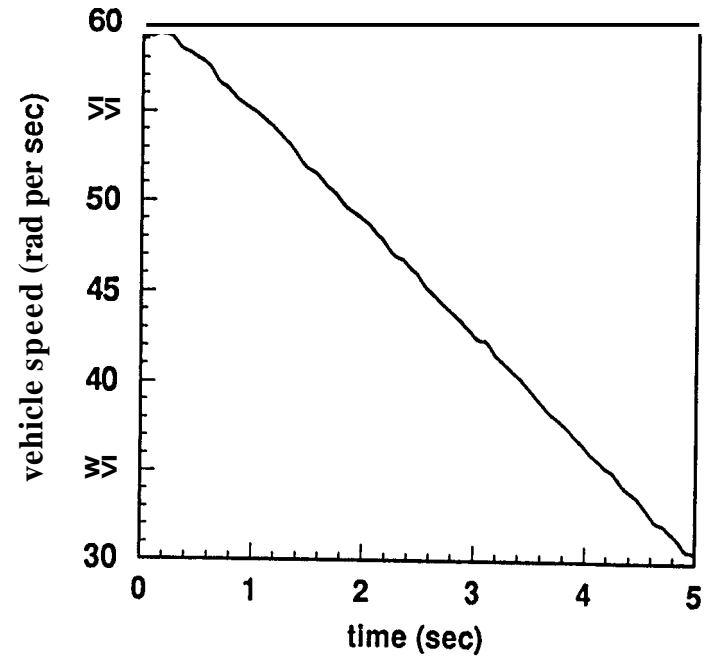
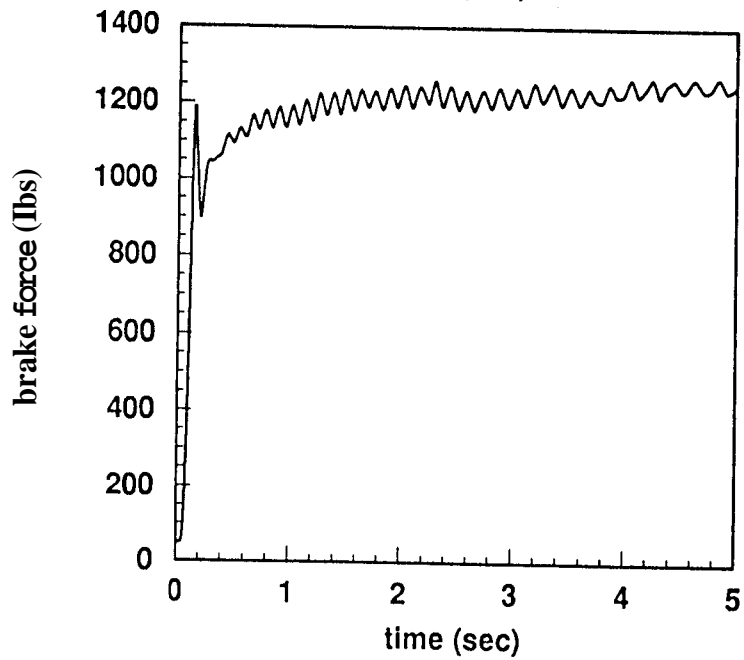
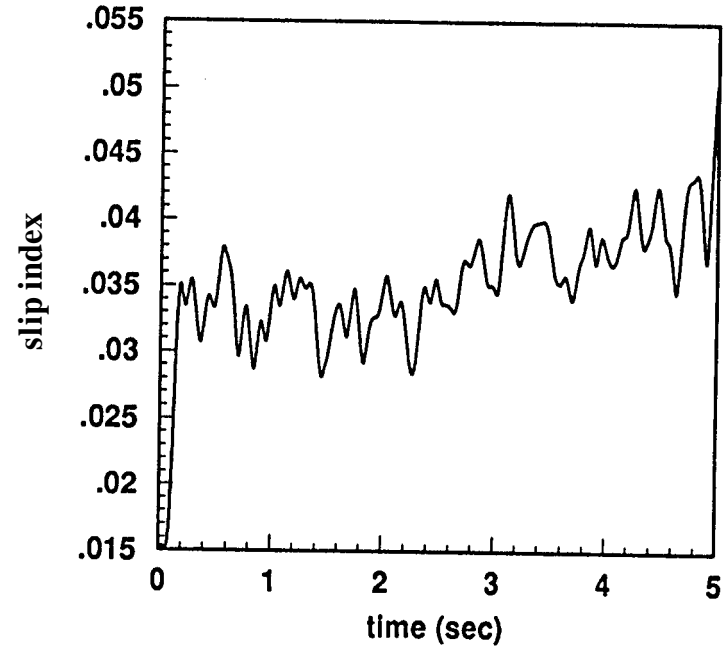
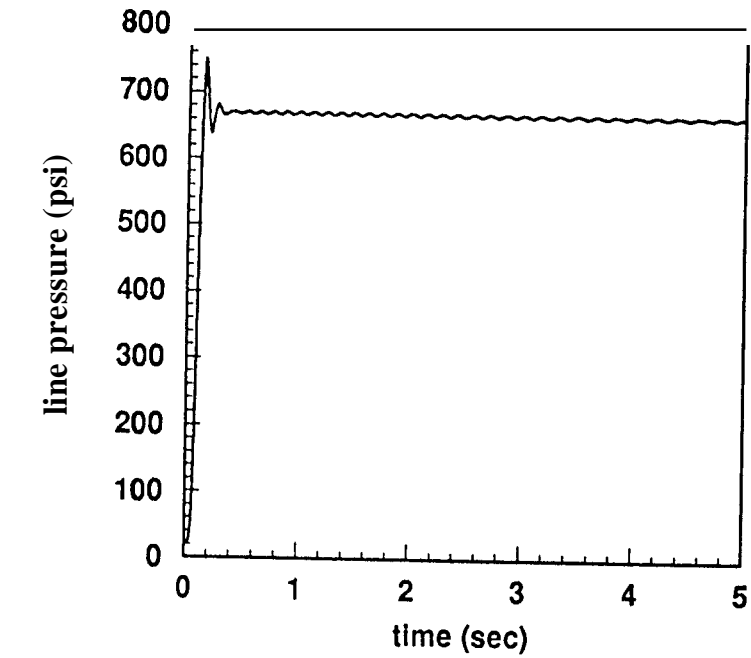


Figure A.34

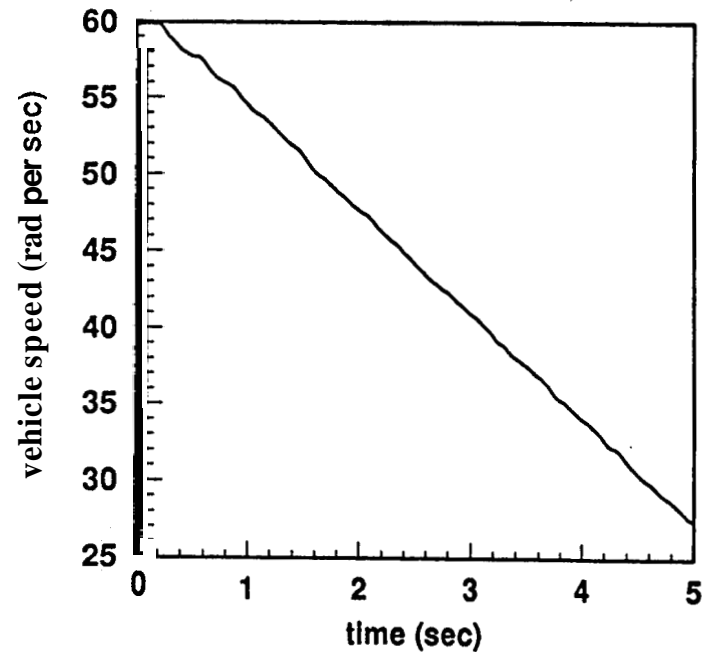
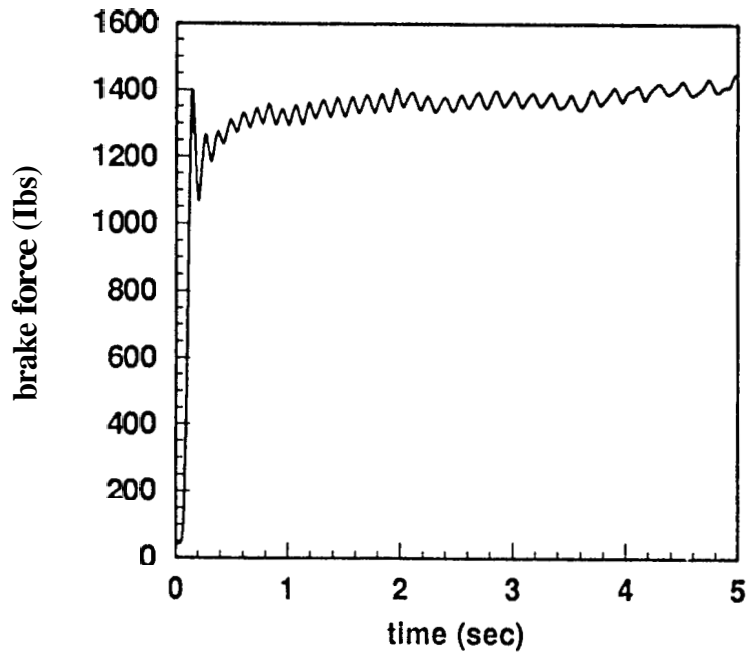
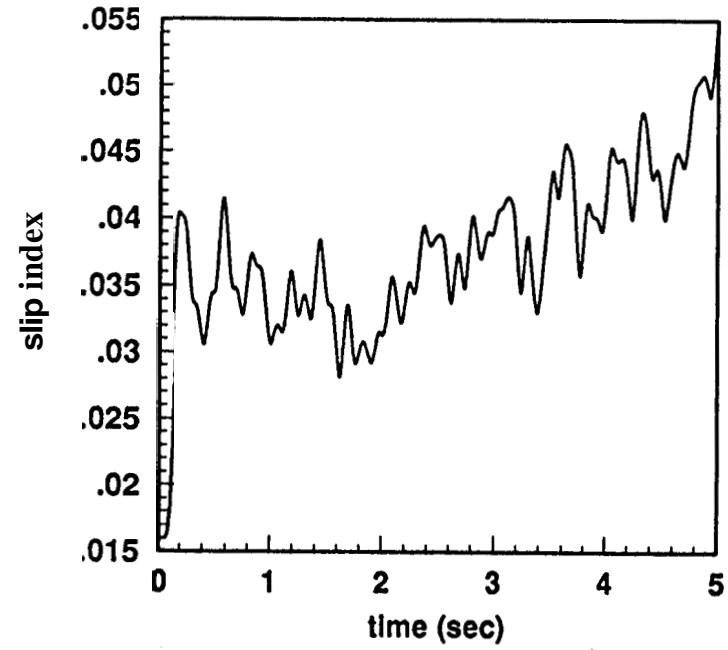
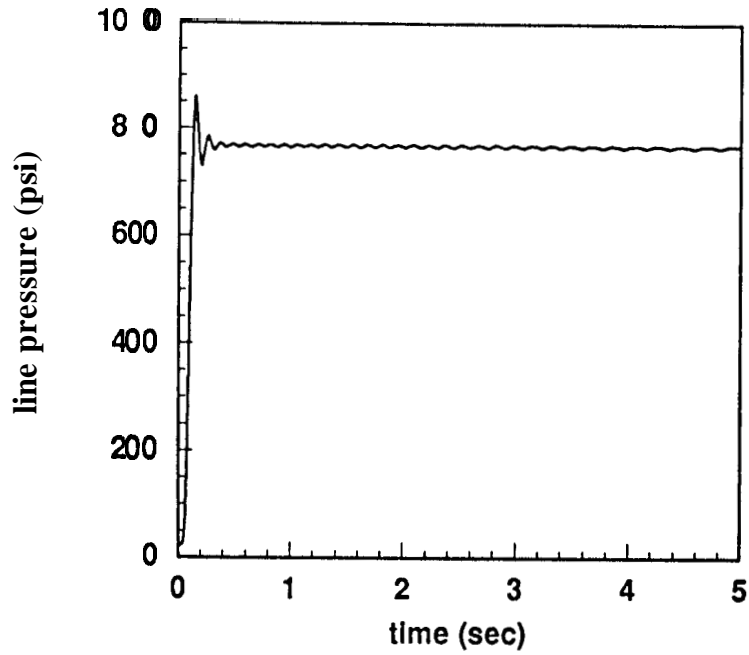


Figure A.35

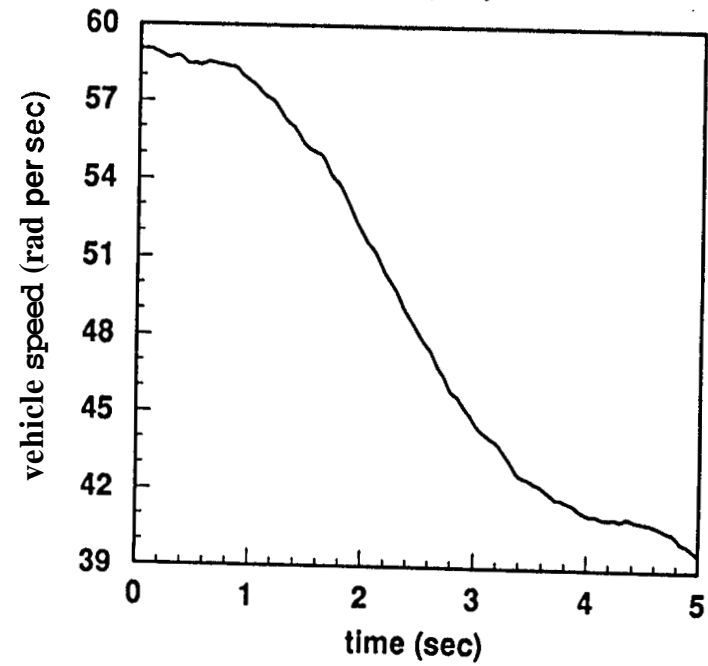
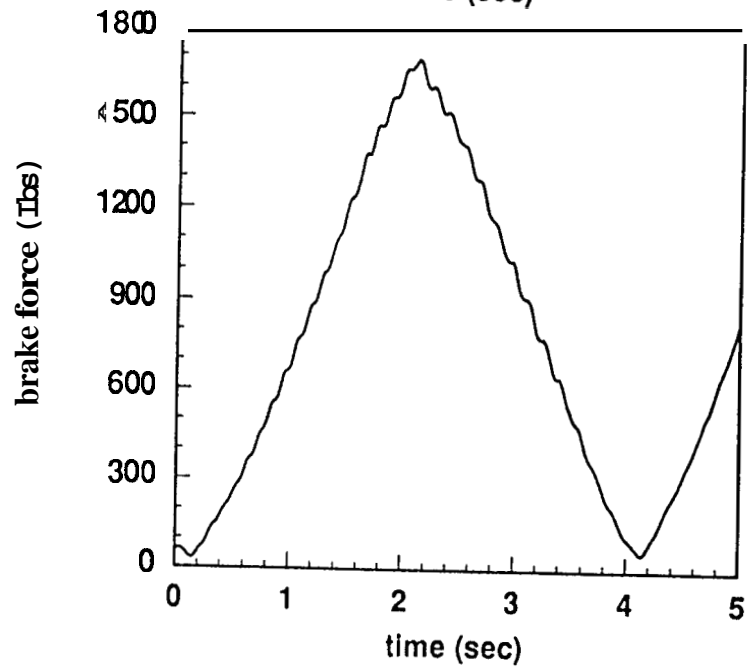
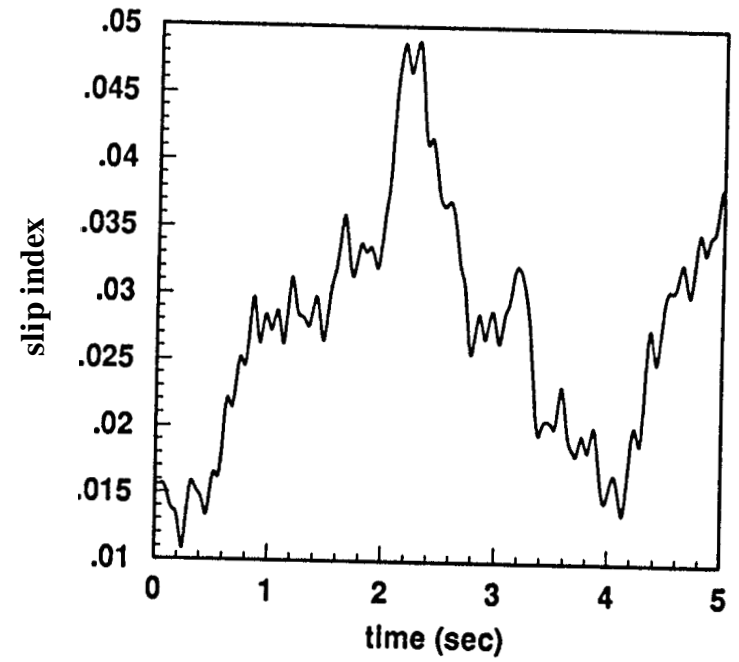
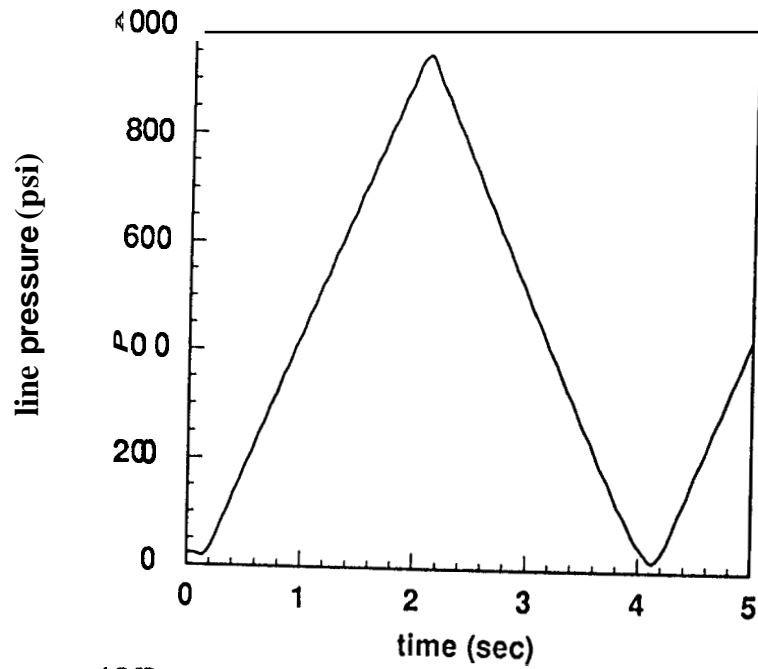


Figure A.36

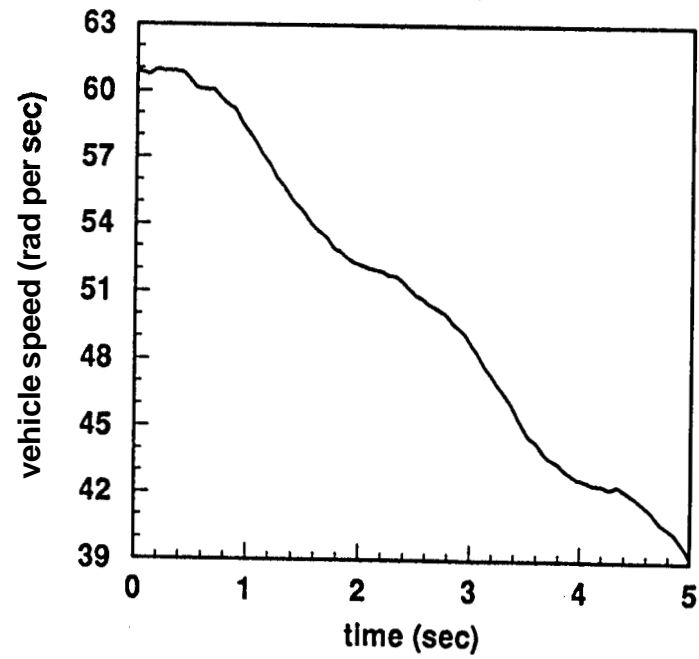
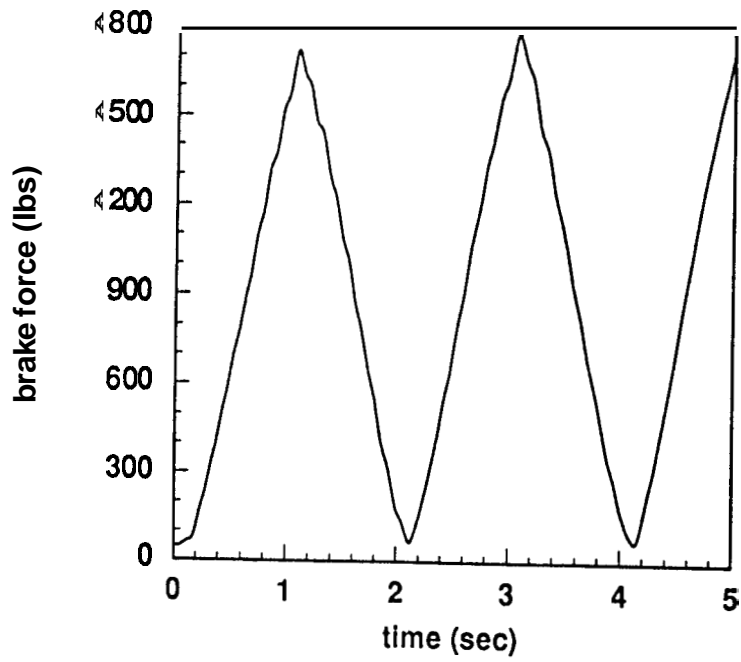
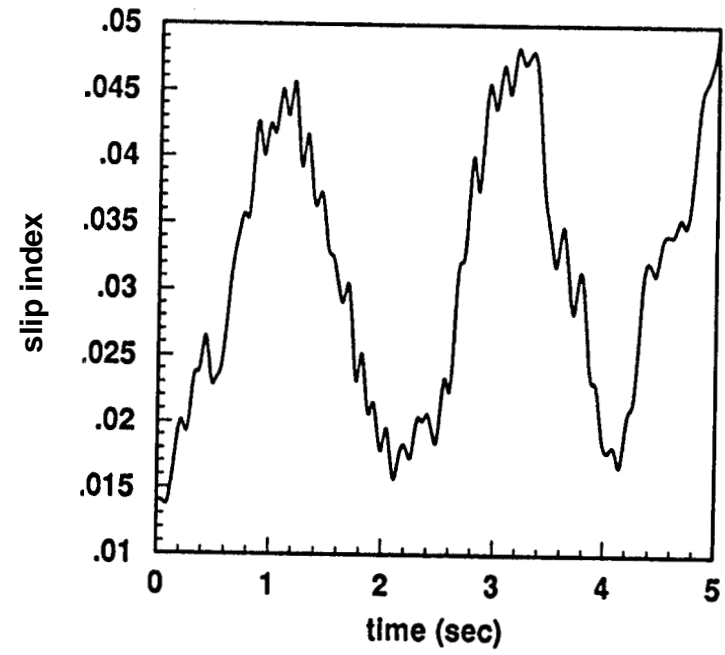
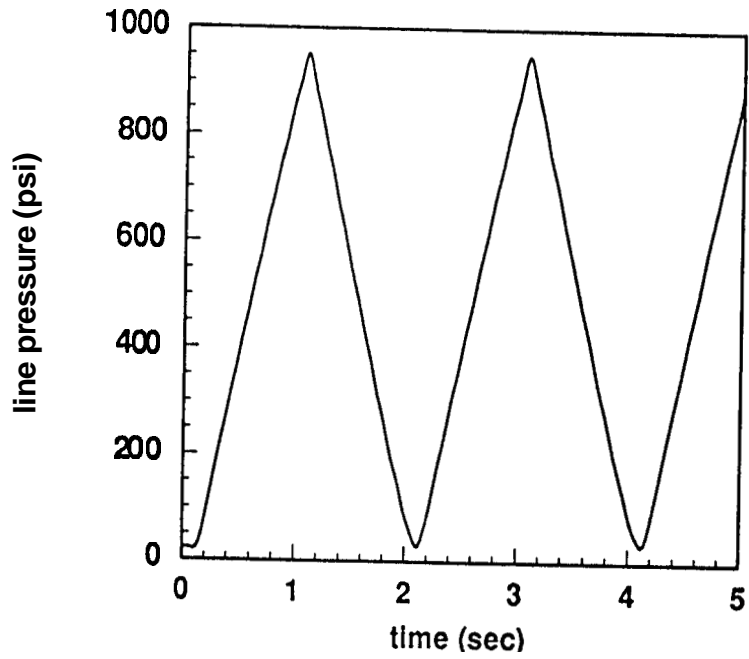


Figure A.37

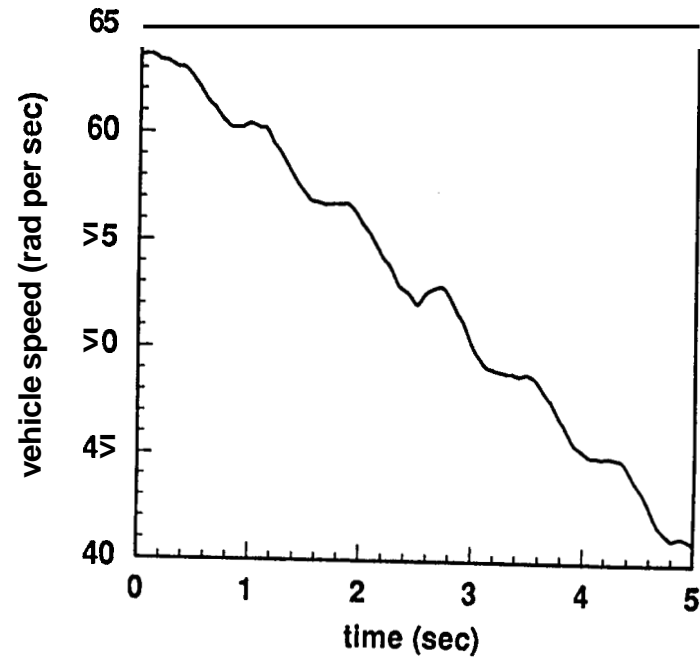
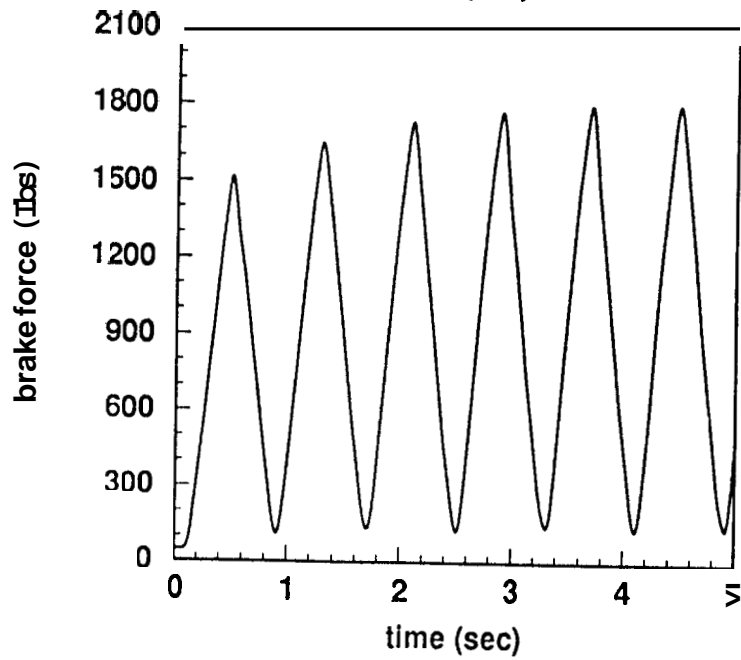
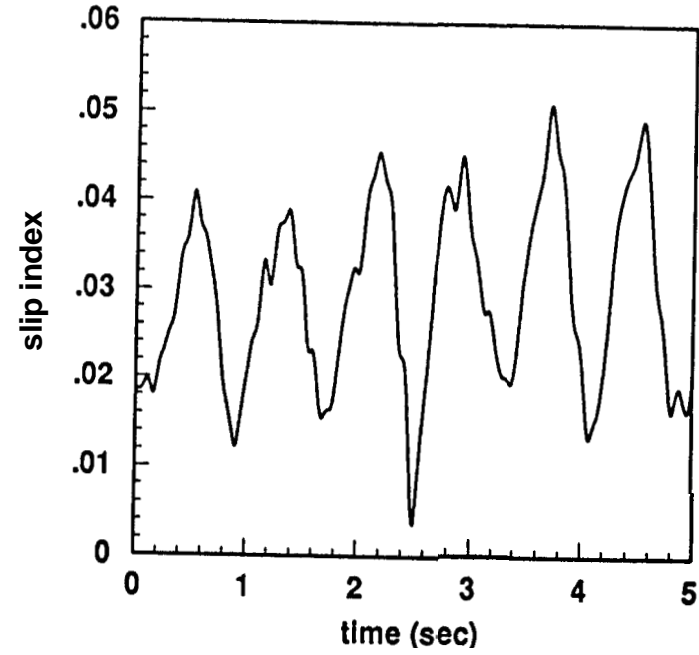
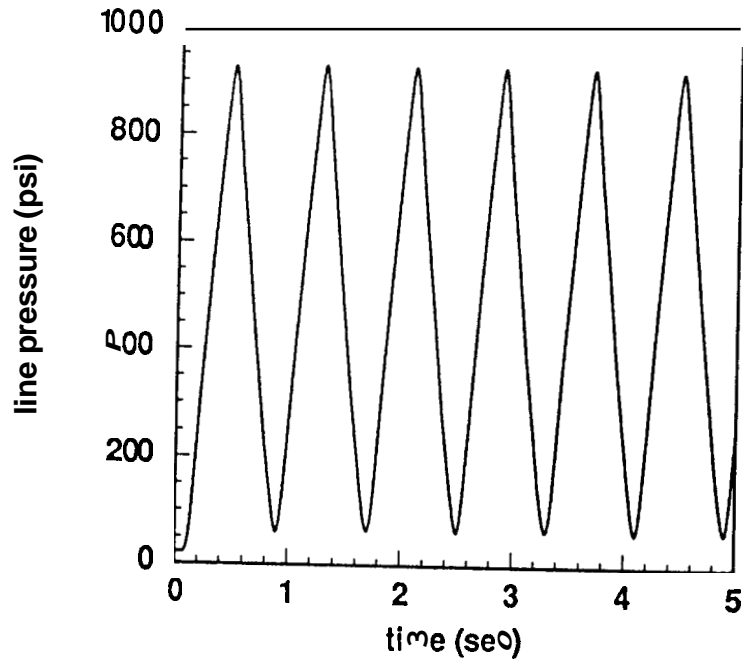


Figure A.38

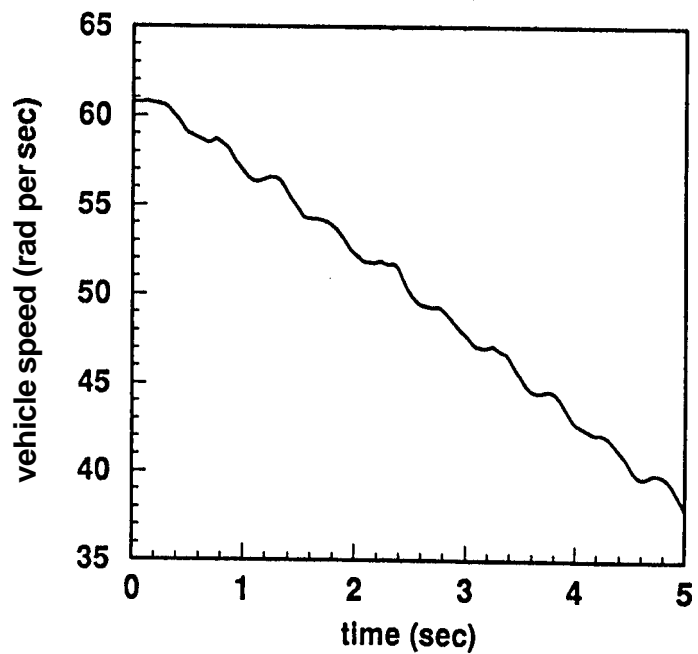
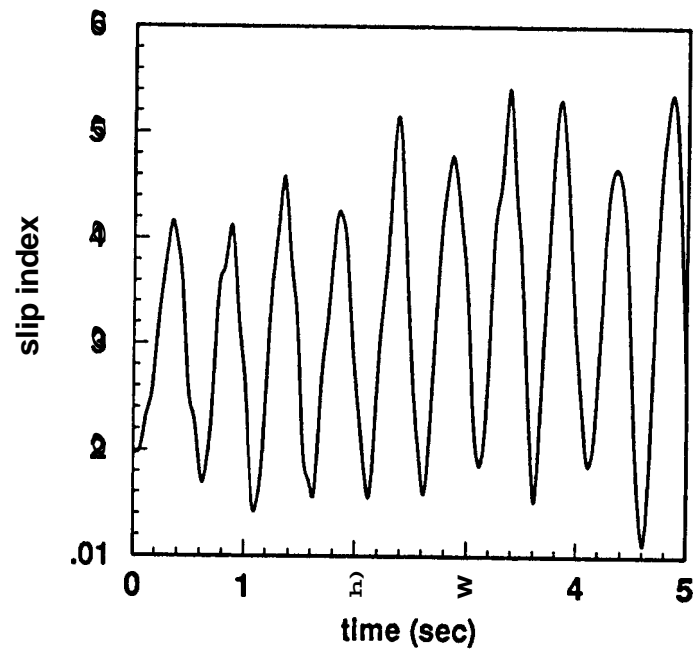
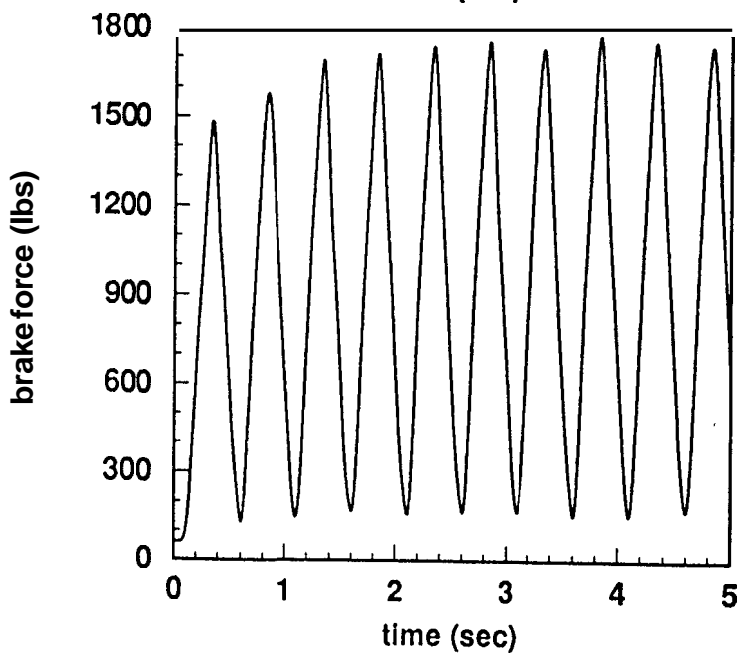
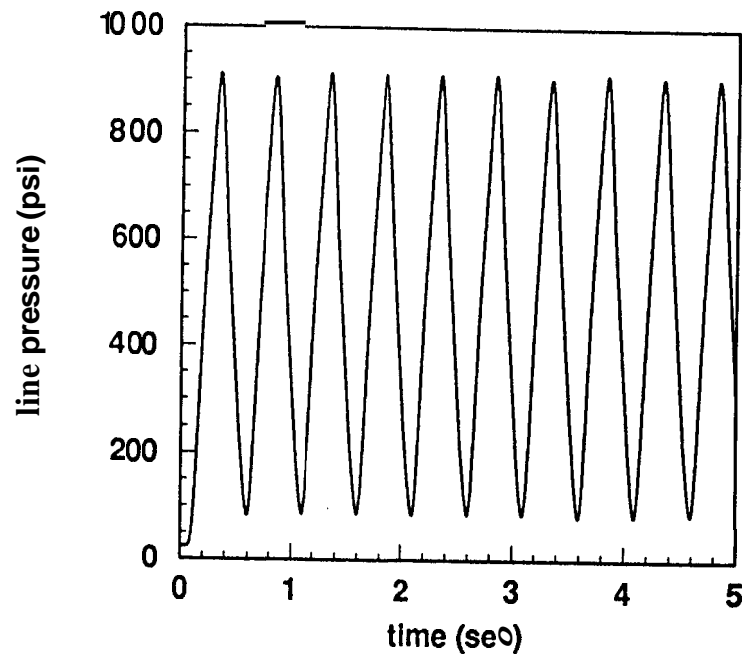


Figure A.39

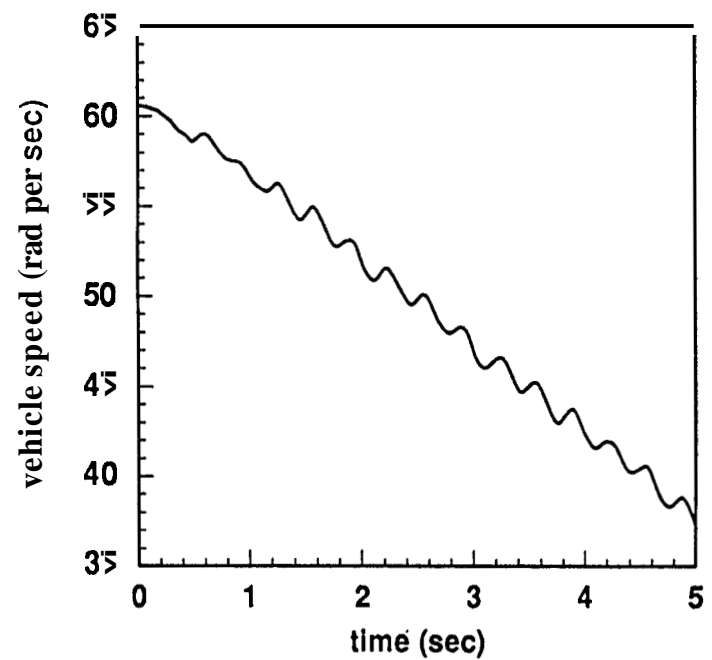
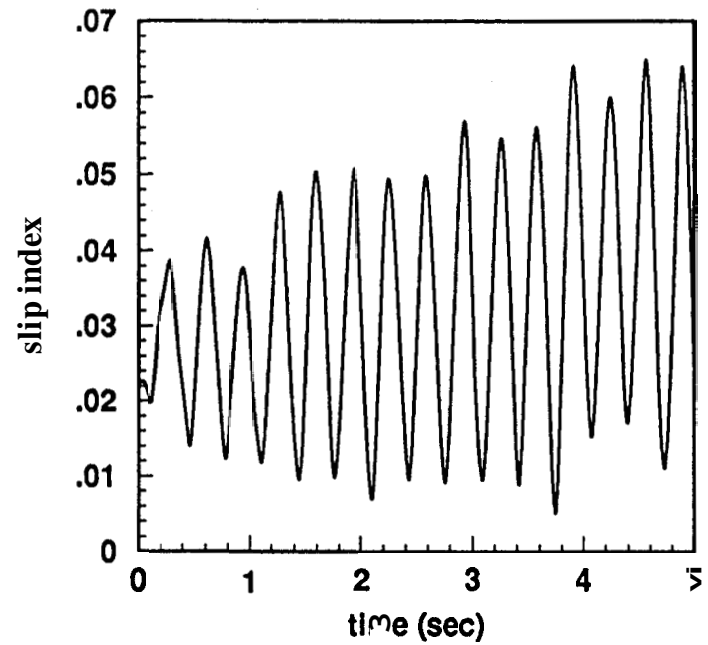
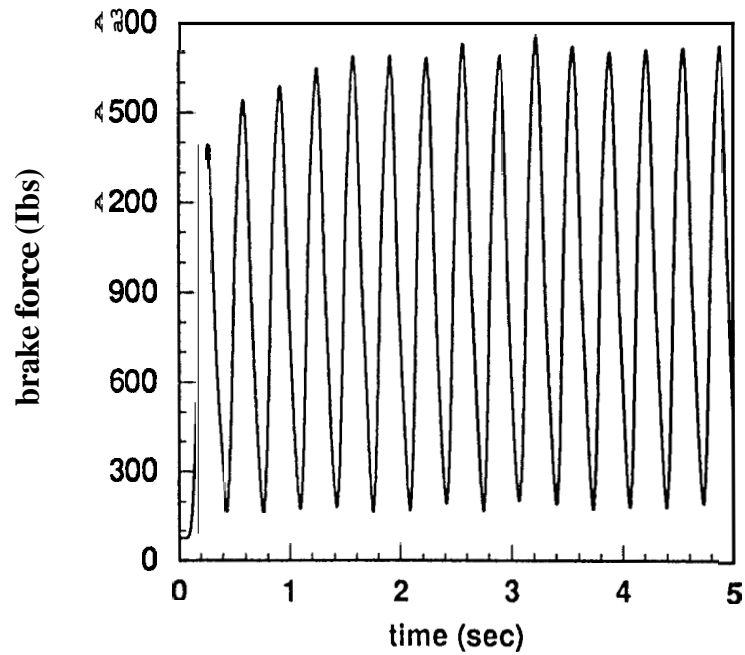
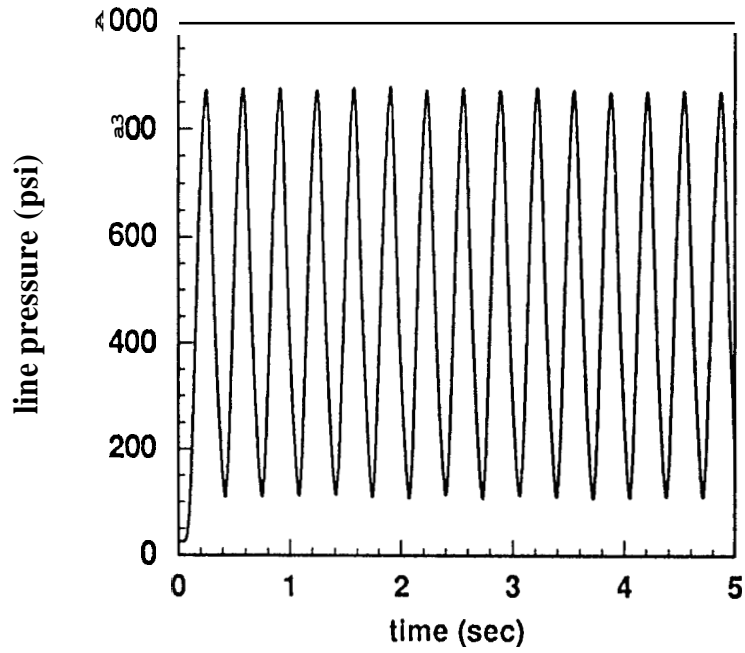


figure A.40

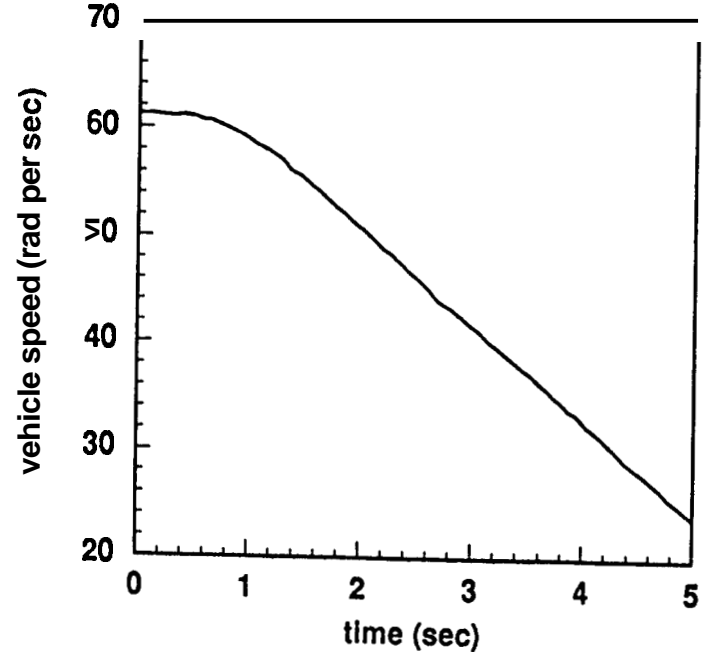
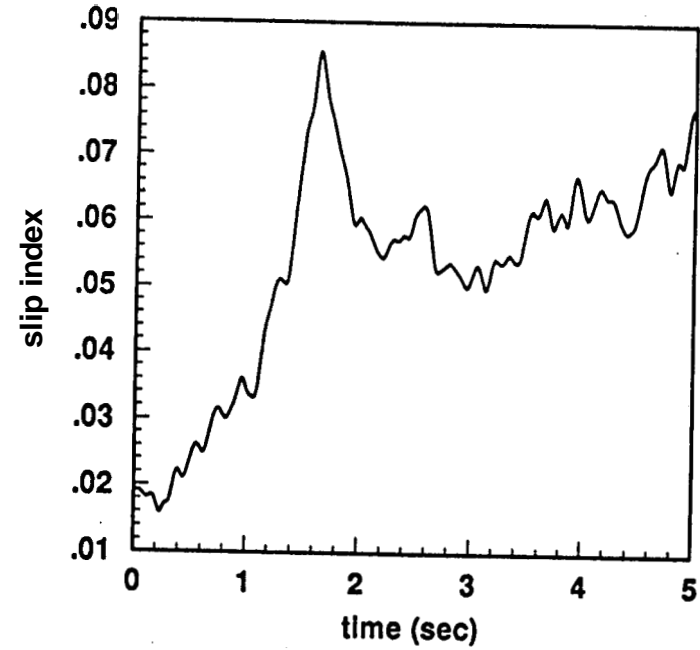
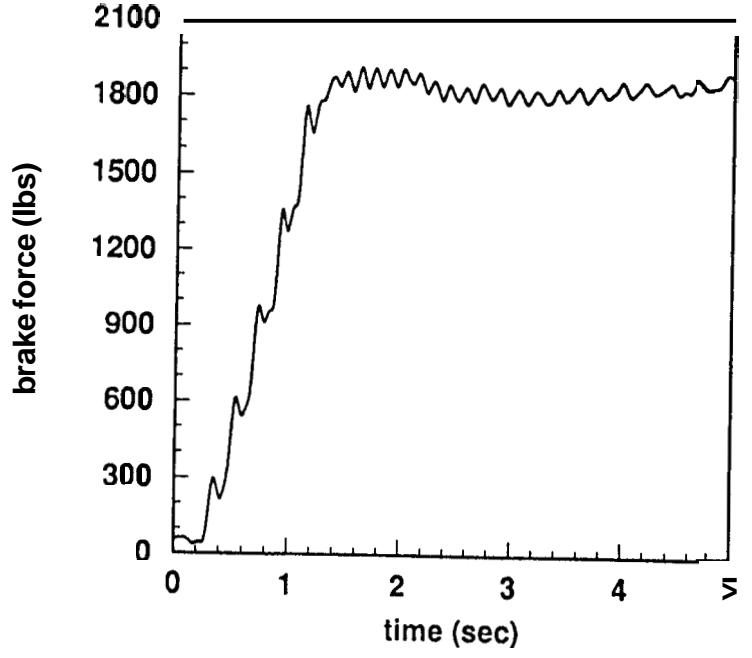
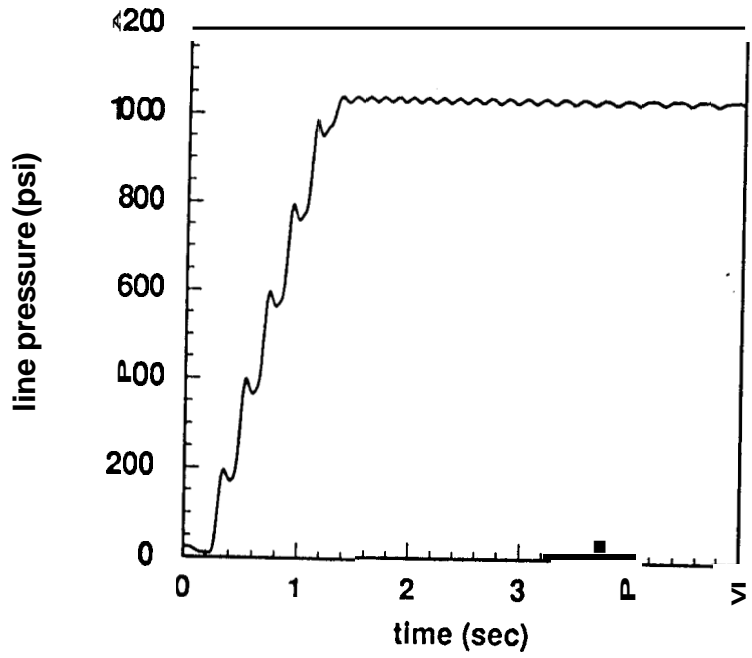


Figure A.41

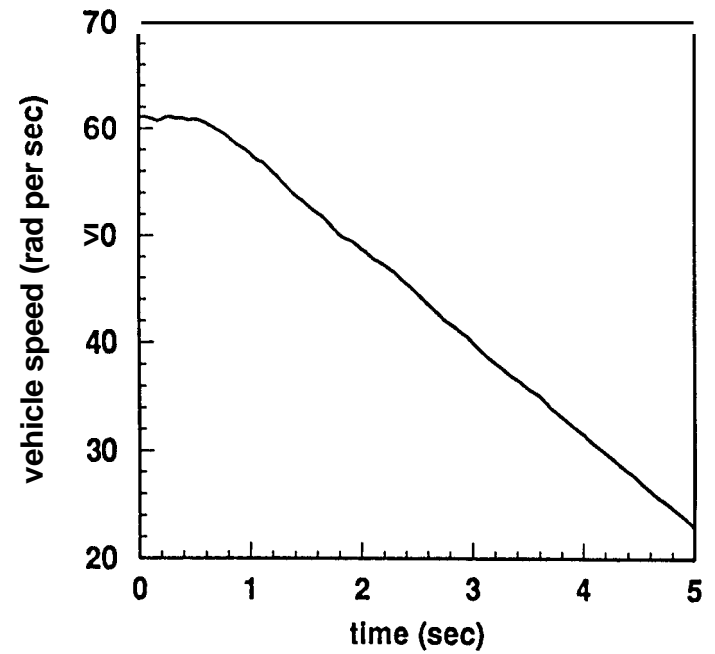
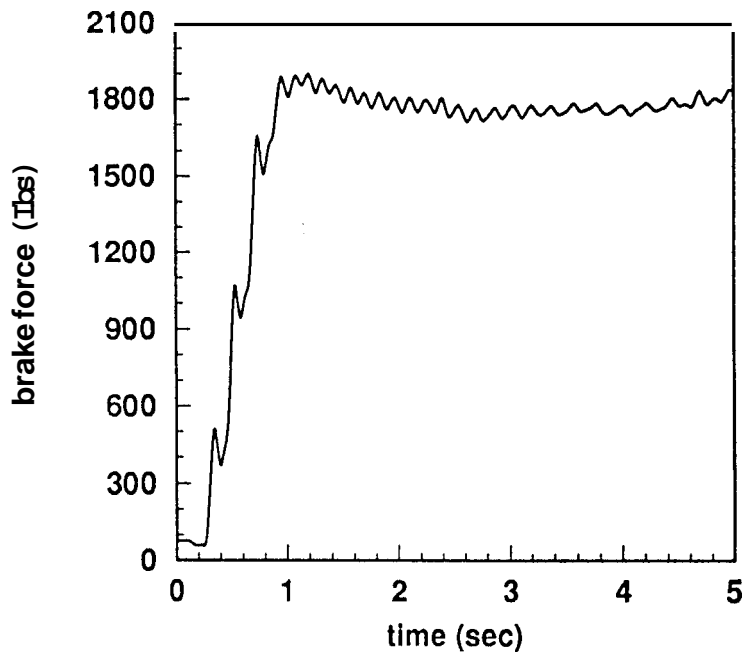
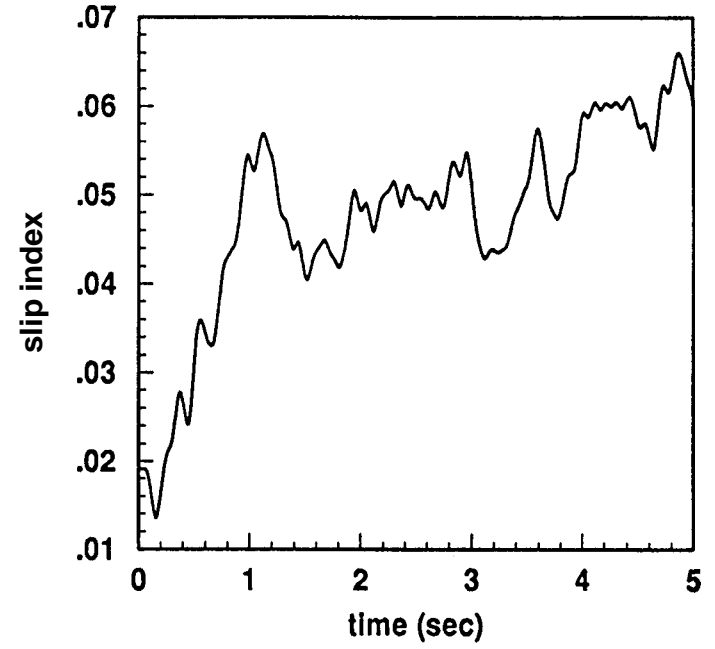
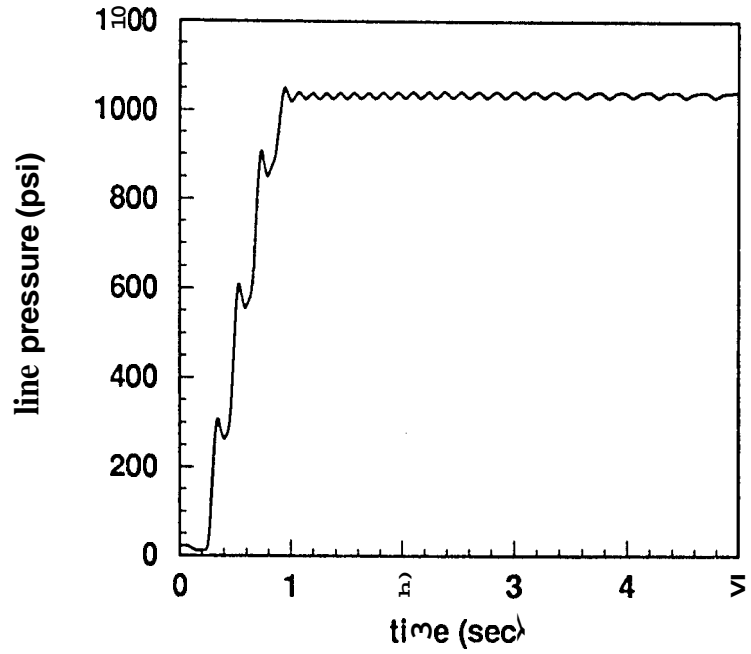


Figure A.42

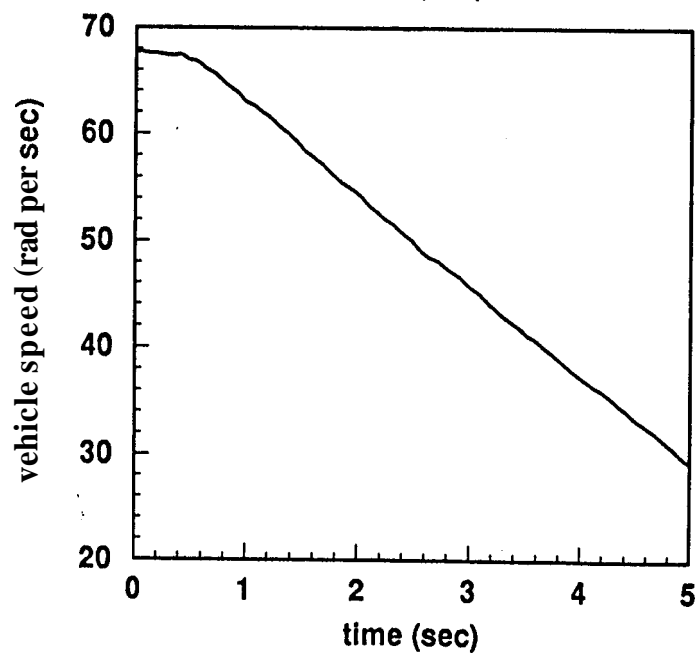
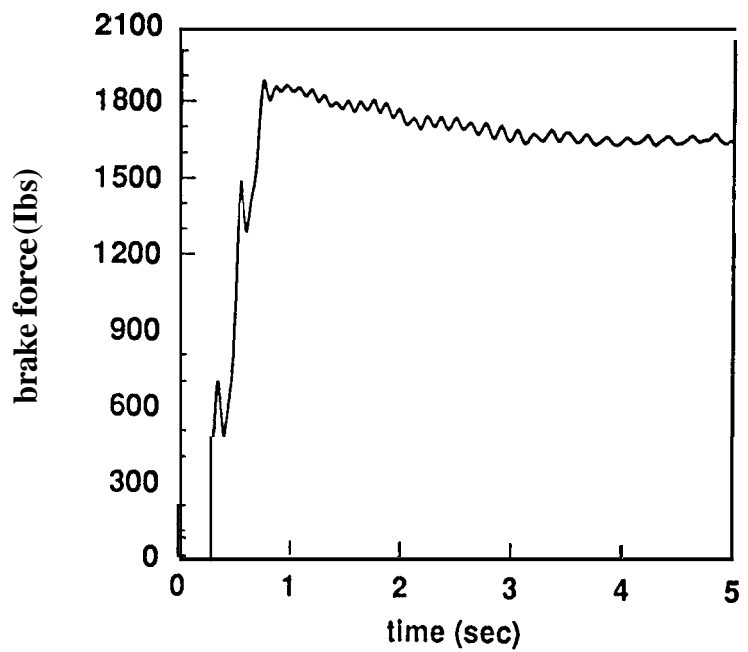
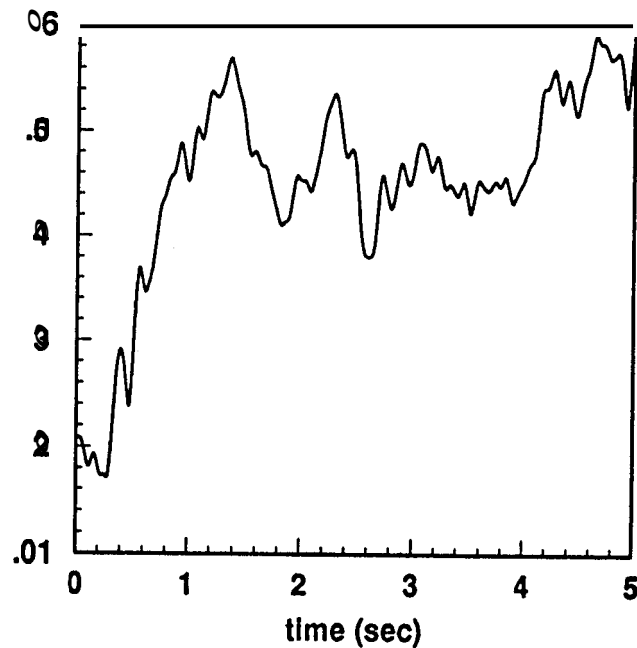
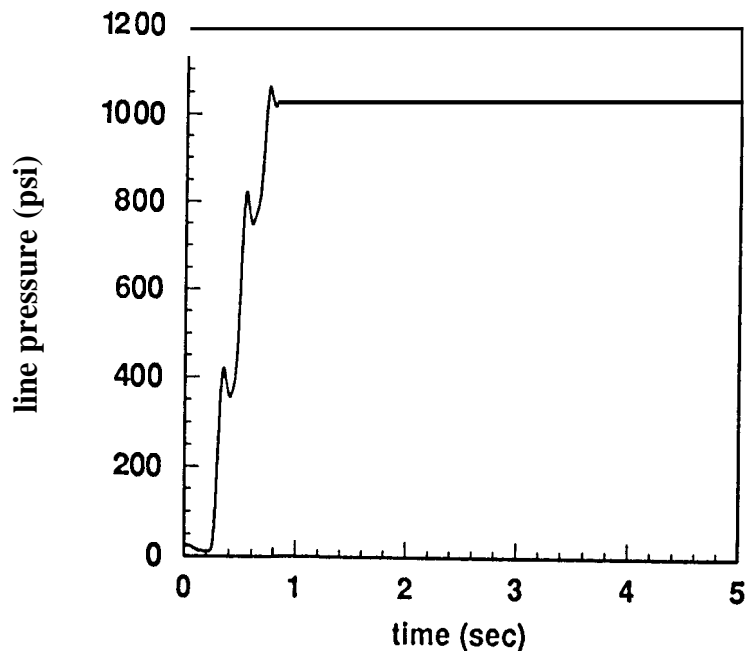


Figure A.43

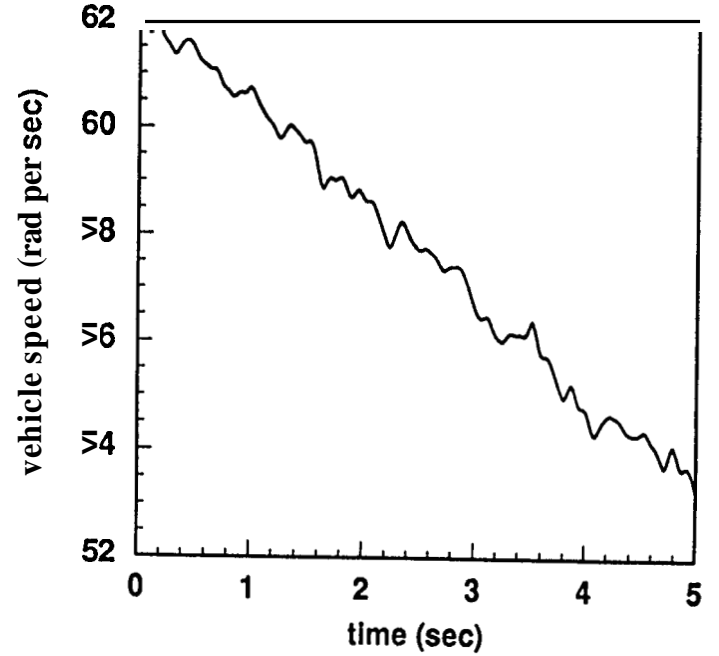
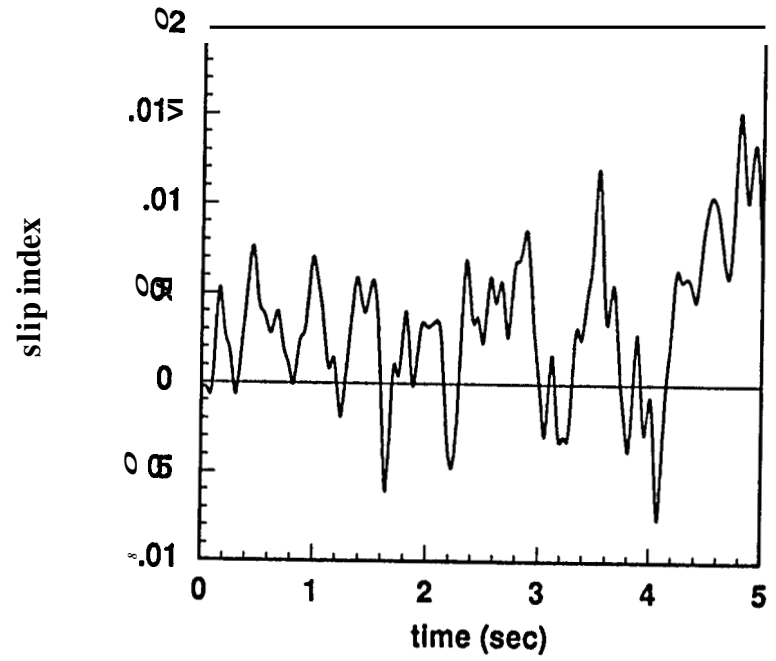
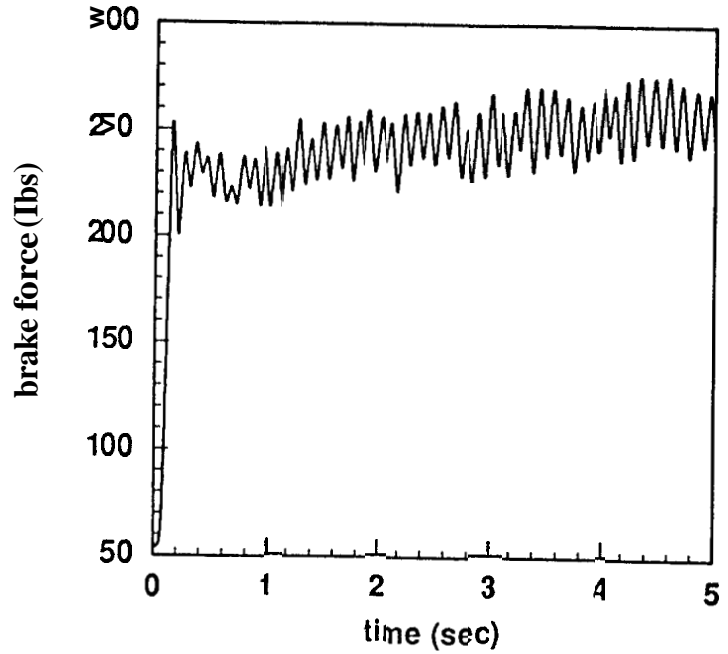
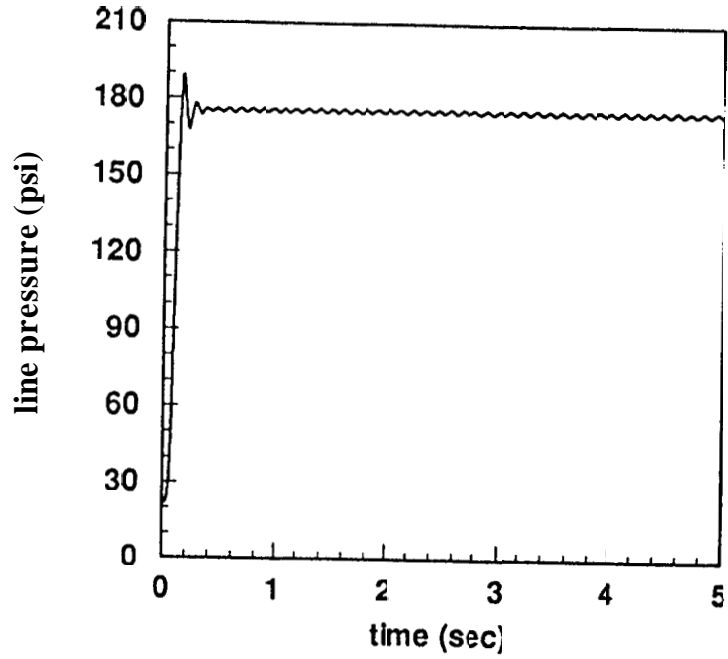


Figure A.44

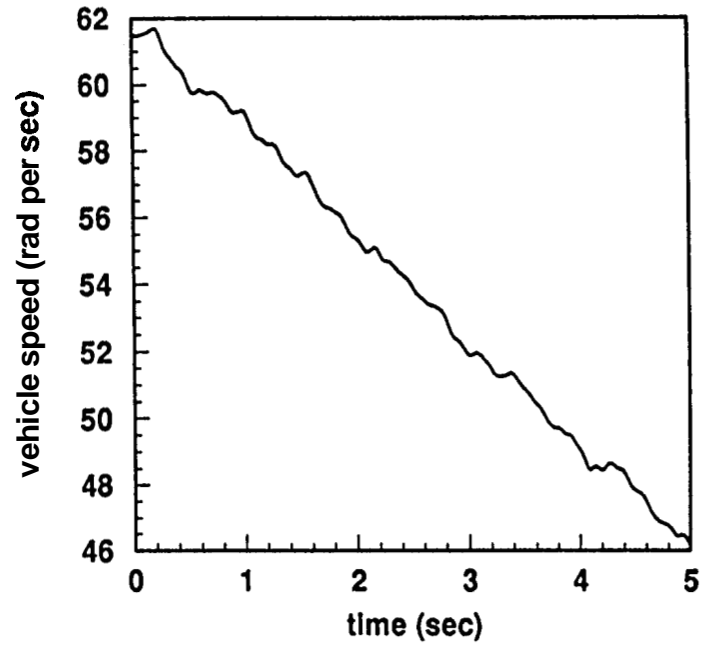
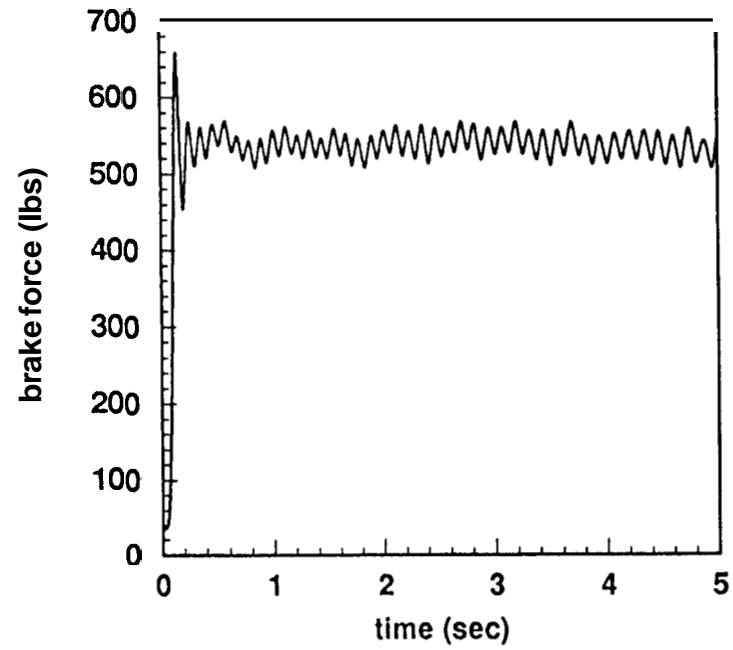
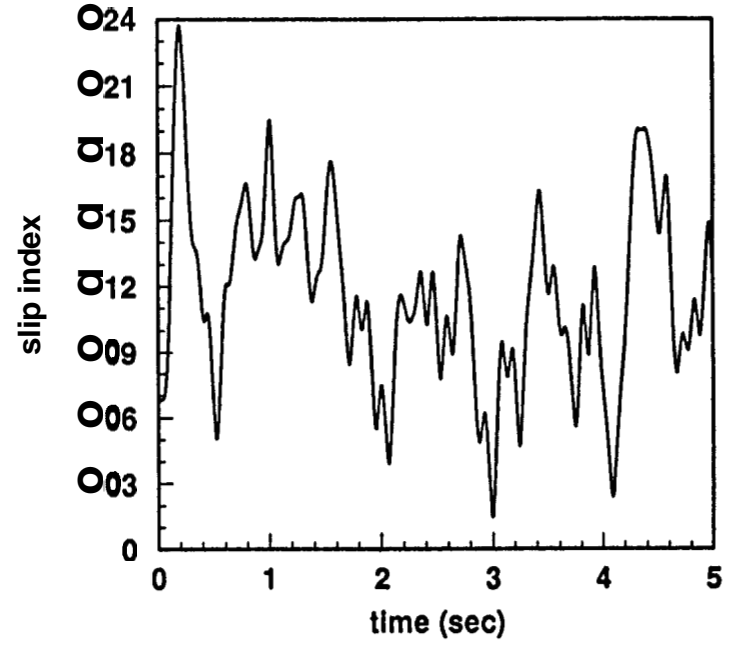
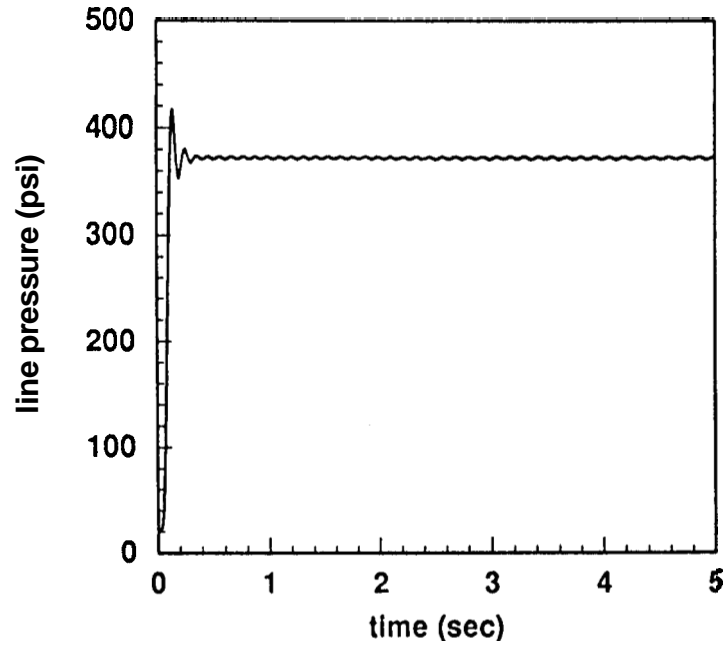


Figure A.45

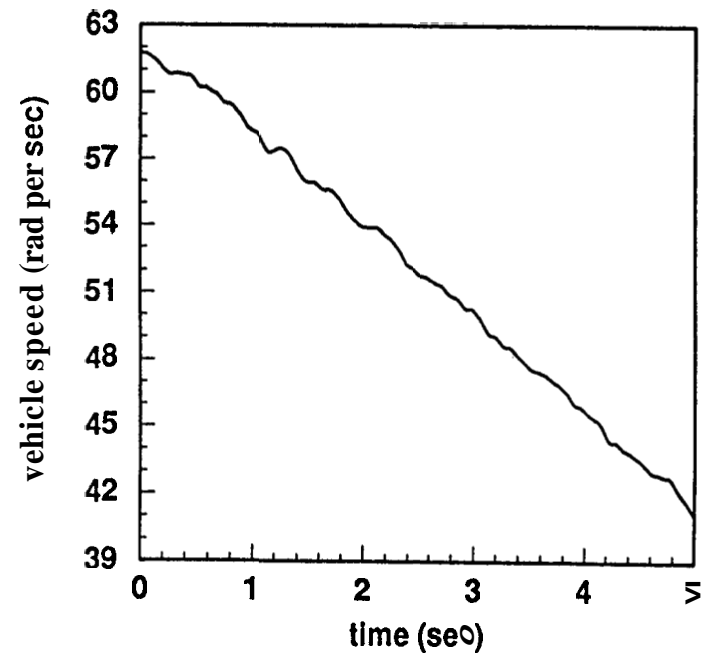
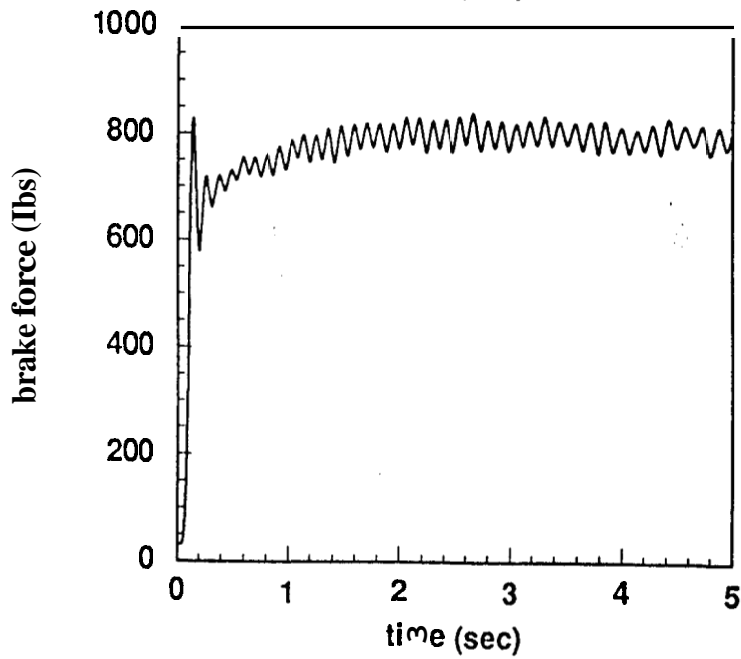
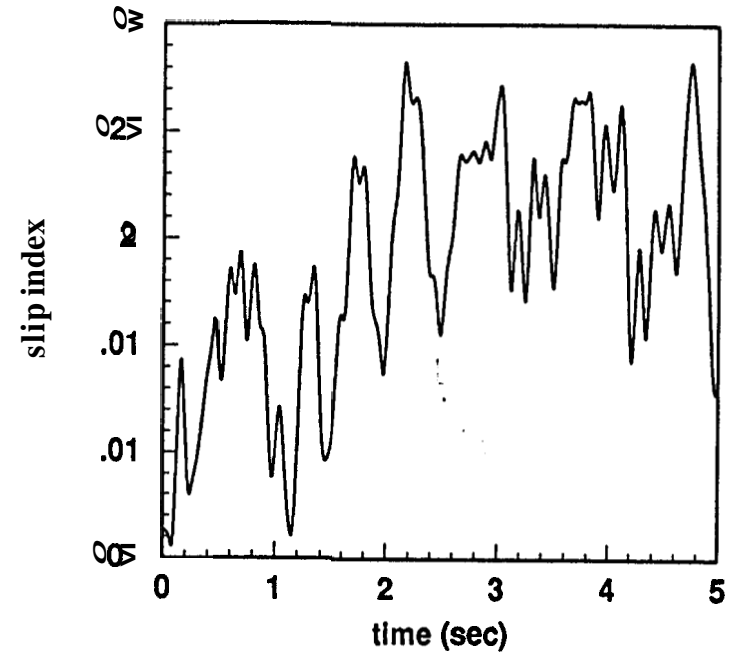
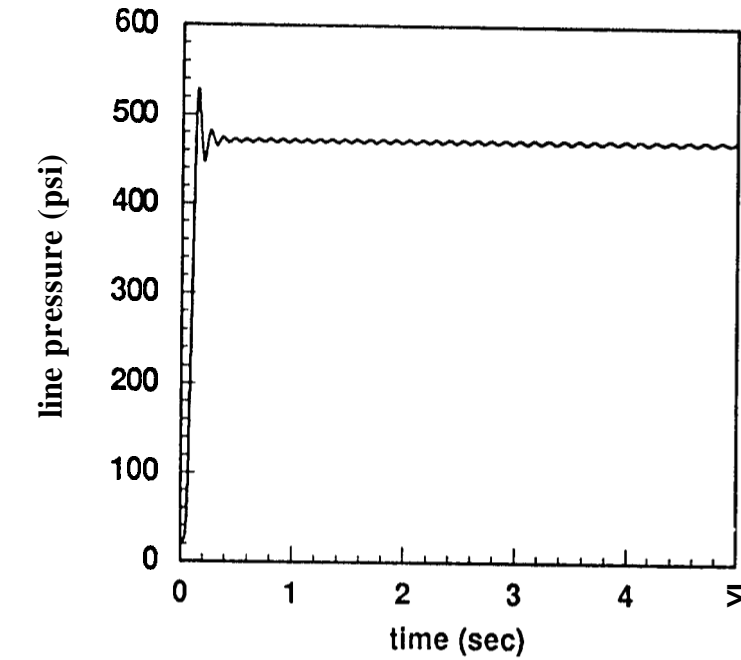


Figure A.46

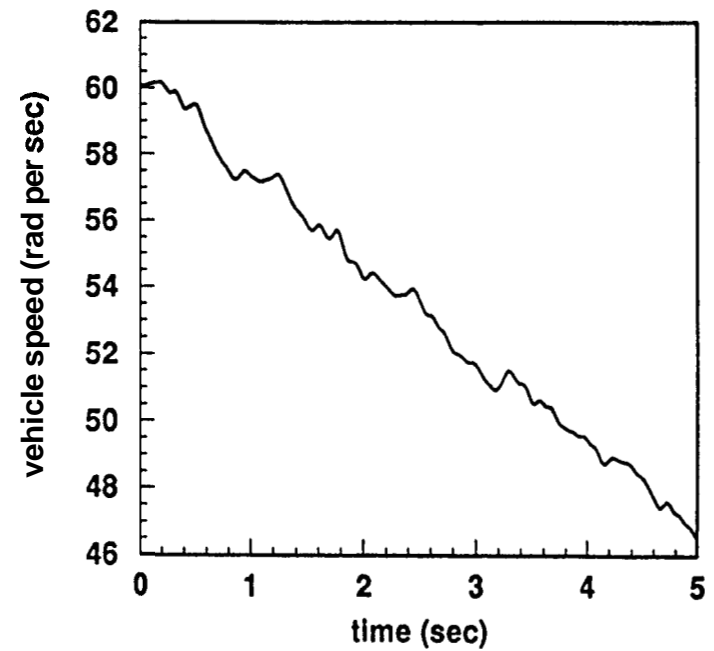
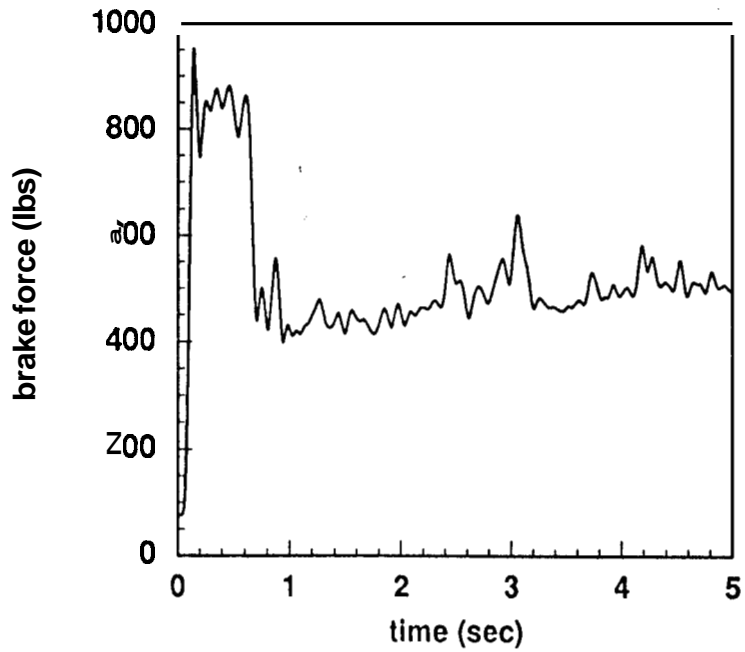
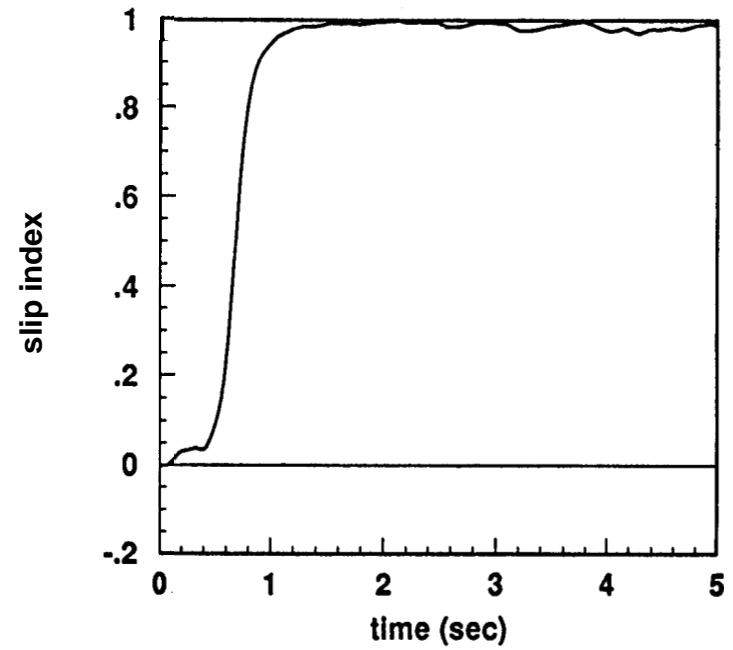
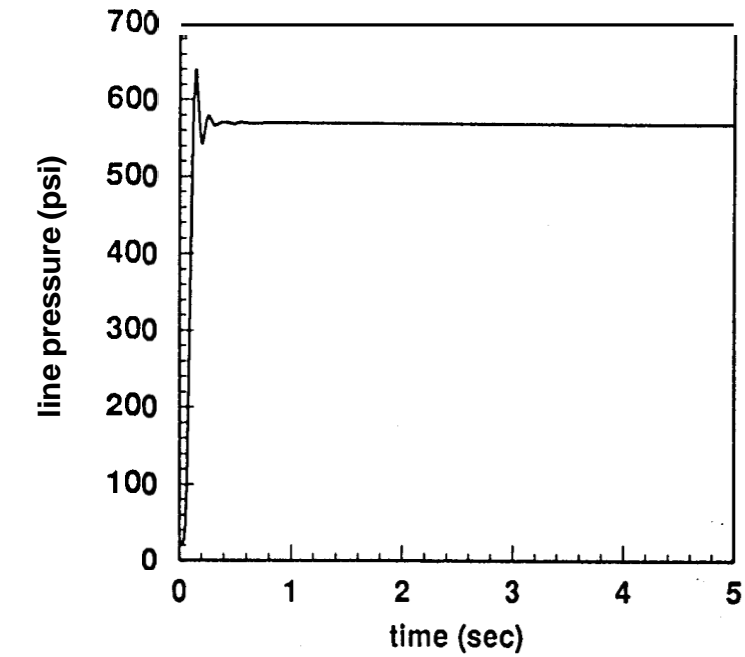


Figure A.47

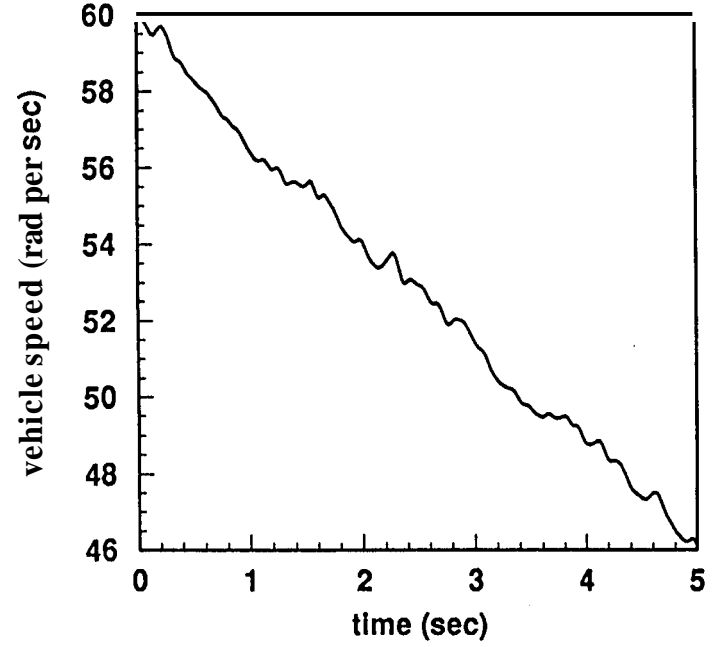
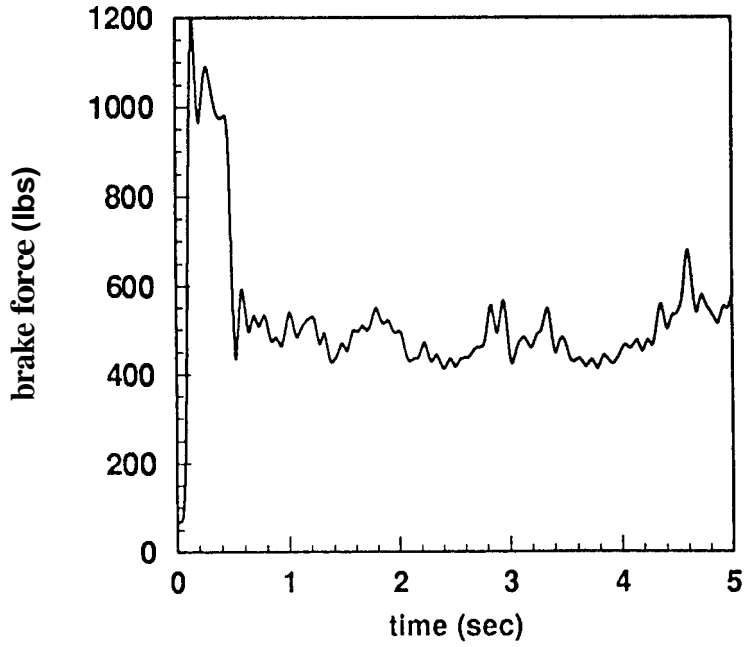
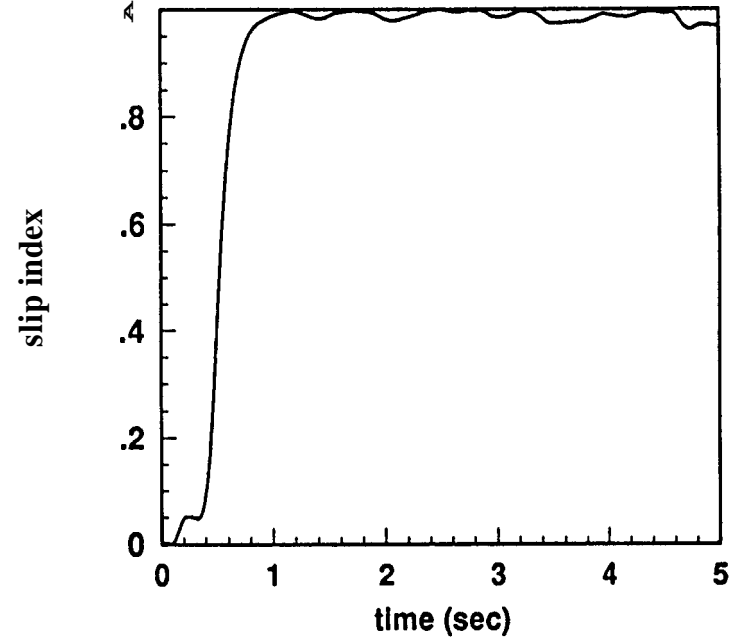
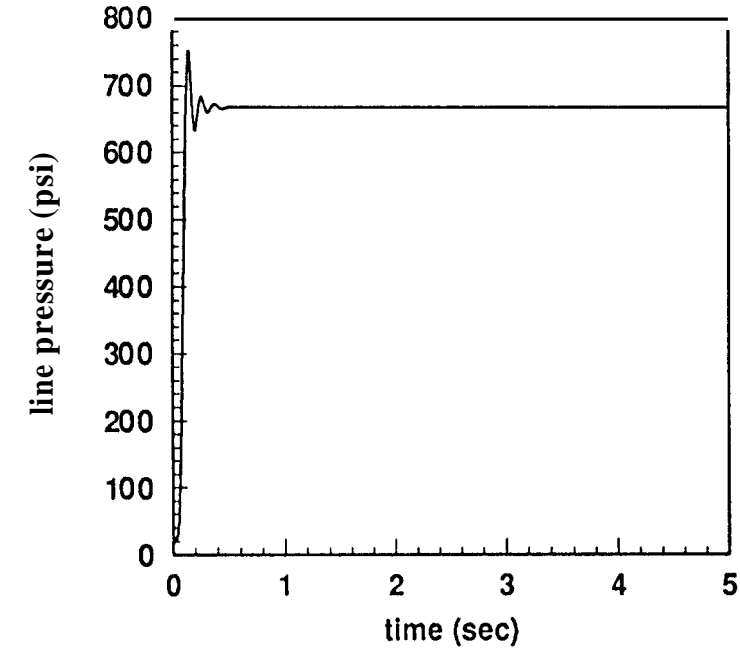


Figure A.48

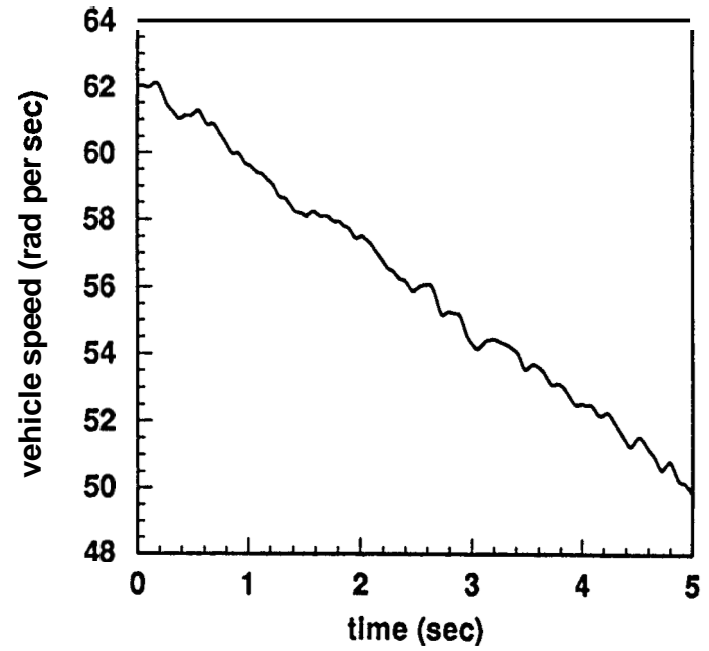
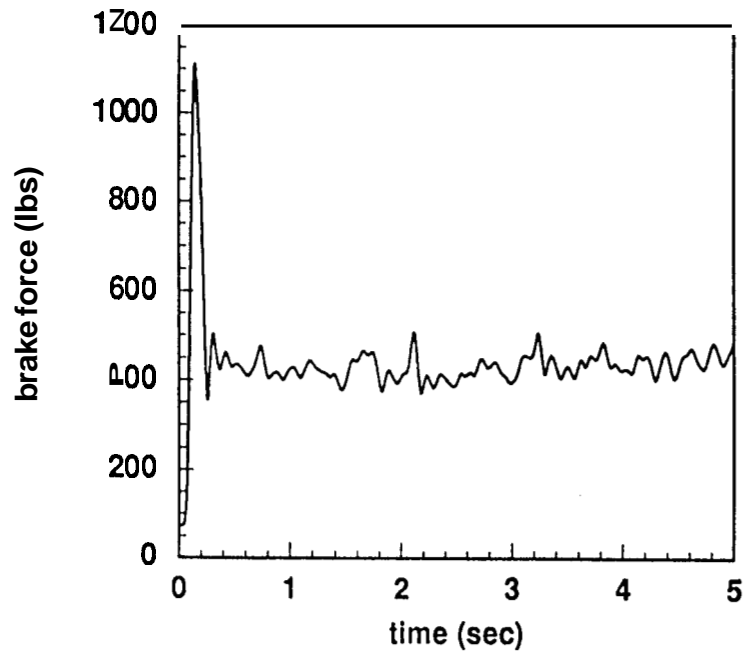
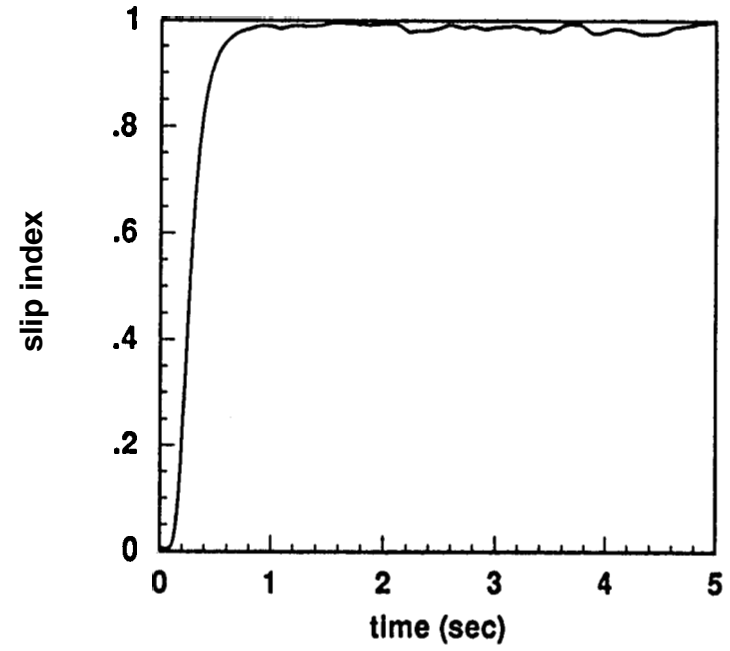
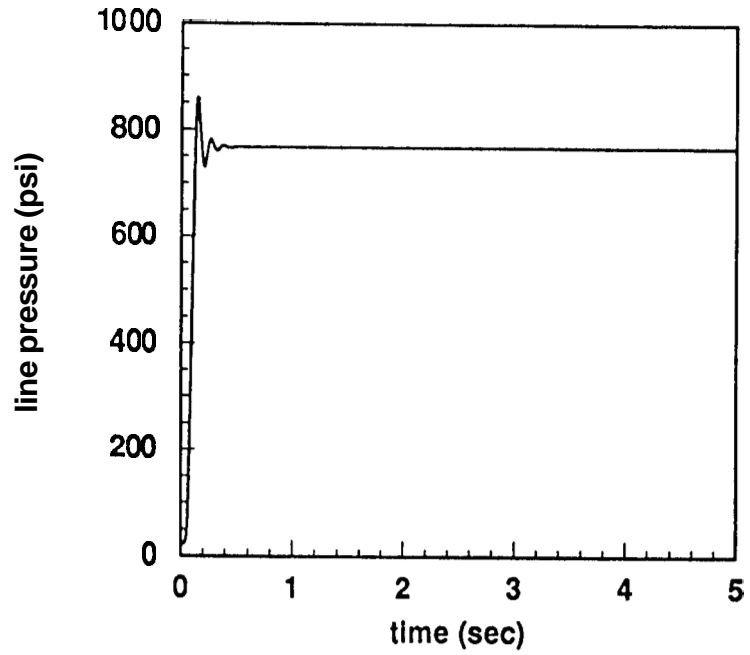


Figure A.49

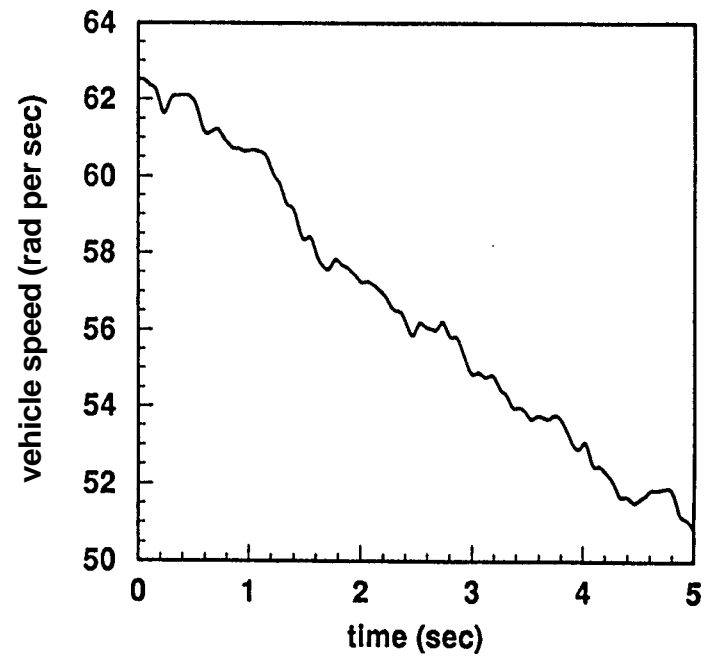
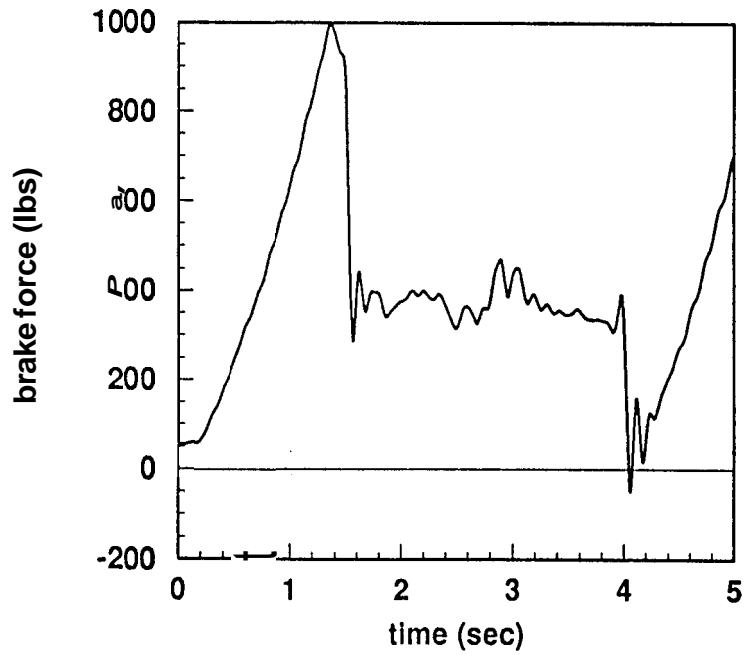
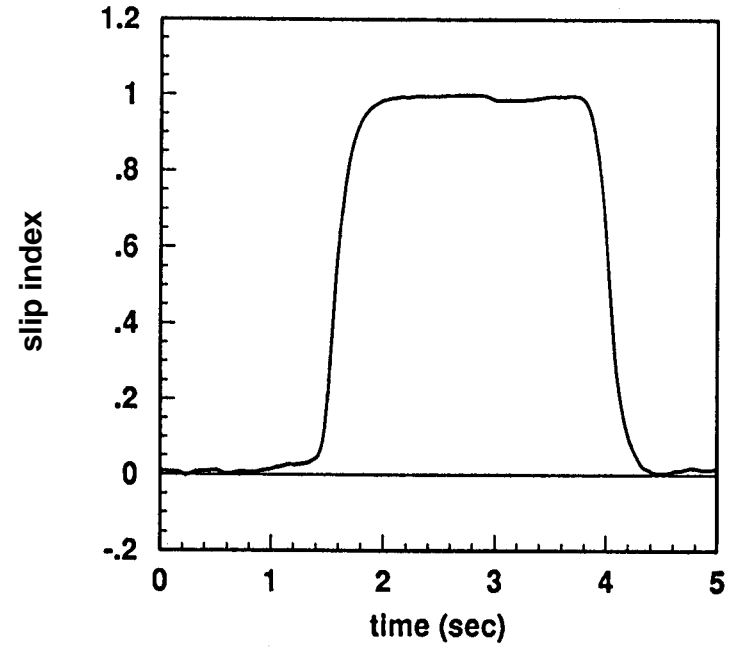
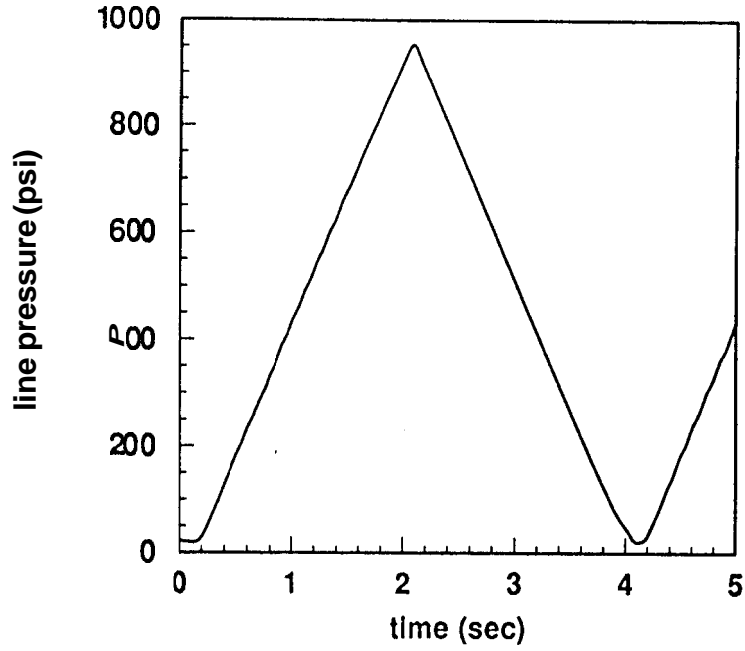


Figure A.50

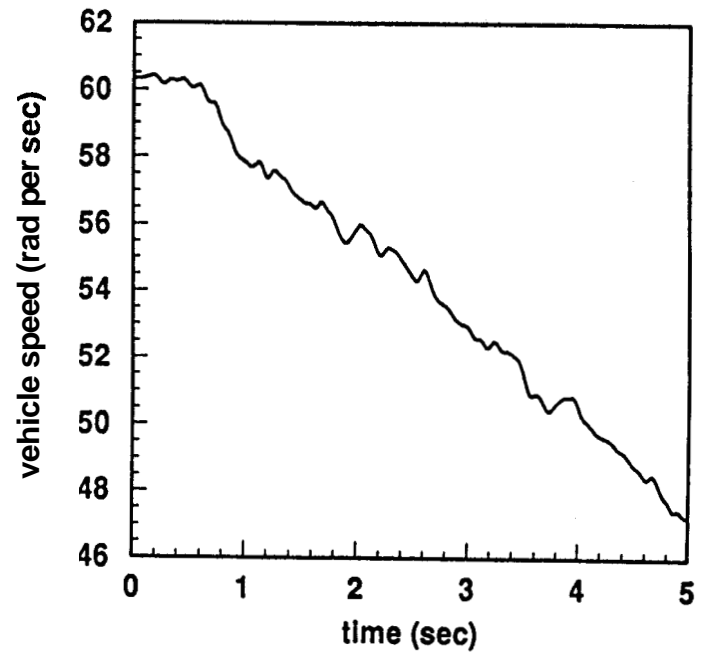
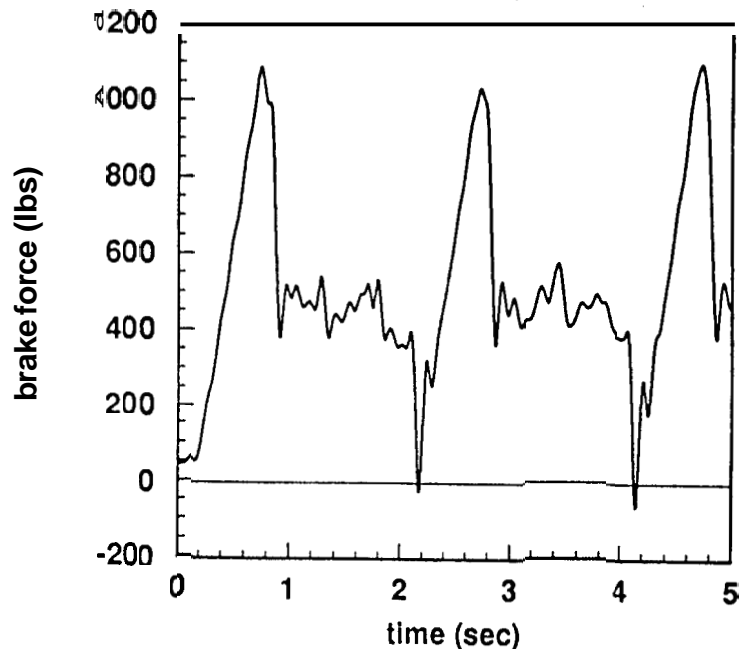
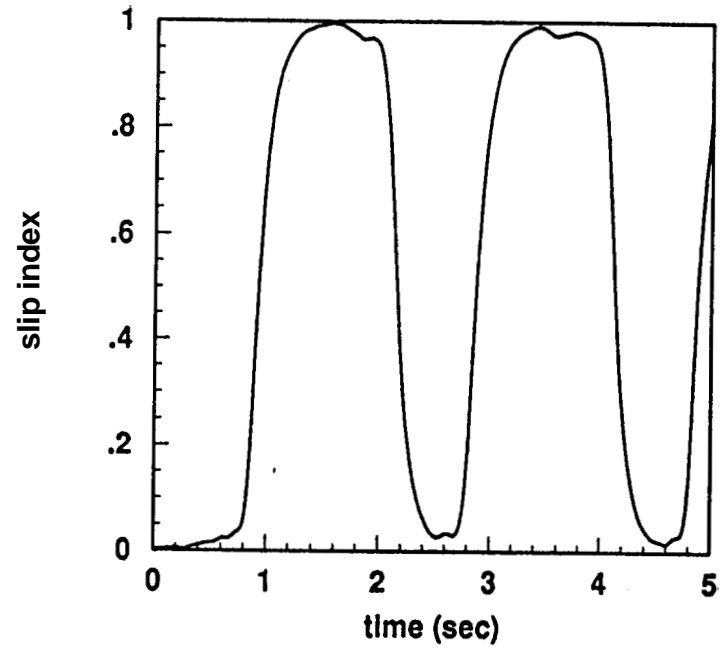
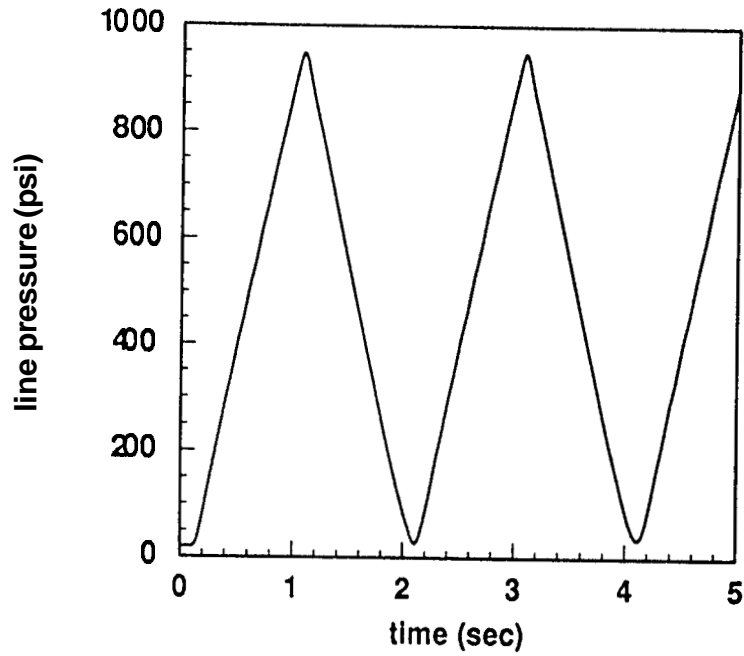


Figure A.51

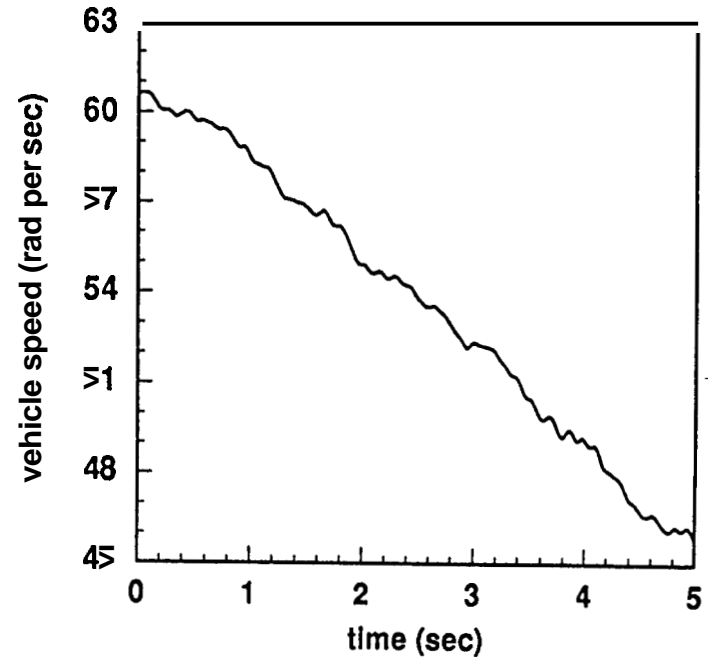
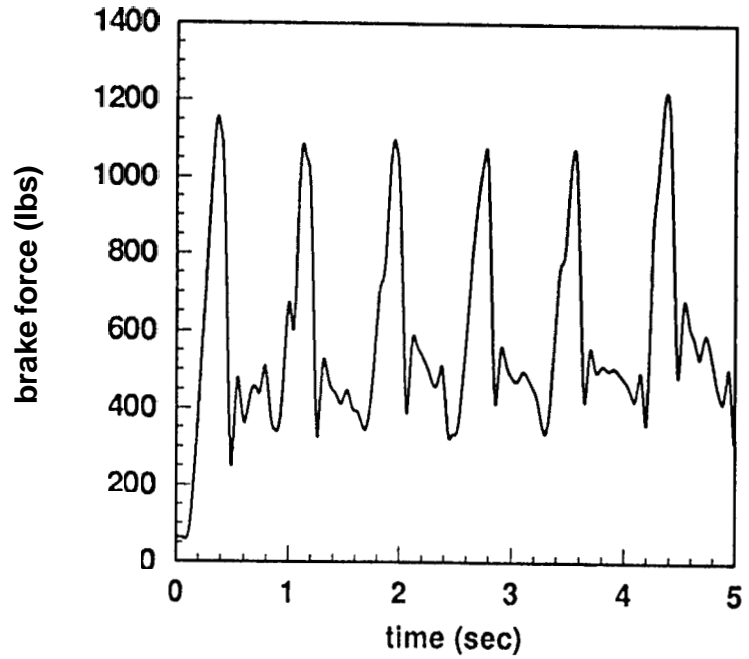
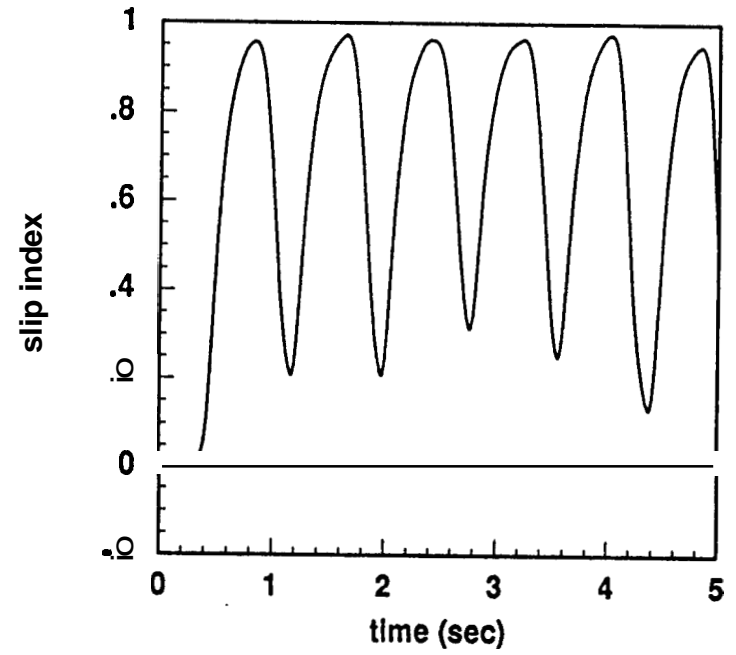
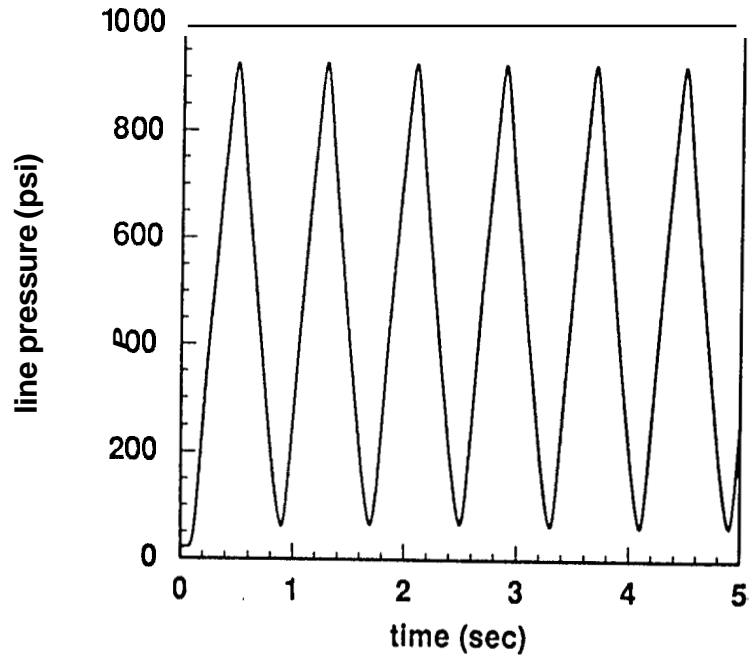


Figure A.52

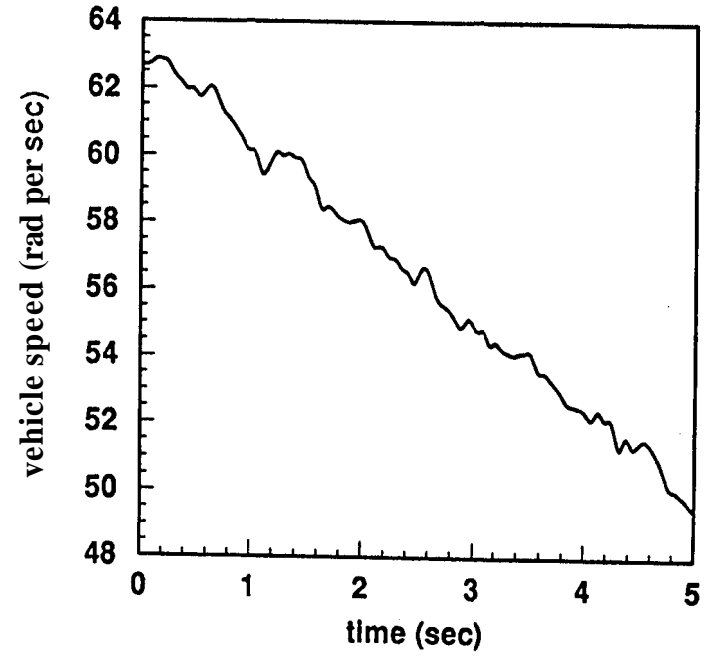
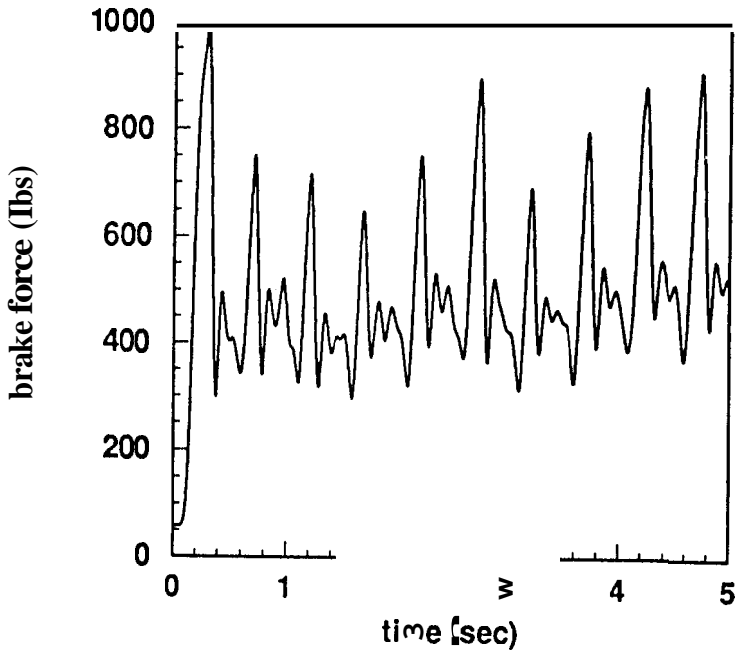
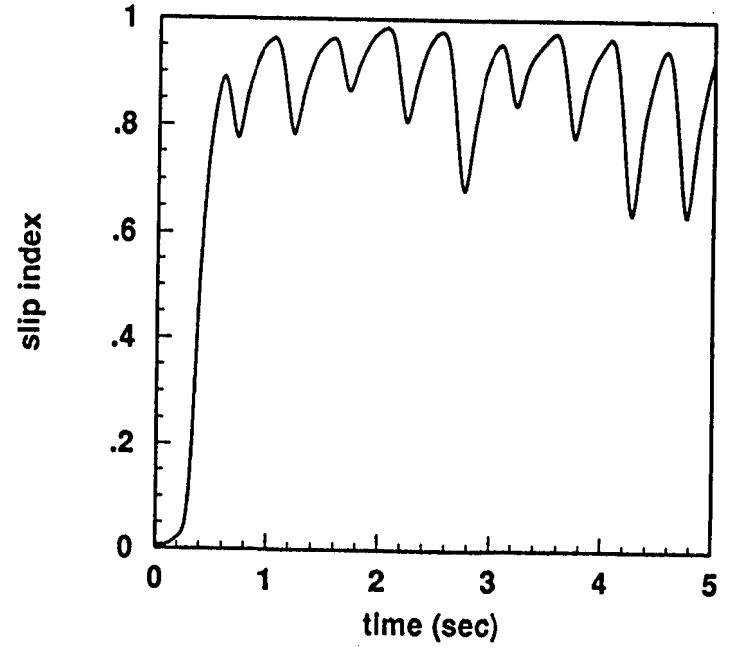
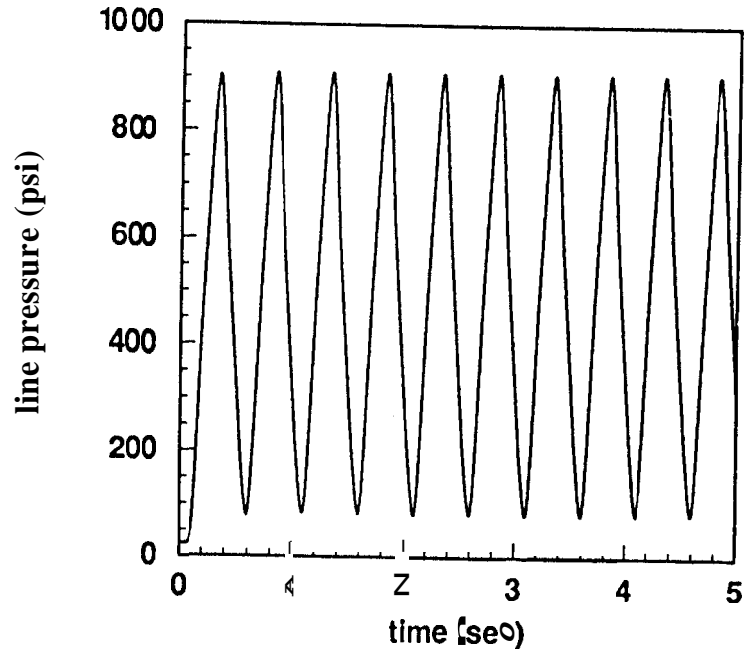


Figure A.53

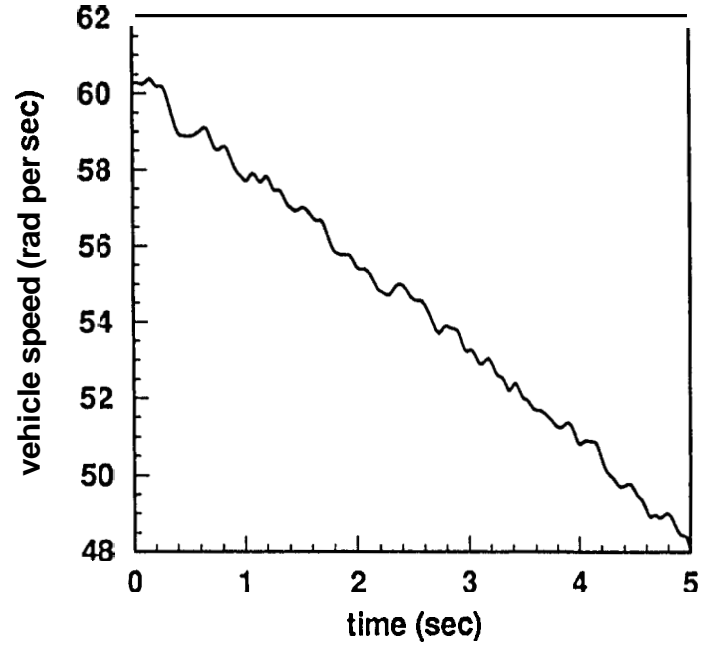
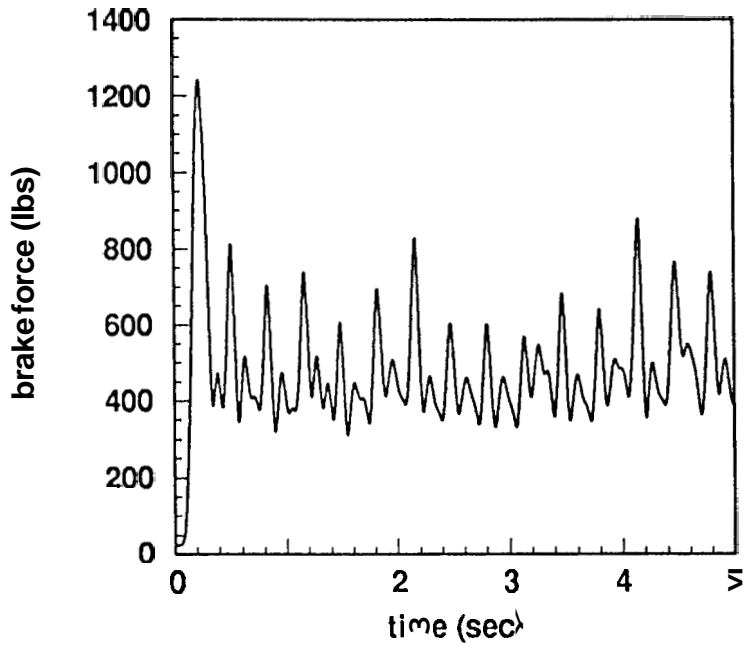
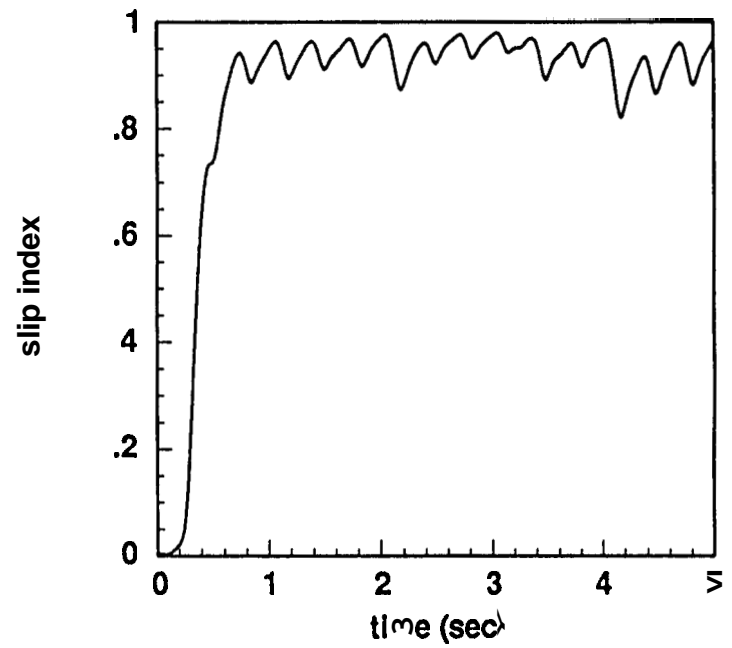
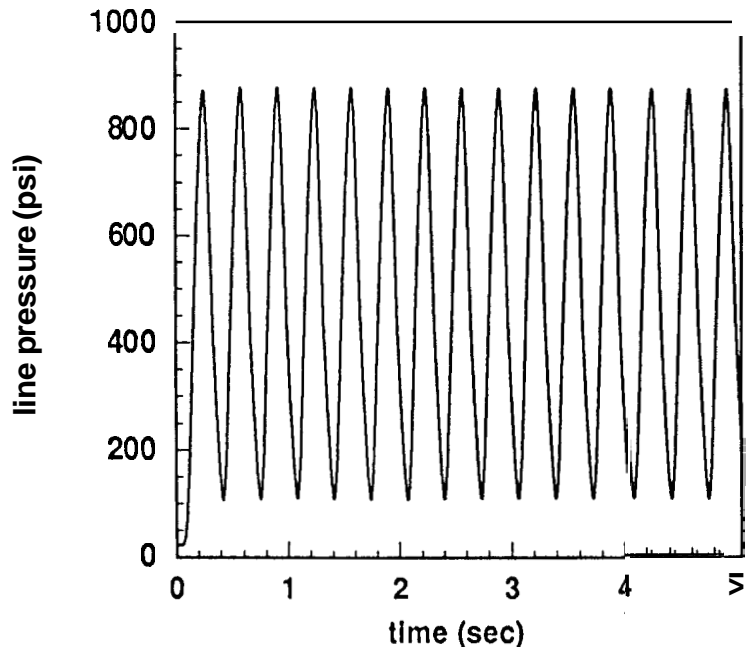


Figure A.54

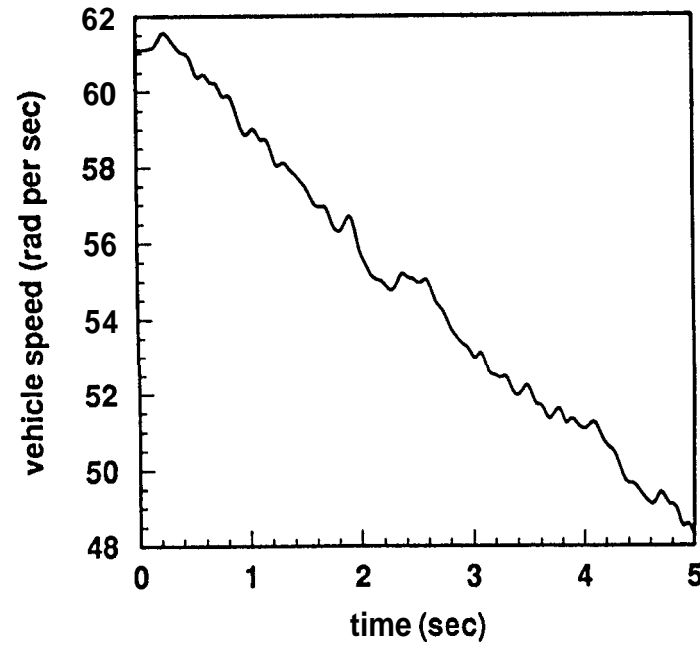
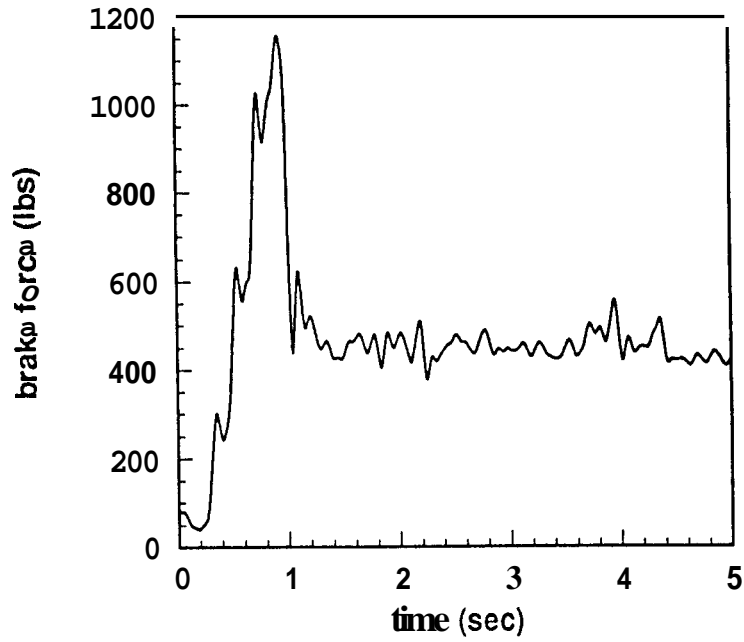
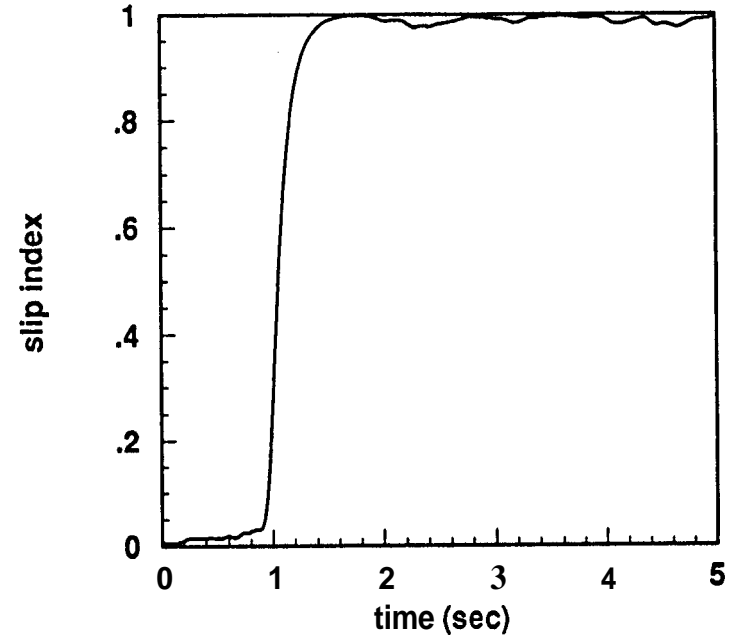
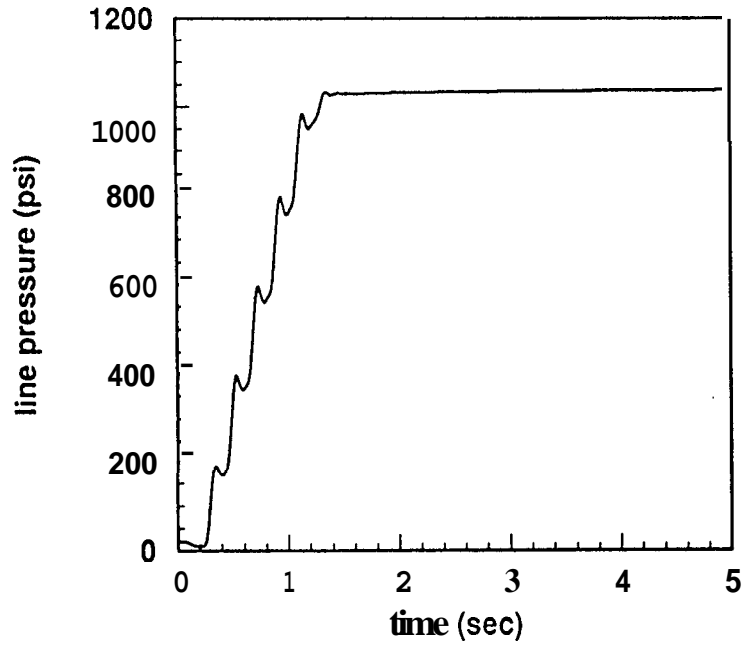
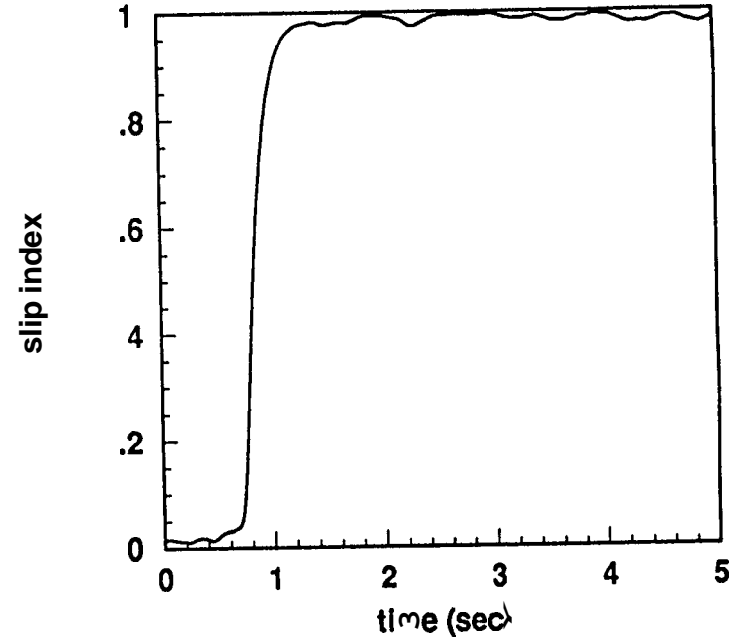
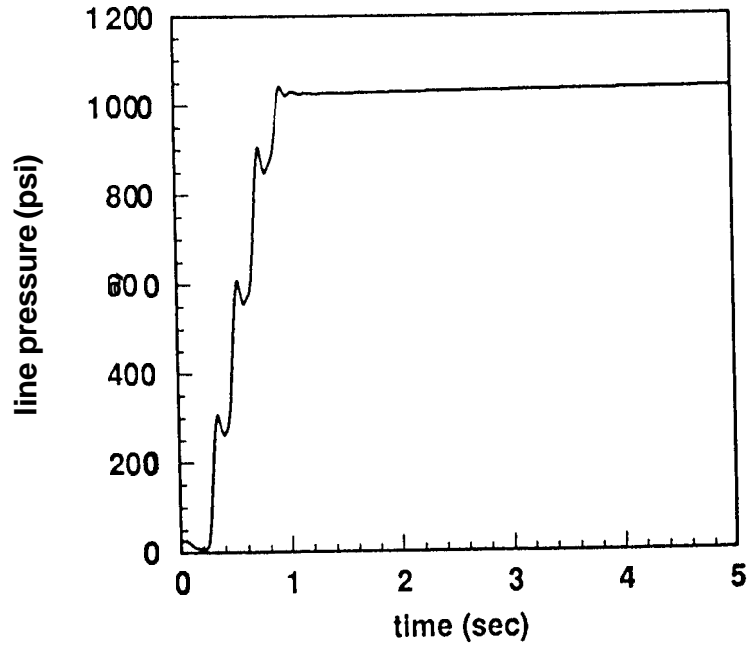


Figure A.55



66

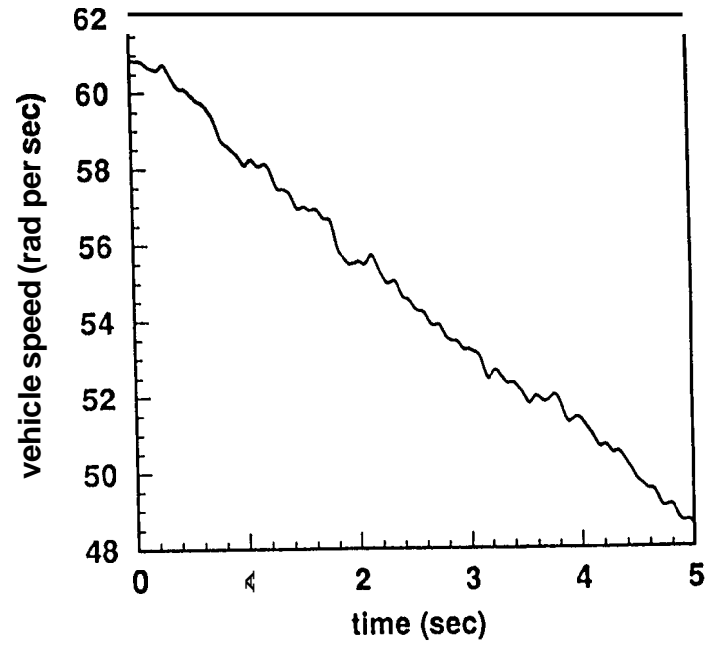
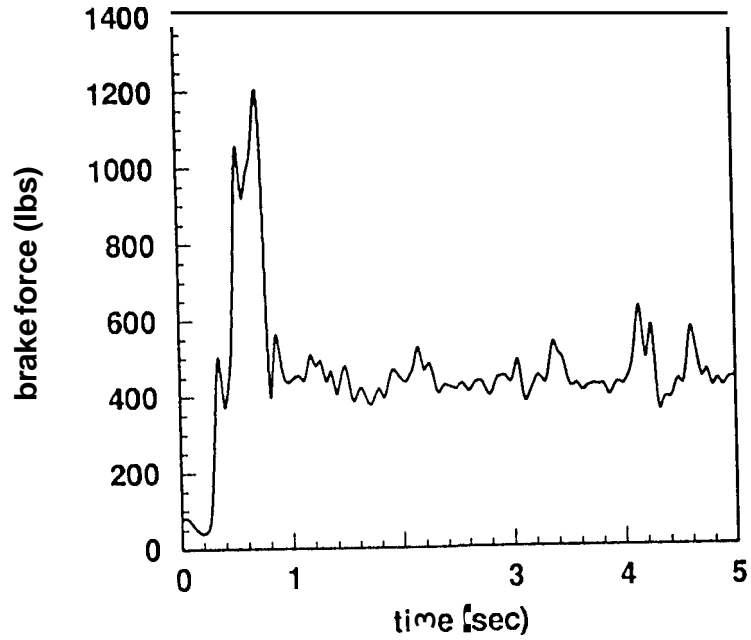


Figure A.56

